Westinghouse Non-Proprietary Class 3

WCAP-15950-NP
Revision 2
(See WCAP-14000-P Rev. 2
For Proprietary Version)

September 2004

Structural Integrity Evaluation of Reactor Vessel Upper Head Penetrations to Support Continued Operation: Point Beach Units 1 and 2

Westinghouse

WCAP-15950-NP
Revision 2
(Revision 1 Not Issued)

Structural Integrity Evaluation of Reactor Vessel Upper Head Penetrations to Support Continued Operation: Point Beach Units 1 and 2

W. H. Bamford
D. Tang

September 2004

Verifier: _____
C. Y. Yang
Piping Analysis and Fracture Mechanics

Approved: _____
S. A. Swamy, Manager
Piping Analysis and Fracture Mechanics

Westinghouse Electric Company LLC
P.O. Box 355
Pittsburgh, PA 15230-0355

© 2004 Westinghouse Electric Company LLC
All Rights Reserved

TABLE OF CONTENTS

1 INTRODUCTION 1-1

2 HISTORY OF CRACKING IN HEAD PENETRATIONS 2-1

3 OVERALL TECHNICAL APPROACH 3-1

3.1 PENETRATION STRESS ANALYSIS 3-1

3.2 FLAW TOLERANCE APPROACH 3-1

4 MATERIAL PROPERTIES, FABRICATION HISTORY AND CRACK GROWTH PREDICTION 4-1

4.1 MATERIALS AND FABRICATION 4-1

4.2 CRACK GROWTH PREDICTION 4-1

5 STRESS ANALYSIS 5-1

5.1 OBJECTIVES OF THE ANALYSIS 5-1

5.2 MODEL 5-1

5.3 STRESS ANALYSIS RESULTS – OUTERMOST CRDM PENETRATION (43.5 DEGREES) 5-1

5.4 STRESS ANALYSIS RESULTS – INTERMEDIATE CRDM PENETRATIONS 5-2

5.5 STRESS ANALYSIS RESULTS – CENTER CRDM PENETRATION 5-2

5.6 STRESS ANALYSIS RESULTS – HEAD VENT 5-2

6 FLAW EVALUATION CHARTS 6-1

6.1 INTRODUCTION 6-1

6.2 OVERALL APPROACH 6-1

6.3 RESULTS: AXIAL FLAWS 6-2

6.4 CIRCUMFERENTIAL CRACK PROPAGATION 6-3

6.5 FLAW ACCEPTANCE CRITERIA 6-5

TABLE OF CONTENTS (Cont.)

7 SUMMARY AND EXAMPLE PROBLEMS 7-1

7.1 SAFETY ASSESSMENT 7-1

7.2 EXAMPLE PROBLEMS 7-2

8 REFERENCES 8-1

APPENDIX A ALLOWABLE AREAS OF LACK OF FUSION: WELD FUSION ZONES A-1

1 INTRODUCTION

In September of 1991, a leak was discovered in the reactor vessel control rod drive (CRDM) head penetration region of an operating plant. This has led to the question of whether such a case could occur at Point Beach Units 1 and 2. The geometry of interest is shown in Figure 1-1. Throughout this report, the penetration rows have been identified by their angle of intersection with the head. For each penetration of each unit, the angle is identified in Table 1-1 for Units 1 and 2.

The issue resulted from cracking, which occurred in the outermost penetrations of a number of operating plants, as discussed in Section 2. This outermost CRDM location, as well as a number of intermediate CRDM penetrations, the head vent, and the center penetration were chosen for fracture mechanics analyses to support continued safe operation of Point Beach Units 1 and 2 if such cracking were to be found. The dimensions of the CRDM penetrations are all identical, with 4.0 inch outside surface (OD) and wall thickness of 0.625 inches. For the head vent, the OD is 1.014 inches, and the wall thickness is 0.122 inches.

The basis of the analyses was a detailed three dimensional elastic-plastic finite element analysis of several penetration locations, as described in detail in Section 5. Results were obtained at a number of locations in each penetration, and used in the fracture analysis.

The fracture analyses were carried out using reference crack growth rates recommended by the EPRI Materials Reliability Project, which are consistent with service experience. The results are presented in the form of flaw evaluation charts for both surface flaws and through wall flaws, to determine the allowable time of safe operation if indications are found. All the times calculated in this handbook are effective full power years (EFPY).

Table 1-1 Point Beach Units 1 and 2 Head Penetration Nozzles, with Intersection Angles Identified

Nozzle No.	Type	Angle (degrees)	Nozzle No.	Type	Angle (degrees)
1	CRDM	0.0	26	CRDM	37.0
2	CRDM	19.5	27	CRDM	37.0
3	CRDM	19.5	28	CRDM	37.0
4	CRDM	19.5	29	CRDM	37.0
5	CRDM	19.5	30	CRDM	37.0
6	CRDM	13.6	31	CRDM	37.0
7	CRDM	13.6	32	CRDM	37.0
8	CRDM	13.6	33	CRDM	37.0
9	CRDM	13.6	34	CRDM	43.5
10	CRDM	28.1	35	CRDM	43.5
11	CRDM	28.1	36	CRDM	43.5
12	CRDM	28.1	37	CRDM	43.5
13	CRDM	28.1	38	CRDM	9.7
14	CRDM	31.8	39	CRDM	9.7
15	CRDM	31.8	40	CRDM	9.7
16	CRDM	31.8	41	CRDM	9.7
17	CRDM	31.8	42	CRDM	22.0
18	CRDM	30.0	43	CRDM	22.0
19	CRDM	30.0	44	CRDM	22.0
20	CRDM	30.0	45	CRDM	22.0
21	CRDM	30.0	46	CRDM	22.0
22	CRDM	31.8	47	CRDM	22.0
23	CRDM	31.8	48	CRDM	22.0
24	CRDM	31.8	49	CRDM	22.0
25	CRDM	31.8			

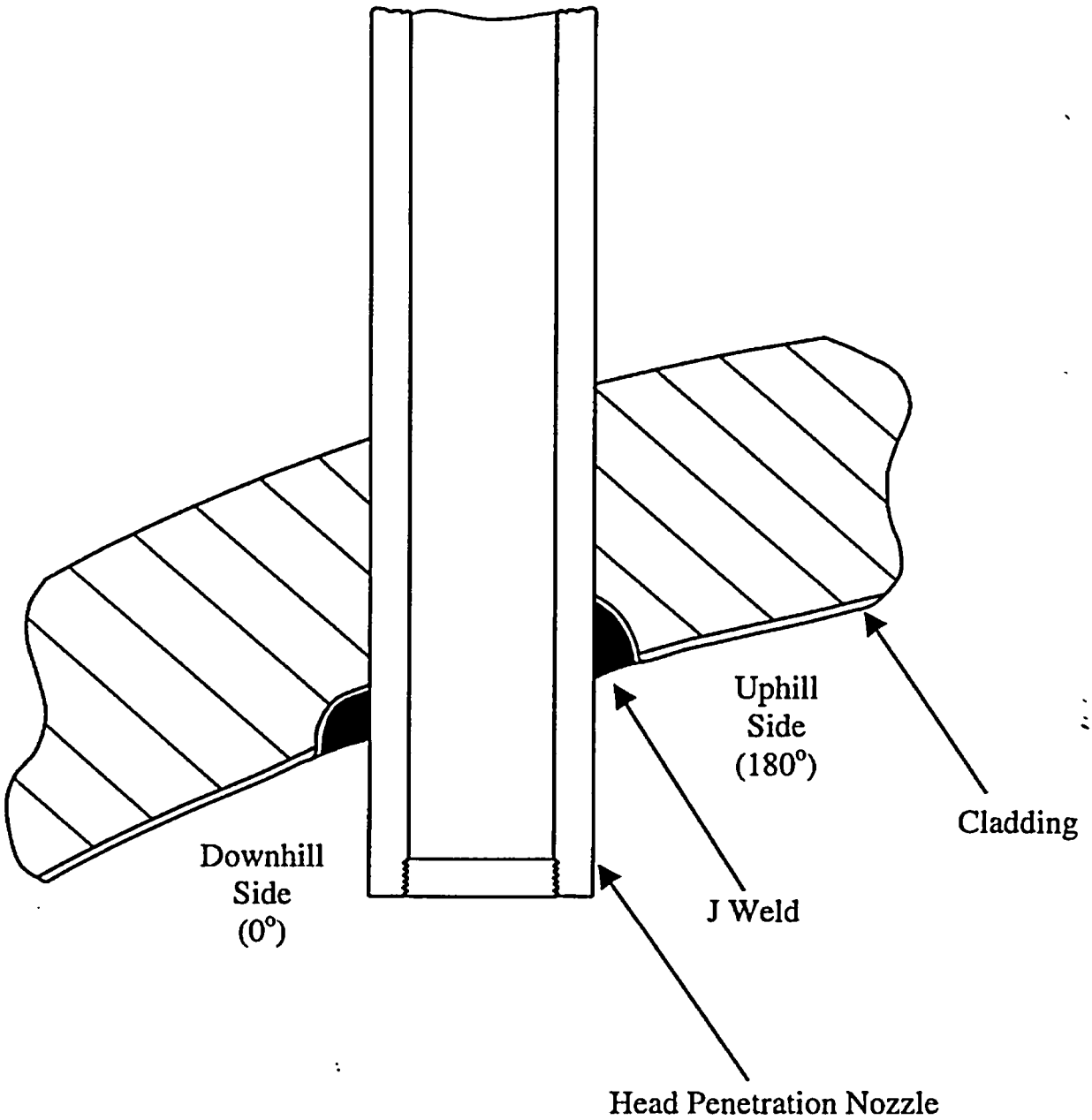

Figure 1-1 Reactor Vessel Control Rod Drive Mechanism (CRDM) Penetration

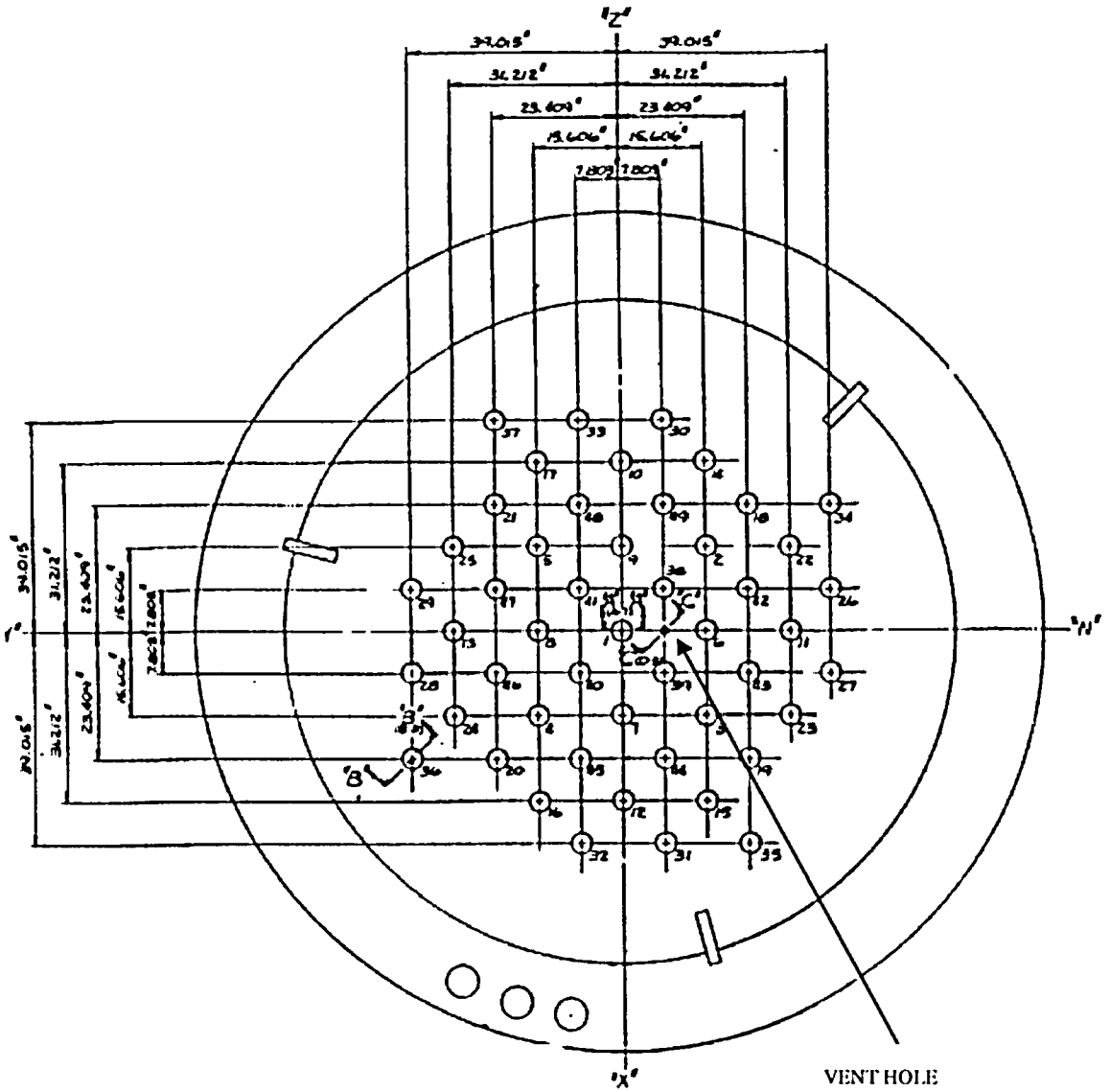

Figure 1-2 Location of Head Penetrations for Point Beach Units 1 and 2

2 HISTORY OF CRACKING IN HEAD PENETRATIONS

In September of 1991, leakage was reported from the reactor vessel CRDM head penetration region of a French plant, Bugey Unit 3. Bugey 3 is a 920 megawatt three-loop PWR which had just completed its tenth fuel cycle. The leak occurred during a post ten year hydrotest conducted at a pressure of approximately 3000 psi (204 bar) and a temperature of 194°F (90°C). The leak was detected by metal microphones located on the top and bottom heads, and the leak rate was estimated to be approximately 0.7 liter/hour (0.003 GPM). The location of the leak was subsequently established on a peripheral penetration with an active control rod (H-14), as seen in Figure 2-1.

The control rod drive mechanism and thermal sleeve were removed from this location to allow further examination. Further study of the head penetration revealed the presence of longitudinal cracks near the head penetration attachment weld. Penetrant and ultrasonic testing confirmed the cracks. The cracked penetration was fabricated from Alloy 600 bar stock (SB-166), and has an outside diameter of 4 inches (10.16 cm) and an inside diameter of 2.75 inches (7.0 cm).

As a result of this finding, all of the control rod drive mechanisms and thermal sleeves at Bugey 3 were removed for inspection of the head penetrations. Only two penetrations were found to be cracked, as shown in Figure 2-1.

An inspection of a sample of penetrations at three additional plants were planned and conducted during the winter of 1991-92. These plants were Bugey 4, Fessenheim 1, and Paluel 3. The three outermost rows of penetrations at each of these plants were examined, and further cracking was found in two of the three plants.

At Bugey 4, eight of the 64 penetrations examined were found to contain axial cracks, while only one of the 26 penetrations examined at Fessenheim 1 was cracked. The locations of all the cracked penetrations are shown in Figure 2-1. None of the 17 CRDM penetrations inspected at Paluel 3 showed indications of cracking, at the time, but further inspection of the French plants have confirmed at least one crack in each operating plant.

Thus far, the cracking in tubes not manufactured by Babcock and Wilcox Tubular Products has been consistent in both its location and extent. All cracks discovered by nondestructive examination have been oriented axially, and have been located in the bottom portion of the penetration in the vicinity of the partial penetration attachment weld to the vessel head as shown schematically in Figure 1-1.

[

]a,c,e

[

.]a,c,e

Non-destructive examinations of the leaking CRDM nozzles showed that most of the cracks originated on the outside surface of the nozzles below the J-groove weld, were axially oriented, and propagated primarily in the nozzle base material to an elevation above the top of the J-groove weld where leakage could then pass through the annulus to the top of the head where it was detected by visual inspection. In some cases the cracks initiated in the weld metal or propagated into the weld metal, and in a few cases the cracks propagated through the nozzle wall thickness to the inside surface (ID).

[

]a,c,e

The cracking has now been confirmed to be primary water stress corrosion cracking. Relatively high residual stresses are produced in the outermost CRDM penetrations due to the welding process. Other important factors which affect this process are temperature and time, with higher temperatures and longer times being more detrimental. It is interesting to note that no head vents have been found to be cracked. The inspection findings for the plants examined thus far are summarized in Table 2-1.

Table 2-1Operational Information and Inspection Results for Units Examined (Results to April 30, 2002)

Country	Plant Type	Units Inspected	K Hours	Head Temp. (°F)	Total Penetrations	Penetrations Inspected	Penetrations With Indications
France	CPO	6	80-107	596-599	390	390	23
	CPY	28	42-97	552	1820	1820	126
	1300MW	20	32-51	558-597	1542	1542	95
Sweden	3 Loop	3	75-115	580-606	195	190	8
Switzerland	2 Loop	2	148-154	575	72	72	2
Japan	2 Loop	7	105-108	590-599	276	243	0
	3 Loop	7	99	610	455	398	0
	4 Loop	3	46	590	229	193	0
Belgium	2 Loop	2	115	588	98	98	0
	3 Loop	5	60-120	554-603	337	337	6
Spain	3 Loop	5	65-70	610	325	102	0
Brazil	2 Loop	1	25	NA	40	40	0
South Africa	3 Loop	1	NA	NA	65	65	6
Slovenia	2 Loop	1	NA	NA	49	49	0
South Korea	2 Loop	3	NA	NA	49	49	3
	3 Loop	2	NA	NA	130	130	2
US	2 Loop	2	170	590	98	98	0
	3 Loop	1	NA	NA	65	20	12
	4 Loop	18	NA	NA	1149	537	35
TOTALS		117	–	–	7384	6373	318

NA = Not Available

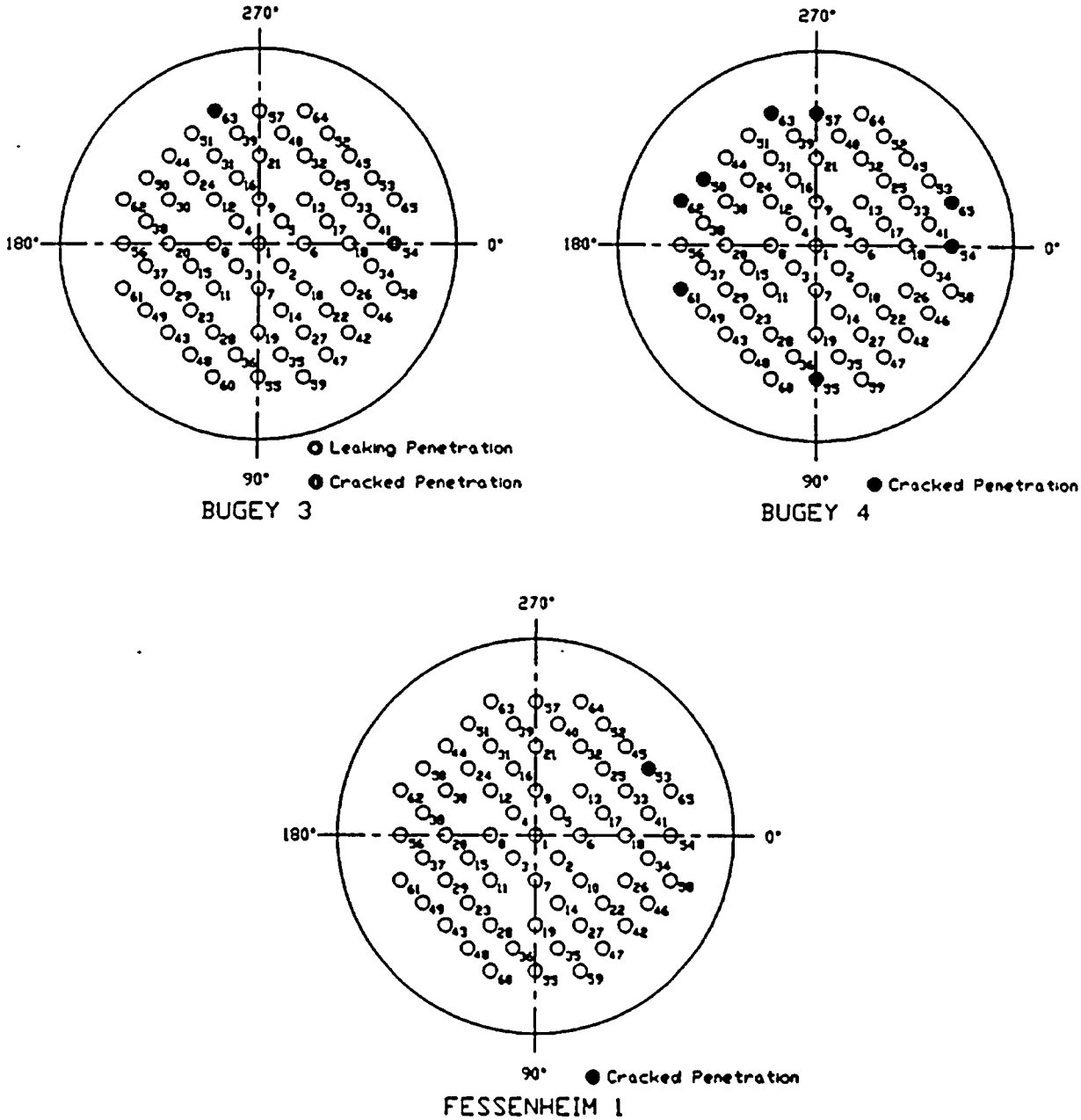

Figure 2-1 French R/V Closure Head CRDM Penetration Cracking EdF Plants – Penetrations with Cracking

3 OVERALL TECHNICAL APPROACH

The primary goal of this work is to provide technical justification for the continued safe operation of Point Beach Units 1 and 2 in the event that cracking is discovered during inservice inspections of the Alloy 600 reactor vessel upper head penetrations.

3.1 PENETRATION STRESS ANALYSIS

Three dimensional elastic-plastic finite element stress analyses have been performed to determine the stresses in the head penetration region (6A, 6B). These analyses have considered the pressure loads associated with steady state operation, as well as the residual stresses which are produced by the fabrication process.

[

]a,c,e

3.2 FLAW TOLERANCE APPROACH

A flaw tolerance approach has been developed to allow continued safe operation until an appropriate time for repair, or the end of plant life. The approach is based on the prediction of future growth of detected flaws, to ensure that such flaws would remain stable.

If an indication is discovered during inservice inspection, its size can be compared with the flaw size which is considered allowable for continued service. This "allowable" flaw size is determined from the actual loadings (including mechanical, residual, and transient loads) on the head penetration for the plant of interest. Suitable margins to ensure the integrity of the reactor vessel as well as safety from unacceptable leakage rates, should also be considered. Acceptance criteria are discussed in Section 6.5.

The time for the observed crack to reach the allowable crack size determines the length of time the plant can remain online before repair, if required. For the crack growth calculation, a best estimate is needed and no additional margins are necessary.

The results of the evaluation are presented in terms of simple charts, which show graphically the time required to reach the allowable length or depth, which represents the additional service life before repair. This result is a function of the loadings on the particular head penetration, as well as the circumferential location of the crack in the penetration tube.

Schematic drawings of the head penetration flaw tolerance charts are presented as Figures 3-1 and 3-2. These two types of charts can be used to provide estimates of the time which remains before a leak would develop from an observed crack. For example, if a part-through flaw was discovered, the user would first refer to Figure 3-1, to determine the time (t_P) which would be remaining before the crack would penetrate the wall or reach the allowable depth (t_A) (eg a/t=.75). Once the crack penetrates the wall, the time (t_B) required to reach an allowable crack length would be determined from Figure 3-2. The total time remaining would then be the simple sum:

$$\text{Time remaining} = t_P + t_B$$

Another way to determine the allowable time of operation with a part-through flaw would be to use Figure 3-2 directly, in effect assuming the part-through flaw is a through-wall flaw. This approach would be more conservative than that above, and the time remaining would then be:

$$\text{Time remaining} = t_B$$

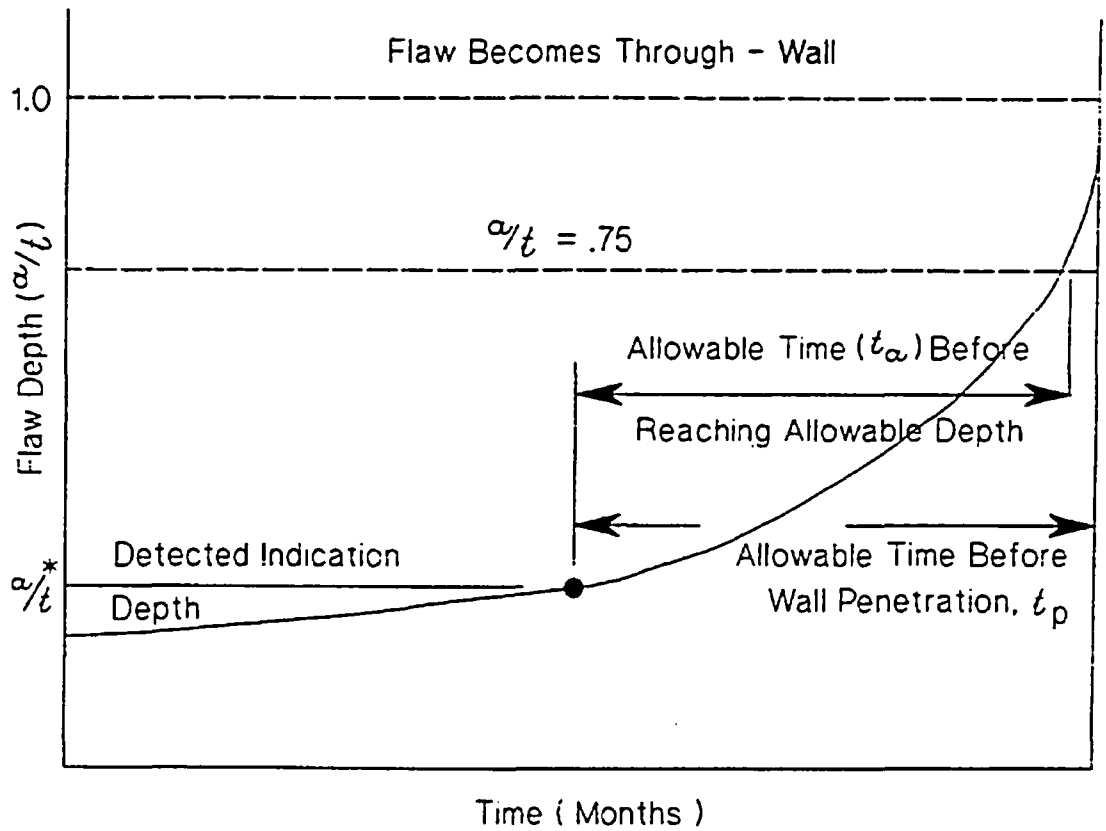

Figure 3-1 Schematic of a Head Penetration Flaw Growth Chart for Part Through Flaws

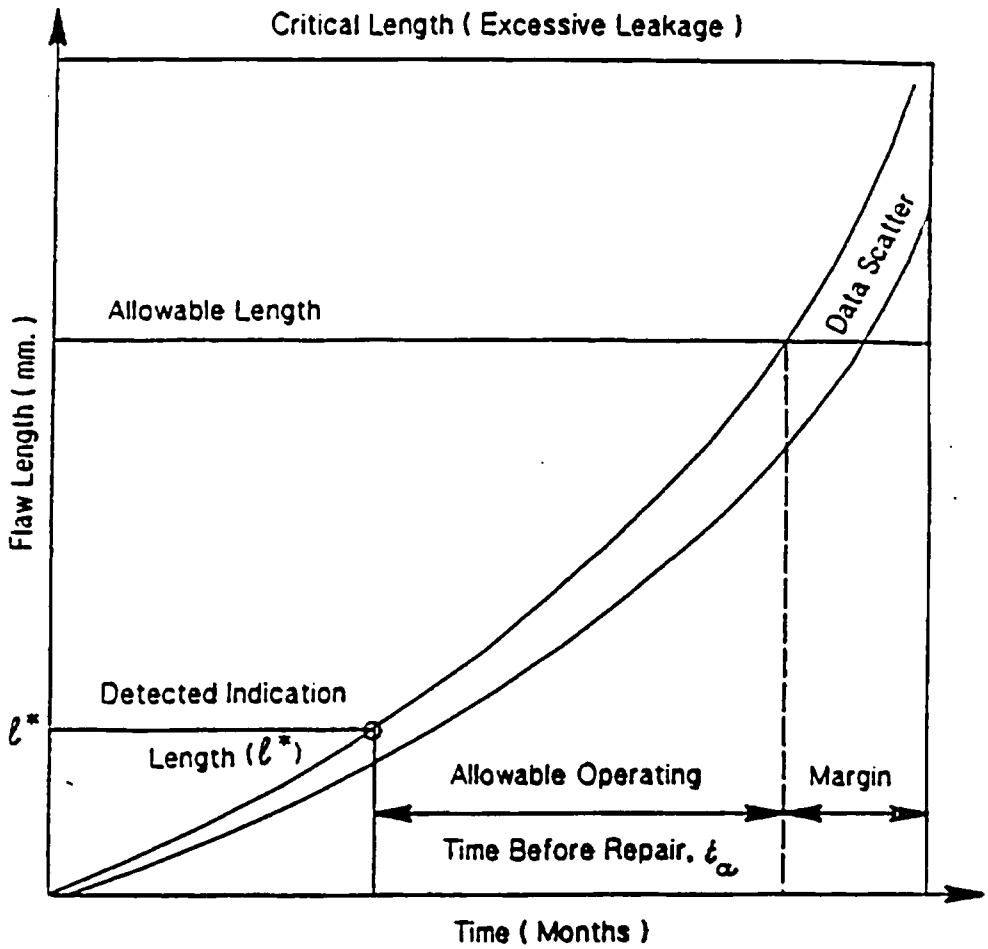

Figure 3-2 Schematic of a Head Penetration Flaw Tolerance Chart for Through-Wall Flaws

4 MATERIAL PROPERTIES, FABRICATION HISTORY AND CRACK GROWTH PREDICTION

4.1 MATERIALS AND FABRICATION

The reactor vessel for Point Beach Unit 1 was manufactured by Babcock and Wilcox, while Unit 2 was manufactured by Combustion Engineering. The head adopters were made by Huntington Alloys, with one heat of Unit 2 made by Babcock and Wilcox tubular products. The carbon content, mechanical properties and heat treatment of the Alloy 600 material used to fabricate the Point Beach vessels are provided in Table 4-1 and Table 4-2 respectively. The certified material test reports (CMTRs) were used to obtain the chemistry and mechanical properties for the vessel head penetrations. The CMTRs for the material supplied by Huntington do not indicate the heat treatment of the material. However, Huntington was contacted and they indicated that, although the records for these heats of material were not available, their best estimate for standard practice applied to the heavy wall extruded tubes was 940.6 °C (1725 °F) in a continuous annealing furnace with approximately 1-1/2 hours in the hot zone. Figures 4-1 and 4-2 illustrates the yield strengths and carbon content, based on percent of heats, of the head adapter penetrations in the Point Beach Units 1 and 2 vessel relative to a sample of the French head penetrations which have experienced cracking. The general trend for the head adapter penetrations in Point Beach Units 1 and 2 are a higher carbon content, higher mill annealing temperature and lower yield strength relative to those on the French vessels. These factors should all have a beneficial effect on the material resistance to PWSCC in the head penetrations.

4.2 CRACK GROWTH PREDICTION

The cracks in the penetration region have been determined to result from primary water stress corrosion cracking in the Alloy 600 base metal, and in some cases the Alloy 182 weld metal. There are a number of available measurements of static load crack growth rates in primary water environment, and in this section the available results will be compared and a representative growth rate established.

Direct measurements of SCC growth rates in Alloy 600 are relatively rare, and care should be used in interpreting the results because the materials may be excessively cold worked, or the loadings applied may be near or exceeding the limit load of the tube, meaning there will be an interaction between tearing and crack growth. In these cases the crack growth rates may not be representative of service conditions.

The effort to develop a reliable crack growth rate model for Alloy 600 began in the spring of 1992, when the Westinghouse Owners Group was developing a safety case to support continued operation of plants. At the time there was no available crack growth rate data for head penetration materials, and only a few publications existed on growth rates of Alloy 600 in any product form.

The best available publication was found to be that of Peter Scott of Framatome, who had developed a growth rate model for PWR steam generator materials (1). His model was based on a study of results obtained by McIlree, Rebak, and Smialowska (2) who had tested short steam generator tubes which had been flattened into thin compact specimens. Upon study of his paper there were several ambiguities, and several phone conversations were held to clarify his conclusions. These discussions led to Scott's

admission that reference 1 contains an error, in that no correction for cold work was applied to the McIllree/Smialowska data. The correct development is below.

An equation was fitted to the data of reference (2) for the results obtained in water chemistries that fell within the standard specification for PWR primary water. Results for chemistries outside the specification were not used. The following equation was fitted to the data at 330°C (626°F):

$$\frac{da}{dt} = 2.8 x 10^{-11} (K-9)^{1.16} m/\sec \tag{4-1}$$

where K is stress intensity factor in MPa $\sqrt{m}$.

The next step described by Scott in his paper was to correct these results for the effects of cold work. Based on work by Cassagne and Gelpi (3), he concluded that dividing the above equation by a factor of 10 would be appropriate to account for the effects of cold work. This step was inadvertently omitted from Scott's paper, even though it is discussed. The crack growth law for 330°C (626°F) then becomes:

$$\frac{da}{dt} = 2.8 x 10^{-12} (K-9)^{1.16} m/\sec \tag{4-2}$$

Scott further corrected this law for the effects of temperature. This forms the basis for the PWR Materials Reliability Program (MRP) recommended crack growth rate (CGR) curve for the evaluation of SCC where a power-law dependence on stress intensity factor was assumed. The MRP recommended CGR curve was used in this report for determining the primary water stress corrosion crack growth rate and a brief discussion on this recommended curve is as follows:

[

]a,c,e

There is a general agreement that crack growth in Alloy 600 materials in the primary water environment can be modeled using a stress intensity factor relationship with differences in temperature accounted for by an activation energy (Arrhenius) model for thermally controlled processes. Figure 4-3 shows the recommended CGR curve along with the laboratory data from Huntington materials used to develop the curve.

[

]a,c,e

[

]a,c,e

[

]a,c,e

The applicability of the MRP recommended model to the head penetrations at the Point Beach Units 1 and 2 were recently confirmed by two independent approaches. The first was a collection of all available data from Huntington Alloys materials tested over the past ten years (4H). The results are shown in Figure 4-3, along with the Scott model for the test temperature.

The MRP crack growth curve was structured to bound 75 percent of the 26 heats for which test results were available. Fits were done on the results for each heat, and the constant term was determined for each heat. The 75th percentile was then determined from these results. This was done to eliminate the concern that the curve might be biased from a large number of results from a single heat. The MRP expert panel on crack growth endorsed the resulting curve unanimously in a meeting on March 6th and 7th 2002. This approach is consistent with the Section XI flaw evaluation philosophy, which is to make a best estimate prediction of future growth of a flaw. Margins are incorporated in the allowable flaw sizes. The entire data set is shown in Figure 4-3, where the data have been adjusted to a single temperature of 325°C.

A second independent set of data were used to validate the model, and these data were obtained from the two inspections carried out on penetration 75 of D.C. Cook Unit 2, which was first found to be cracked in 1994 (4C). The plant operated for one fuel cycle before the penetration was repaired in 1996 and the flaw

was measured again before being repaired. These results were used to estimate the PWSCC growth rate, for both the length of the flaw and its depth. These two points are also shown in Figure 4-4, and are consistent with the laboratory data for Huntington and Standard Steel materials. In fact, Figure 4-4 demonstrates that the MRP model is nearly an upper bound for these materials. The D.C. Cook Unit 2 penetrations were made from Huntington materials.

Since Point Beach Units operates at a temperature lower than 325°C (617°F) in the head region, and the crack growth rate is strongly affected by temperature, a temperature adjustment is necessary. This temperature correction was obtained from study of both laboratory and field data for stress corrosion crack growth rates for Alloy 600 in primary water environments. The available data showing the effect of temperature are summarized in Figure 4-5. Most of the results shown here are from steam generator tube materials, with several sets of data from operating plants, and results from two heats of materials tested in a laboratory (4A).

Study of the data shown in Figure 4-4 results in an activation energy of 31-33 Kcal/mole, which can then be used to adjust for the lower operating temperature. This value is slightly lower than the generally accepted activation energy of 44-50 Kcal/mole used to characterize the effect of temperature on crack initiation, but the trend of the actual data for many different sources is unmistakable.

[

].[a,c,e] Therefore the following growth rate model was used for the Point Beach Units 1 and 2 head penetrations:

$$\frac{da}{dt} = 1.67x10^{-12}(K-9)^{1.16}\, m/\sec$$

where K = applied stress intensity factor, in $MPa\sqrt{m}$. This equation implies a threshold for cracking susceptibility, $K_{ISCC} = 9\ MPa\sqrt{m}$. The crack growth is applicable to propagation in both axial and circumferential directions.

a,c,e

Table 4-1 Point Beach Unit 1 Head Penetration Material Information

a,c,e

Table 4-2 Point Beach Unit 2 Head Penetration Material Information

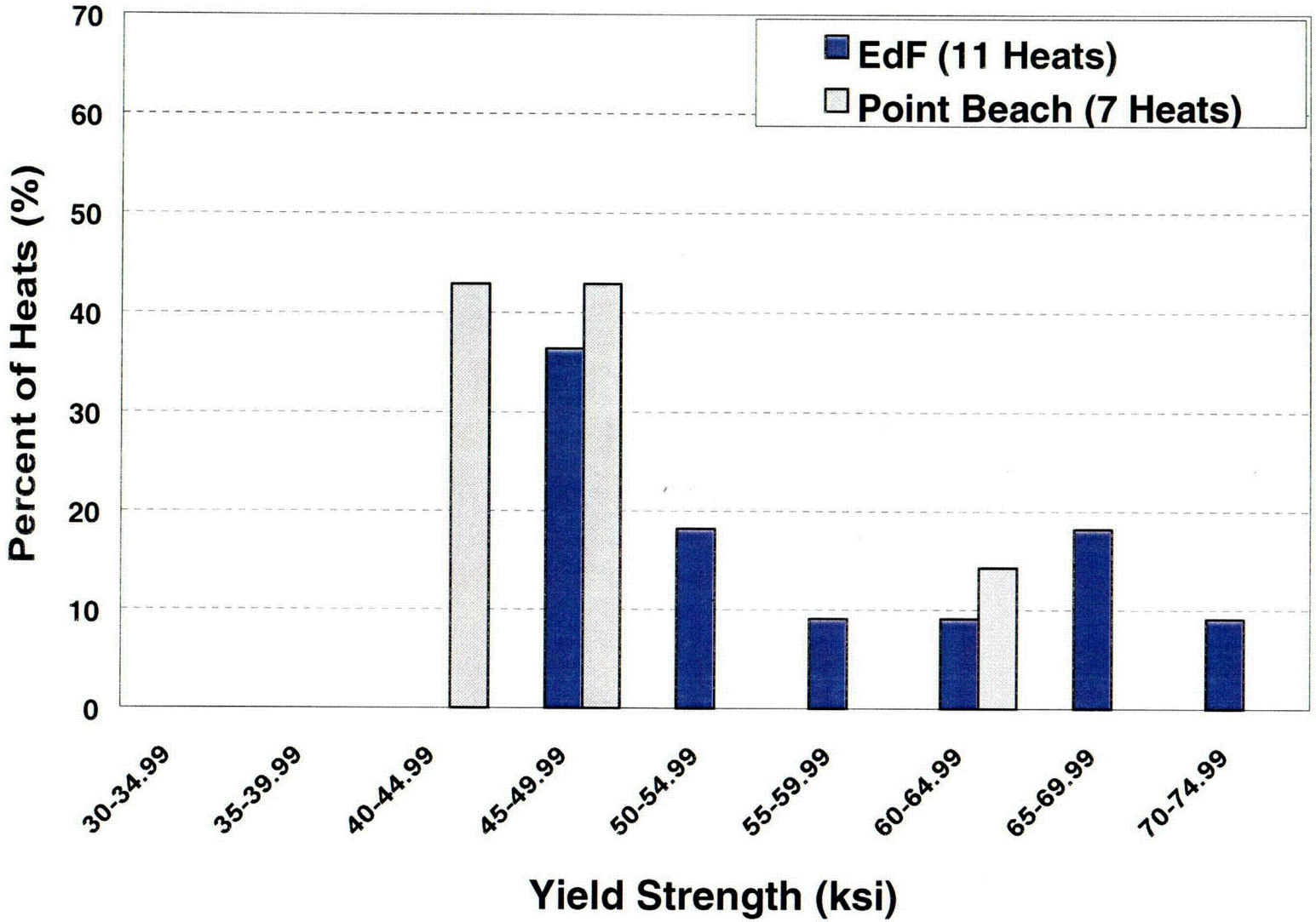

Figure 4-1 Yield Strength of the Various Heats of Alloy 600 Used in Fabricating the Point Beach and French Head Penetrations

C01

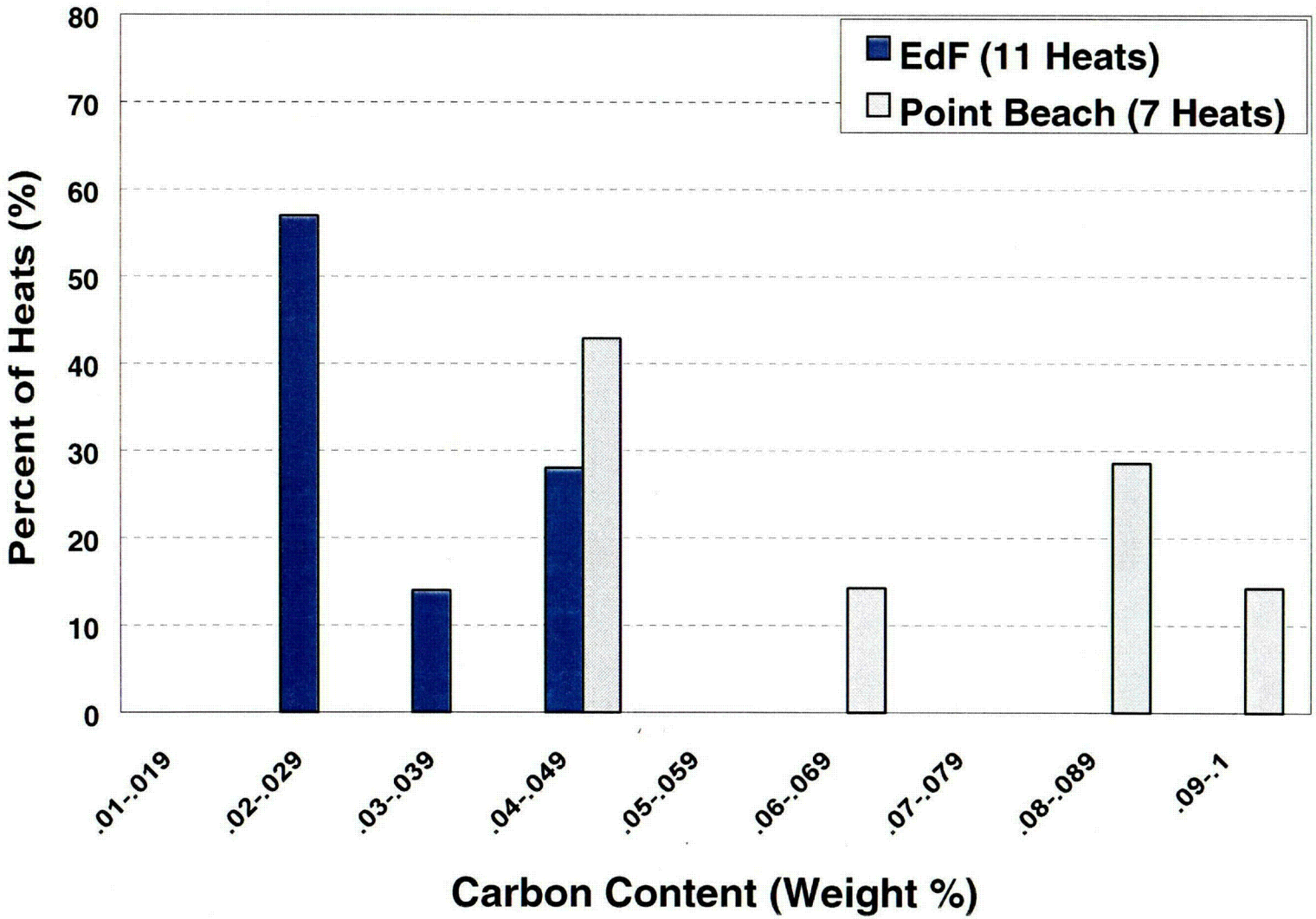

Figure 4-2 Carbon Content of the Various Heats of Alloy 600 Used in Fabricating the Point Beach and French Head Penetration

C02

a,c,e

Figure 4-3 Screened Laboratory Data for Alloy 600, with the MRP Recommended 75/50 Curve. Note that the Modified Scott Model is also Shown (4H)

a.c.e

Figure 4-4 Model for PWSCC Growth Rates in Alloy 600 in Primary Water Environments (325°C), With Supporting Data from Standard Steel, Huntingdon, and Sanvik Materials (4H)

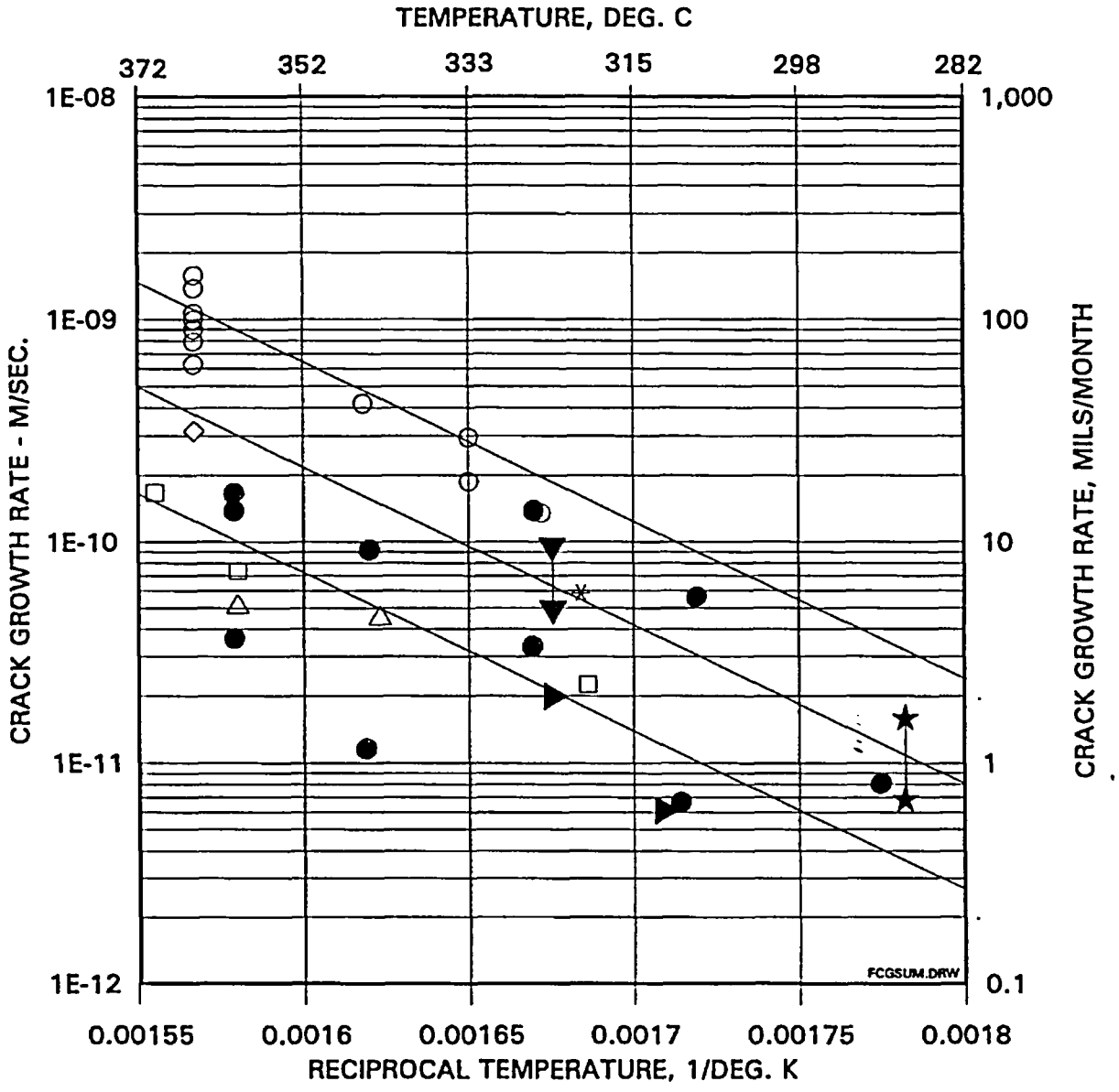

Note: All symbols are for steam generator materials, except the solid circles, which are head penetration laboratory data.

Figure 4-5 Summary of Temperature Effects on PWSCC Growth Rates for Alloy 600 in Primary Water (4A)

5 STRESS ANALYSIS

5.1 OBJECTIVES OF THE ANALYSIS

The objective of this analysis was to obtain accurate stresses in each CRDM or head vent and its immediate vicinity. To do so requires a three dimensional analysis which considers all the pertinent loadings on the penetration (6A, 6B). An investigation of deformations at the lower end of the housing was also performed using the same model. Four CRDM locations were considered: the outermost row (43.5 degrees), rows at 30 degrees, 13.6 degrees and the center location. In addition, the head vent was analyzed.

The analyses were used to provide information for the flaw tolerance evaluation which follows in Section 6. Also, the results of the stress analysis were compared to the findings from service experience, to help assess the causes of the cracking which has been observed.

5.2 MODEL

A three dimensional finite element model comprised of isoparametric brick and wedge elements with a midside node on each element brim, was used to obtain the stresses and deflections. A view of the outermost CRDM model is shown in Figure 5-1. Taking advantage of symmetry through the vessel and penetration centerlines only half of the penetration geometry plus the surrounding vessel material were modeled for each CRDM nozzle. The difference between the hillside penetrations and the center penetration was that there was no differential height across the weld for the center penetration. The differential height increases as the nozzle angle increases.

In the models, the lower portion of the Control Rod Drive Mechanism (CRDM) penetration tube, or head vent, the adjacent section of the vessel closure head, and the joining weld were modeled. The vessel to penetration tube weld was simulated with two layers of elements. The penetration tube, weld metal and cladding were modeled as Alloy 600 and the vessel head shell as carbon steel. The models were consistent with, but slightly more refined, than previous models used to evaluate Combustion Engineering designed head penetration nozzles. The benchmarking of models is described in reference 6A.

The only loads used in the analysis are the steady state operating loads. External loads such as seismic loads have been studied, and have no impact, because the penetration tubes are captured by the full thickness of the reactor vessel head, over seven inches of steel into which the penetrations are shrink fit during construction. The area of interest is in the penetration near the attachment weld, which is totally unaffected by these external loads.

5.3 STRESS ANALYSIS RESULTS – OUTERMOST CRDM PENETRATION (43.5 DEGREES)

Figure 5-2 presents the hoop and axial stresses for the steady state condition for the outermost penetration.

[

]a,c,e

[

]a,c,e

[

]a,c,e

5.4 STRESS ANALYSIS RESULTS – INTERMEDIATE CRDM PENETRATIONS

[

]a,c,e

5.5 STRESS ANALYSIS RESULTS – CENTER CRDM PENETRATION

[

]a,c,e

5.6 STRESS ANALYSIS RESULTS – HEAD VENT

[

]a,c,e

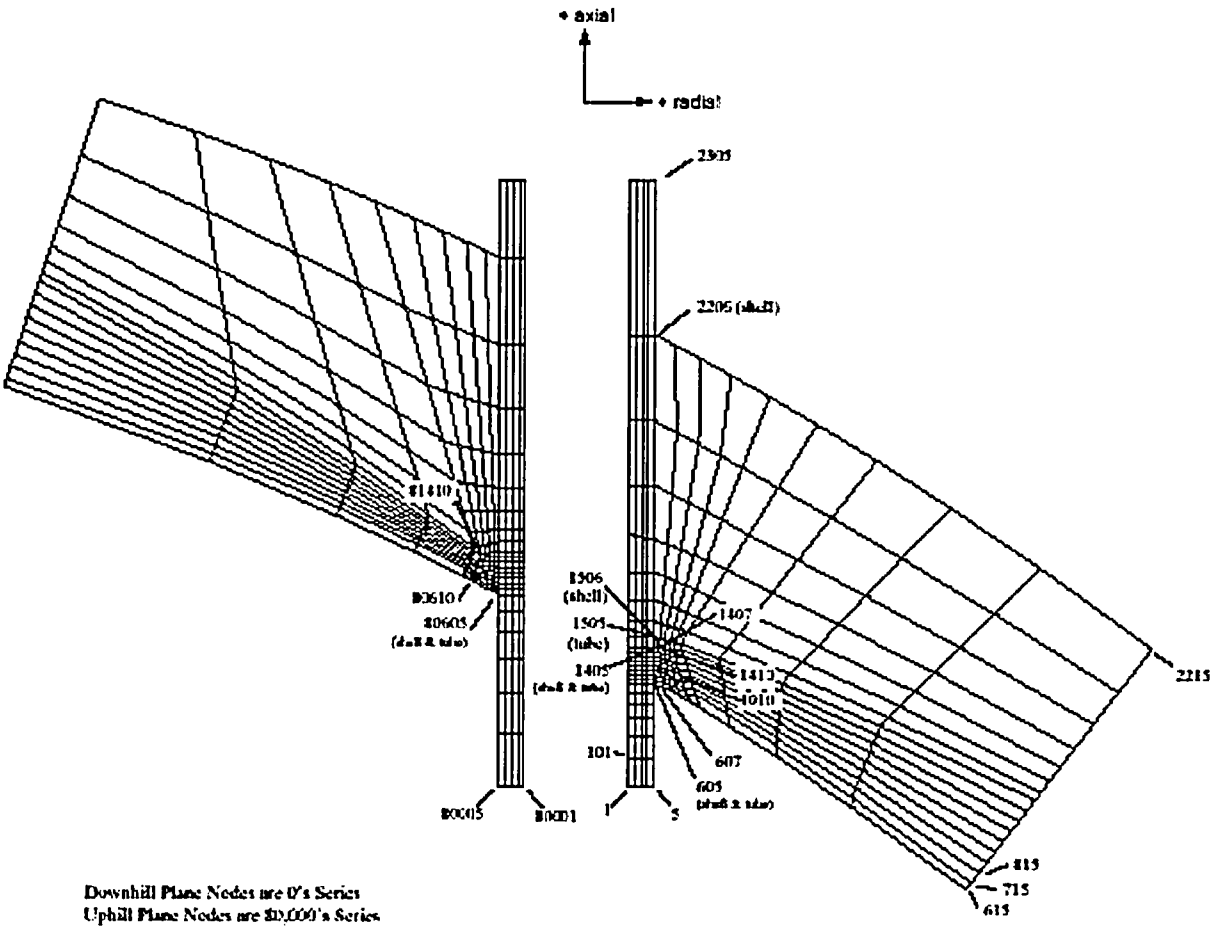

Figure 5-1 A Cut-view of the Three-Dimensional Model of the Outermost CRDM Penetration (43.5 Degrees) (6A)

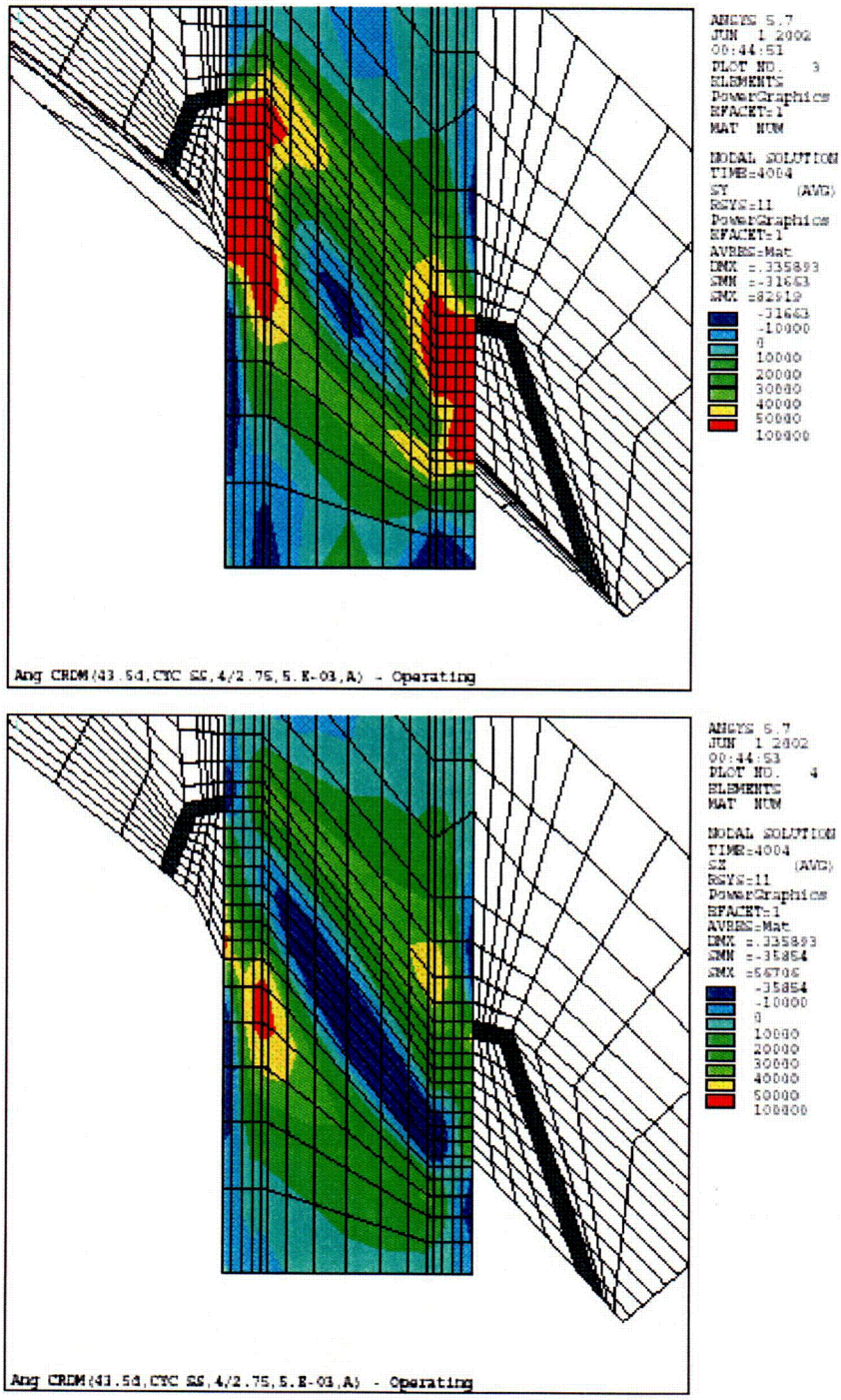

Figure 5-2 **Stress Distributions at Steady State Conditions: Outermost CRDM Penetration (43.5 Degrees) (Top: Hoop Stress; Bottom: Axial Stress) (6A)**

C02A

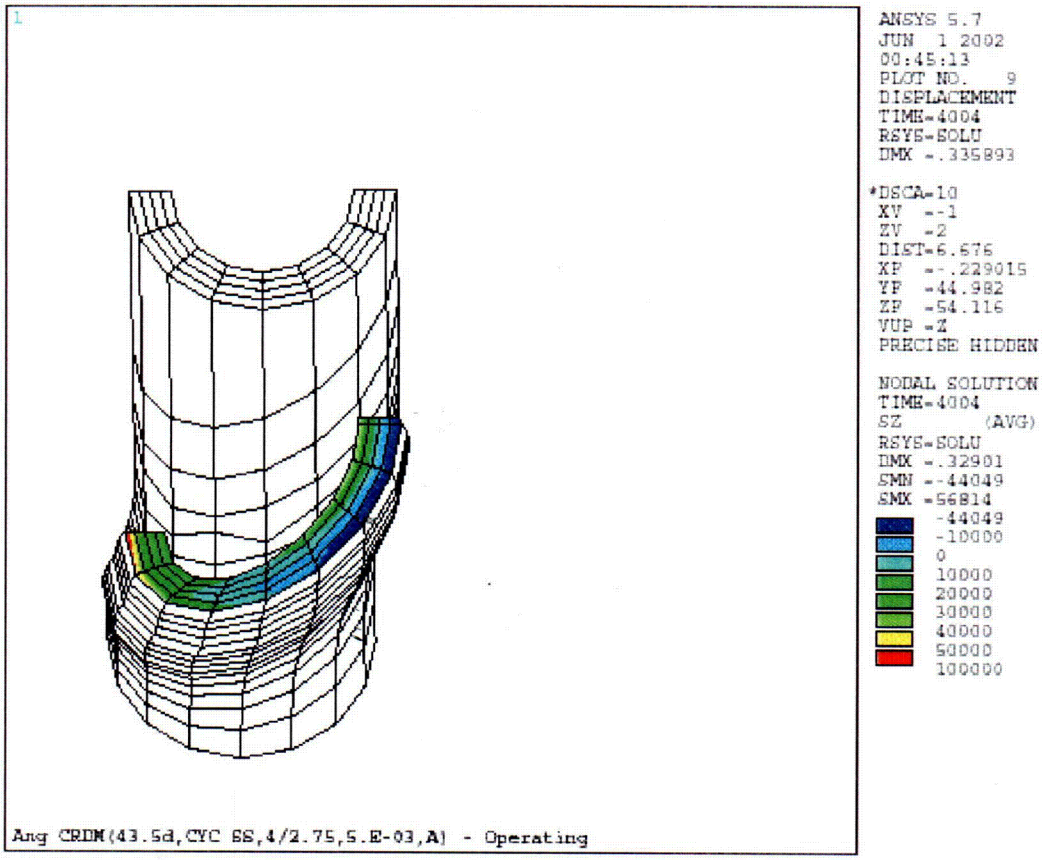

Figure 5-3 **Axial Stress Distribution at Steady State for the Outermost CRDM (43.5 Degrees) Penetration, Along a Plane Oriented Parallel to, and Just Above, the Attachment Weld (6A)**

C03

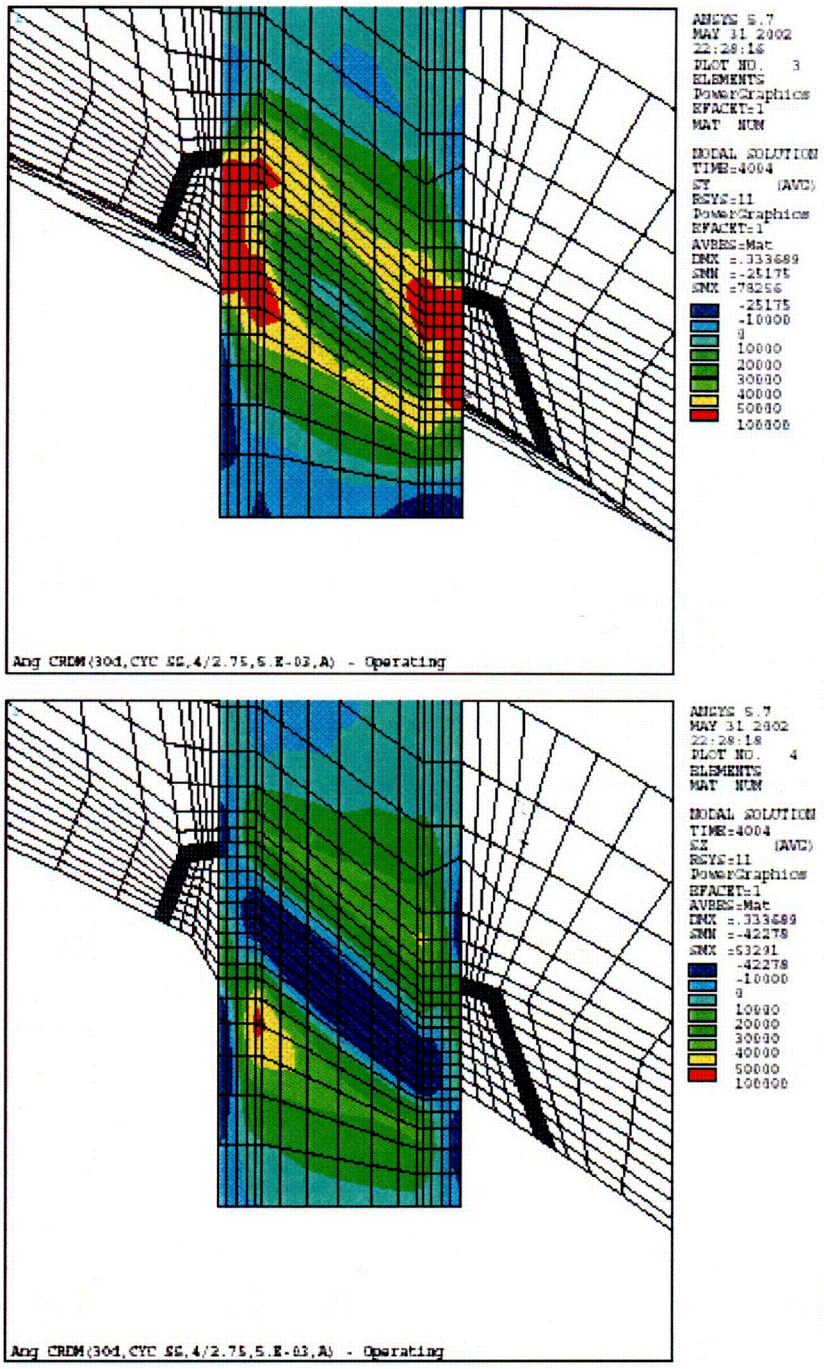

Figure 5-4 Stress Distribution at Steady State Condition for the 30.0 Degree CRDM Penetration (Top: Hoop Stress; Bottom: Axial Stress) (6A)

C04

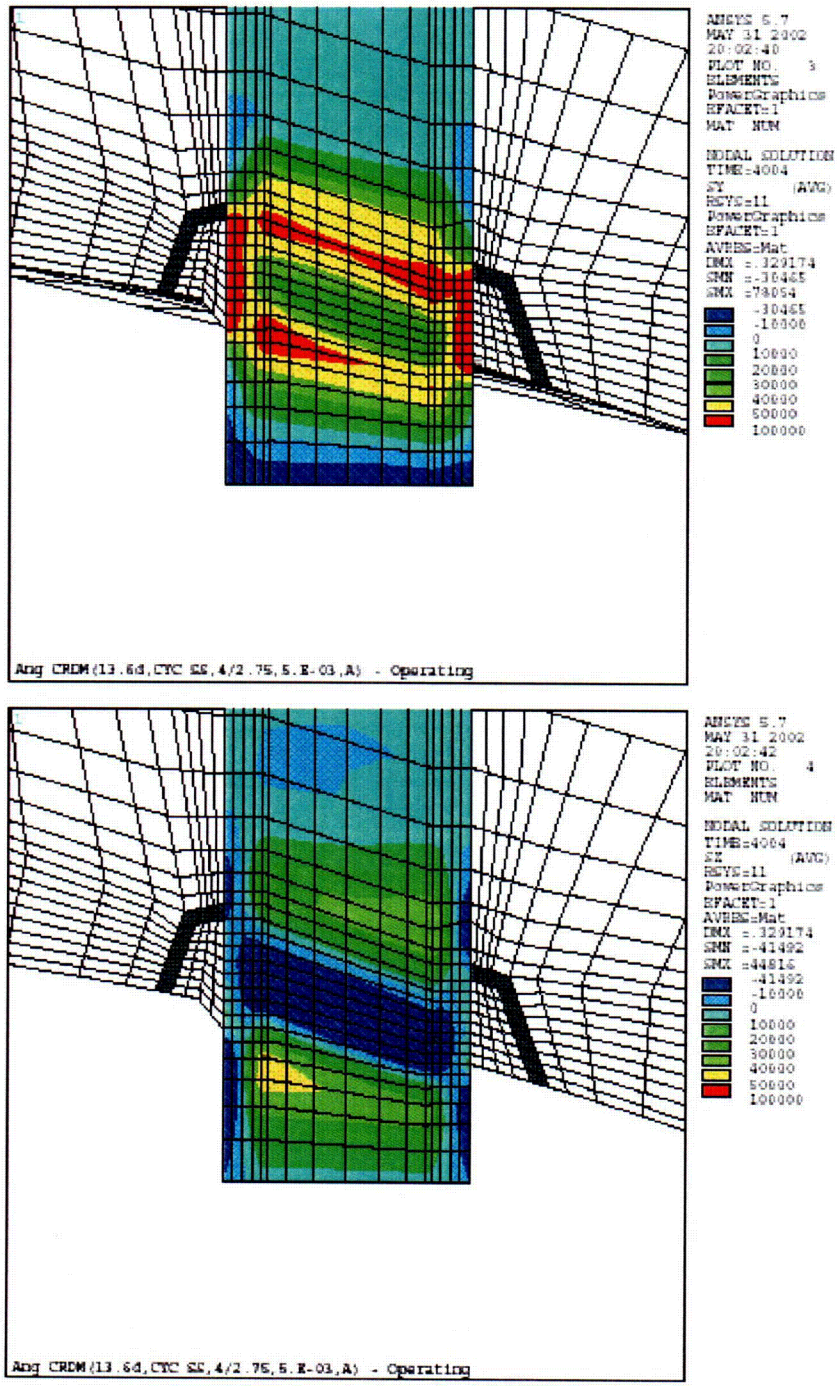

Figure 5-5 Stress Distribution at Steady State Conditions for the 13.6 Degree CRDM Penetration (Top: Hoop Stress; Bottom: Axial Stress) (6A)

C05

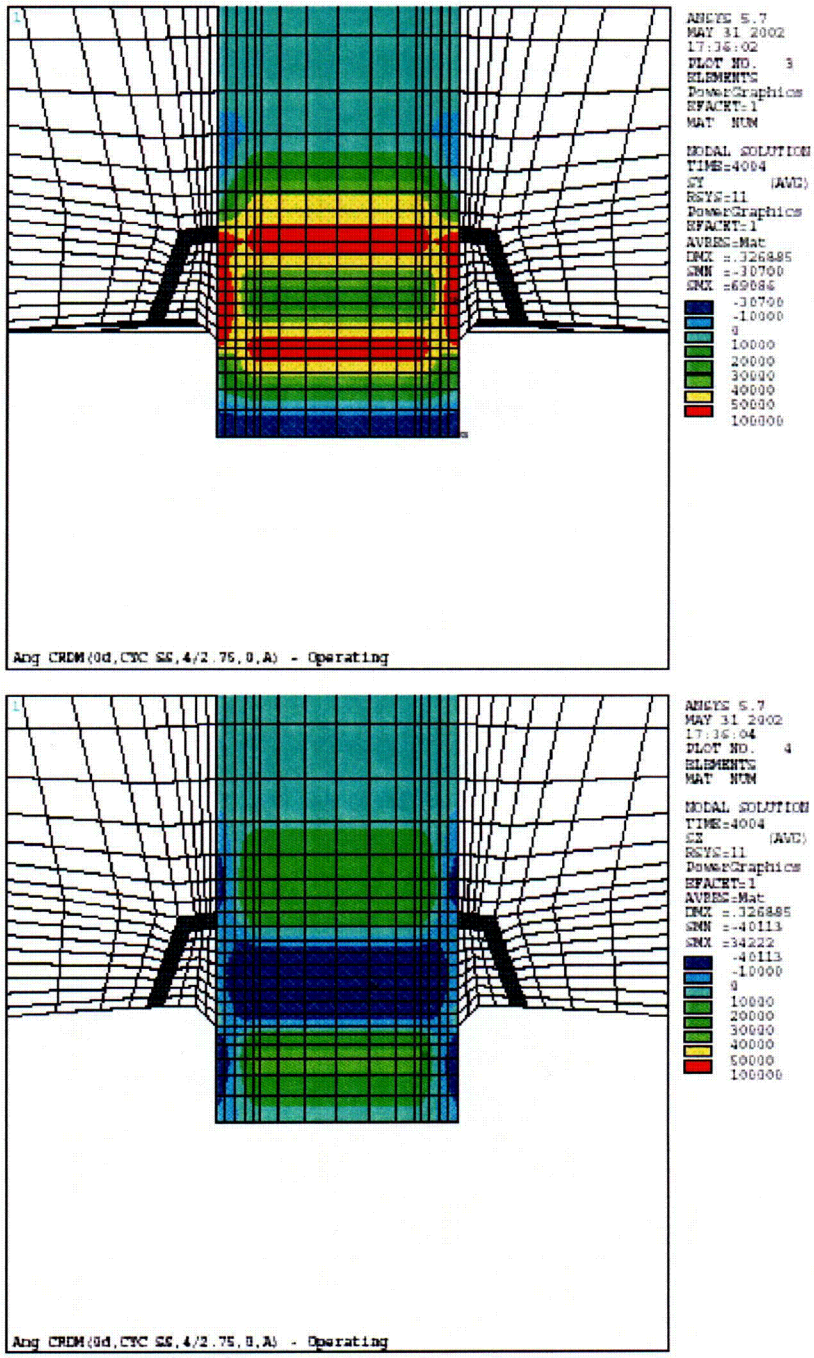

Figure 5-6 Stress Distribution at Steady State Condition for the Center Penetration (Top: Hoop Stress; Bottom: Axial Stress) (6A)

C06

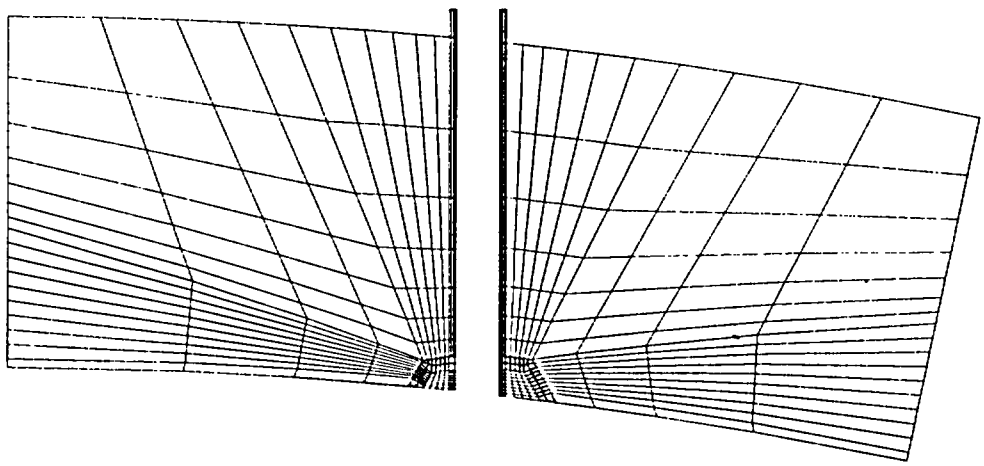

Figure 5-7 A Cut-view of the 3-D Finite Element Model of the Head Vent Penetration (6B)

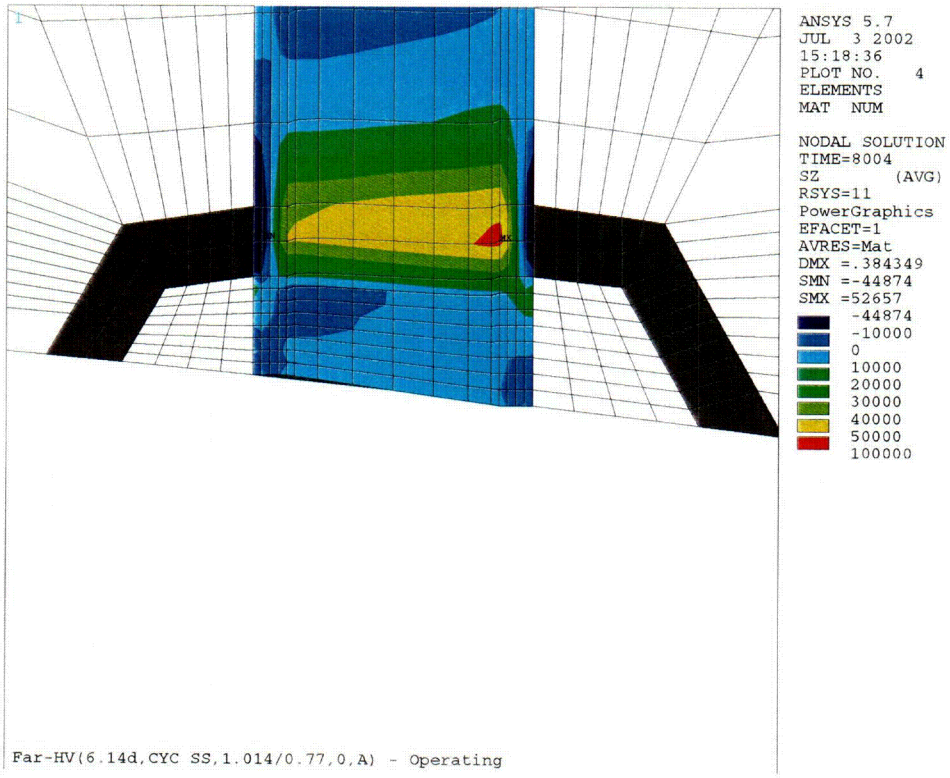

Figure 5-8 Stress Distribution in the Head Vent Under Steady State Condition, including Residual Stresses (Top: Hoop Stress; Bottom: Axial Stress) (6B)

C07

6 FLAW EVALUATION CHARTS

6.1 INTRODUCTION

The flaw evaluation charts were developed from the stress analysis of each of the penetration locations, as discussed in Section 5. The crack growth law developed for Point Beach Units 1 and 2 in Section 4.2 was used for each case, and several flaw tolerance charts were developed for each penetration location. The first series of charts characterizes the growth of a part through flaw, and the second series of charts characterizes the growth of a through-wall flaw in the length direction. The allowable safe operating life of the penetration may then be directly determined, using the combined results of the two charts. All times resulting from these calculations are effective full power years, since crack growth will only occur at operating temperatures.

6.2 OVERALL APPROACH

The results of the three-dimensional stress analysis of the penetration locations were used directly in the flaw tolerance evaluation.

The crack growth evaluation for the part-through flaws was based on the stress distribution through the penetration wall at the location which corresponds to the highest stress along the inner surface of the penetration. The highest stressed location was found to be in the immediate vicinity of the weld for both the center and outermost penetrations.

The stress profile was represented by a cubic polynomial:

$$\sigma(x) = A_0 + A_1 x + A_2 x^2 + A_3 x^3 \tag{6-1}$$

where x = the coordinate distance into the wall
σ = stress perpendicular to the plane of the crack
A_i = coefficients of the cubic fit

For the surface flaw with length six times its depth, the stress intensity factor expression of Raju and Newman (5A) was used. The stress intensity factor $K_I(\phi)$ can be calculated anywhere along the crack front, where ϕ is the elliptical angle of a point on the crack front. The point of maximum crack depth is represented by $\phi = 0$, and this location was found to also be the point of maximum K_I for the cases considered here. The following expression is used for calculating $K_I(\phi)$.

$$K_I(\phi) = \left[\frac{\pi a}{Q}\right]^{0.5} \sum_{j=1}^{3} G_j\left(a/c,\ a/t,\ t/R,\ \phi\right) A_j\, a^j \tag{6-2}$$

The boundary correction factors $G_1(\phi)$, $G_2(\phi)$, $G_3(\phi)$ and $G_4(\phi)$ are obtained by the procedure outlined in reference (5A). The dimension "a" is the crack depth, and "c" is the crack semi-length, while t is the wall thickness, R is the mean radius of the tube, and Q is the shape factor.

[

]a,c,e

6.3 RESULTS: AXIAL FLAWS

CRDM Surface Flaws

The results of the calculated crack growth through the wall thickness of the CRDMs for surface flaws are shown in Figures 6-2 through 6-7 for inside surface flaws. For outside surface flaws the results are shown in Figures 6-8 and 6-9. These crack growth curves begin at a flaw depth that results in a stress intensity factor that exceeds the threshold value of 9 $MPa\sqrt{m}$. This sometimes results in curves with different initial flaw sizes, as seen for example in Figure 6-8. Note that results are only provided for the uphill and downhill sides of each penetration nozzle; the stresses for the regions 90 degrees from these locations are compressive. If flaws are found in such a location, use the results for either the uphill or downhill location, whichever is closer.

Each of these figures allows the future allowable service time to be estimated graphically, as discussed in Section 3. Results are shown for each of the penetrations analyzed in each of these figures. The stresses are much higher near the attachment weld than below or above it, so separate figures have been provided for these three regions. Also, the stresses are different on the downhill side of the penetration as opposed to the uphill side, so these two cross sections have also been treated separately.

Examples have been provided in Section 7 for a range of possible flaw types, so the graphical approach can be completely understood.

CRDM Through-Wall Flaws

Crack growth from surface flaws in the CRDMs is the primary concern in evaluation of the structural integrity of head penetrations, but in some cases the surface flaw may be sufficiently below the attachment weld that additional time may be required to grow the flaw up to the attachment weld. To provide a means to evaluate this time, a series of flaw evaluation charts for through-wall flaws were prepared.

Charts were prepared for each of the penetrations evaluated, for both the uphill and downhill locations, as shown in Figures 6-10 through 6-17. In each figure, the through-wall crack length is measured from the bottom of the nozzle itself. Note that in all the cases, the crack slows down significantly as it grows above the weld, due to the decreasing stress field. This provides further reassurance that axial flaws will not extend to a critical length, regardless of time, as the critical length exceeds 15 inches.

Head Vent

The only flaw evaluation chart necessary for the head vent region is for flaws at and above the weld, since there is no portion of the head vent which extends below the weld. Figure 6-19 provides the projected growth of a part through flaw in the head vent just above the attachment weld. The growth through the wall is relatively rapid, because the thickness of the head vent is small.

6.4 CIRCUMFERENTIAL CRACK PROPAGATION

Since circumferentially oriented flaws have been found at five plants (Bugey 3, Oconee 2, Crystal River 3, Davis Besse, and Oconee 3), it is important to consider the possibility of crack extension in the circumferential direction. The first case was discovered as part of the destructive examination of the tube with the most extensive longitudinal cracking at Bugey 3. The crack was found to have extended to a depth of 2.25 mm in a wall thickness of 16 mm, from the outside surface of the penetration number 54, at the lower hillside location, just above the weld.

The circumferential flaws in Oconee Unit 3 were discovered during the process of repairing a number of axial flaws, while the circumferential flaw in Oconee Unit 2 and Crystal River Unit 3 were discovered by UT. Experience gained from these findings has enabled the development of UT procedures capable of detecting circumferential flaws reliably.

It is important to realize that a flaw would have to propagate through the penetration or the attachment weld, and result in a leak, before the outer surface of the penetration would be exposed to the water. Cracking could then begin for an outside surface flaw. (This is believed to have been the case at all four plants in which circumferential flaws were found). This time period was conservatively ignored in the calculations to be discussed.

To investigate this issue completely, a series of crack growth calculations were carried out for a postulated surface circumferential flaw located just above the head penetration weld, in a plane parallel to the weld

itself. This is the only plane in which the flaw could propagate and result in a complete separation of the penetration, since all others would result in propagation below the weld, and therefore no chance of complete separation because the remaining weld would hold the penetration in place.

[

]a,c,e

The results of this calculation are shown in Figure 6-18, where it may be seen that the time required for propagation of a circumferential flaw to a point where the integrity of the penetration would be affected (330-350 degrees) would be at least 45 years. Because of the conservatism in the calculations, as discussed above, it is likely to be even longer.

Head Vent

Figure 6-19 provides the projected growth of a circumferential outside surface part through flaw in the head vent just above the attachment weld. It may be seen that the flaw requires about 4.75 years to propagate to become a through-wall flaw.

6.5 FLAW ACCEPTANCE CRITERIA

Now that projected crack growth curves have been developed, the question which remains to be addressed is what size flaw would be acceptable for further service.

Acceptance criteria have been developed for indications found during inspection of reactor vessel upper head penetrations. These criteria were developed as part of an industry program coordinated by NUMARC (now NEI). Such criteria are normally found in Section XI of the ASME Code, but Section XI does not require inservice inspection of these regions and therefore acceptance criteria are not available. In developing the enclosed acceptance criteria, the approach used was very similar to that used by Section XI, in that an industry consensus was reached using input from both operating utility technical staff and each of the three PWR vendors. The criteria developed are applicable to all PWR plant designs.

Since the discovery of the leaks at Oconee and ANO-1, the acceptance criteria have been revised slightly, to cover flaws on the outside diameter of the penetration below the attachment weld, and flaws in the attachment weld. These revised criteria are now in draft form, but they are expected to be acceptable to the NRC, and will be used in these evaluations. The draft portions of the acceptance criteria will be noted below.

The criteria which are presented herein are limits on flaw sizes which are acceptable. The criteria are to be applied to inspection results. It should be noted that determination of the future service during which the criteria are satisfied is plant-specific and dependent on flaw geometry and loading conditions.

It has been previously demonstrated by each of the owners groups that the penetrations are very tolerant of flaws and there is only a small likelihood of flaw extension to large sizes. Therefore, it was concluded that complete fracture of the penetration is highly unlikely. The approach used here is more conservative than that used in Section XI applications where the acceptable flaw size is calculated by putting a margin on the critical flaw size. In this case, the critical flaw size is far too large to allow a practical application of this approach so protection against leakage is the priority.

The acceptance criteria presented herein apply to all flaw types regardless of orientation and shape. Similar to the approach used in Section XI, flaws are characterized according to established rules and then compared with acceptance criteria.

Flaw Characterization

Flaws detected must be characterized by length and preferably depth. The proximity rules of Section XI for considering flaws as separate, should be used directly (Section XI, Figure IWA 3400-1). This figure is reproduced here as Figure 6-20.

When a flaw is found, its projections in both the axial and circumferential directions must be determined. Note that the axial direction is always the same for each penetration, but the circumferential direction will be different depending on the angle of intersection of the penetration with the head. The "circumferential" direction of interest here is along the top of the attachment weld, as illustrated in Figure 6-21. It is this angle which will change for each penetration and which is also the plane which could cause separation of the penetration tube from the head. The location of the flaw relative to both the

top and bottom of the partial penetration attachment weld must be determined since a potential leak path exists when a flaw progresses through the wall and up the penetration past this weld. A schematic of a typical weld geometry is shown in Figure 6-22.

Flaw Acceptance Criteria

The maximum allowable depth (a_f) for axial flaws on the inside surface of the penetration, at or above the weld is 75 percent of the penetration wall thickness. The term a_f is defined as the maximum size to which the detected flaw is calculated to grow in a specified time period. This 75 percent limitation was selected to be consistent with the maximum acceptable flaw depth in Section XI and to provide an additional margin against through wall penetration. There is no concern about separation of the head penetration from the head, unless the flaw is above the attachment weld and oriented circumferentially. Calculations have been completed to show that all penetrations geometries can support a continuous circumferential flaw with a depth of 75 percent of the wall.

Axial inside surface flaws found below the weld are acceptable regardless of depth as long as their upper extremity does not reach the bottom of the weld during the period of service until the next inspection. Axial flaws which extend above the bottom of the weld are limited to 75 percent of the wall.

Axial flaws on the OD of the penetration below the attachment weld are acceptable regardless of depth, as long as they do not extend into the attachment weld during the period of service until next inspection. OD flaws above the attachment weld must be evaluated on a case by case basis, and must be discussed with the regulatory authority.

Circumferential flaws located below the weld are acceptable regardless of their depth, provided the length is less than 75 percent of the circumference for the period of service until the next inspection. Flaws in this area have no structural significance but loose parts must be avoided. To this end, intersecting axial and circumferential flaws shall be removed or repaired. Circumferential flaws at and above the weld must be discussed with the regulatory authority on a case by case basis.

Surface flaws located in the attachment welds themselves are not acceptable regardless of their depth. This is because the crack propagation rate is several times faster than that of the Alloy 600 tube material, and also because depth sizing capability does not yet exist for indications in the weld.

These criteria are summarized in Table 6-1. Flaws which exceed these criteria must be repaired unless analytically justified for further service. These criteria have been reviewed and approved by the NRC, as documented in references 7 and 8, with the exception of the draft criteria discussed above, for outside surface flaws and flaws in the attachment weld. These criteria are identical with the draft acceptance criteria now being considered for Section XI, for head penetrations.

It is expected that the use of these criteria and crack growth curves will provide conservative predictions of the allowable time of service.

Table 6-1 Summary of R.V. Head Penetration Flaw Acceptance Criteria (limits for future growth)

Location	Axial		Circumferential	
	a_f	ℓ	a_f	ℓ
Below Weld (ID)	t	no limit	t	.75 circ.
At and Above Weld (ID)	0.75 t	no limit	*	*
Below Weld (OD)	t	no limit	t	.75 circ.
Above Weld (OD)	*	*	*	*

Note: Surface flaws of any size in the attachment weld are not acceptable.

* Requires case-by-case evaluation and discussion with regulatory authority.

a_f = Flaw Depth as defined in IWB 3600
ℓ = Flaw Length
t = Wall Thickness

Table 6-2 Penetration Geometrics

Penetration Type	Wall Thickness (in.)	Penetration OD (in.)
CRDM	0.625	4.000
Head Vent	0.122	1.014

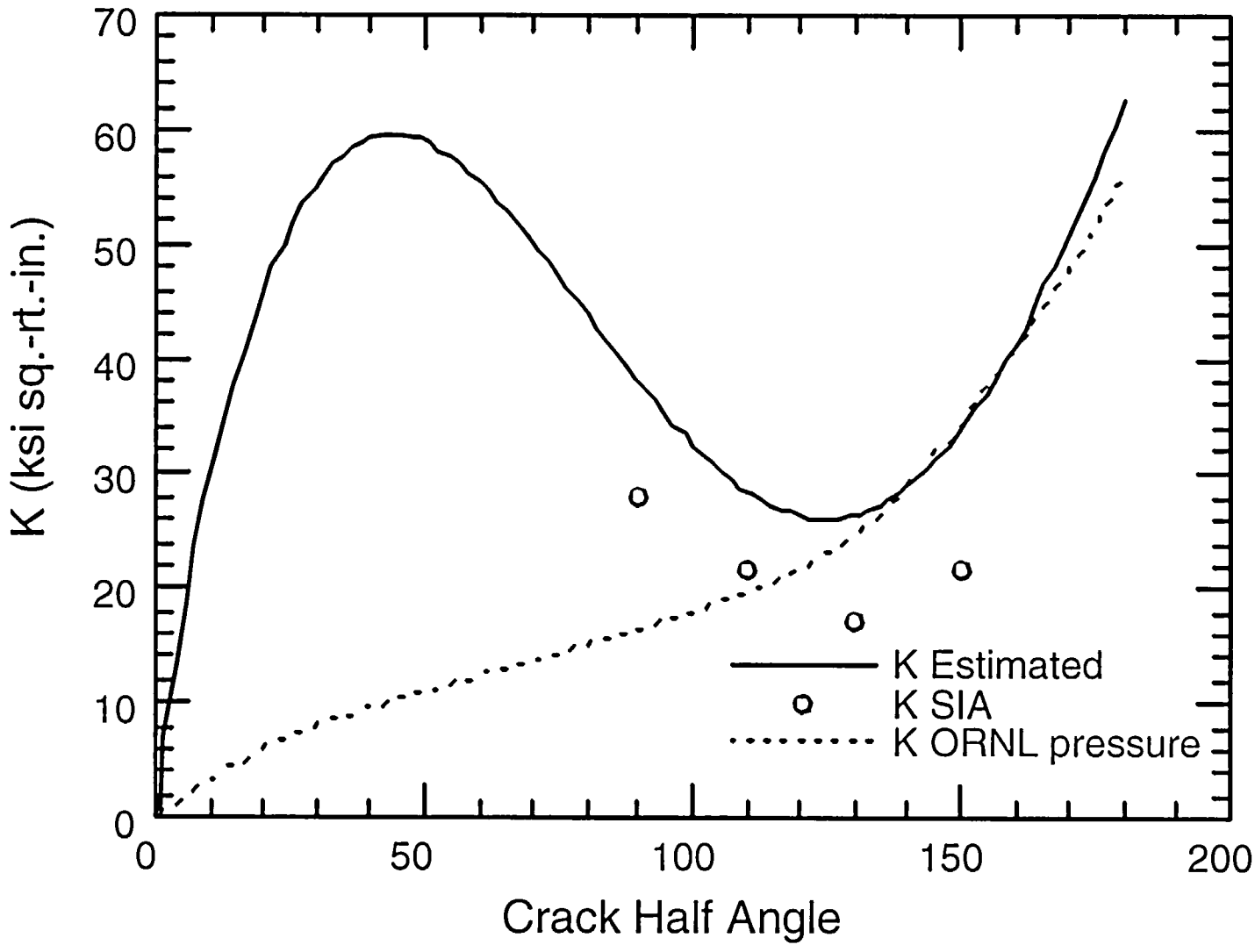

Figure 6-1 Stress Intensity Factor for a Through-Wall Circumferential Flaw in a Head Penetration (5B)

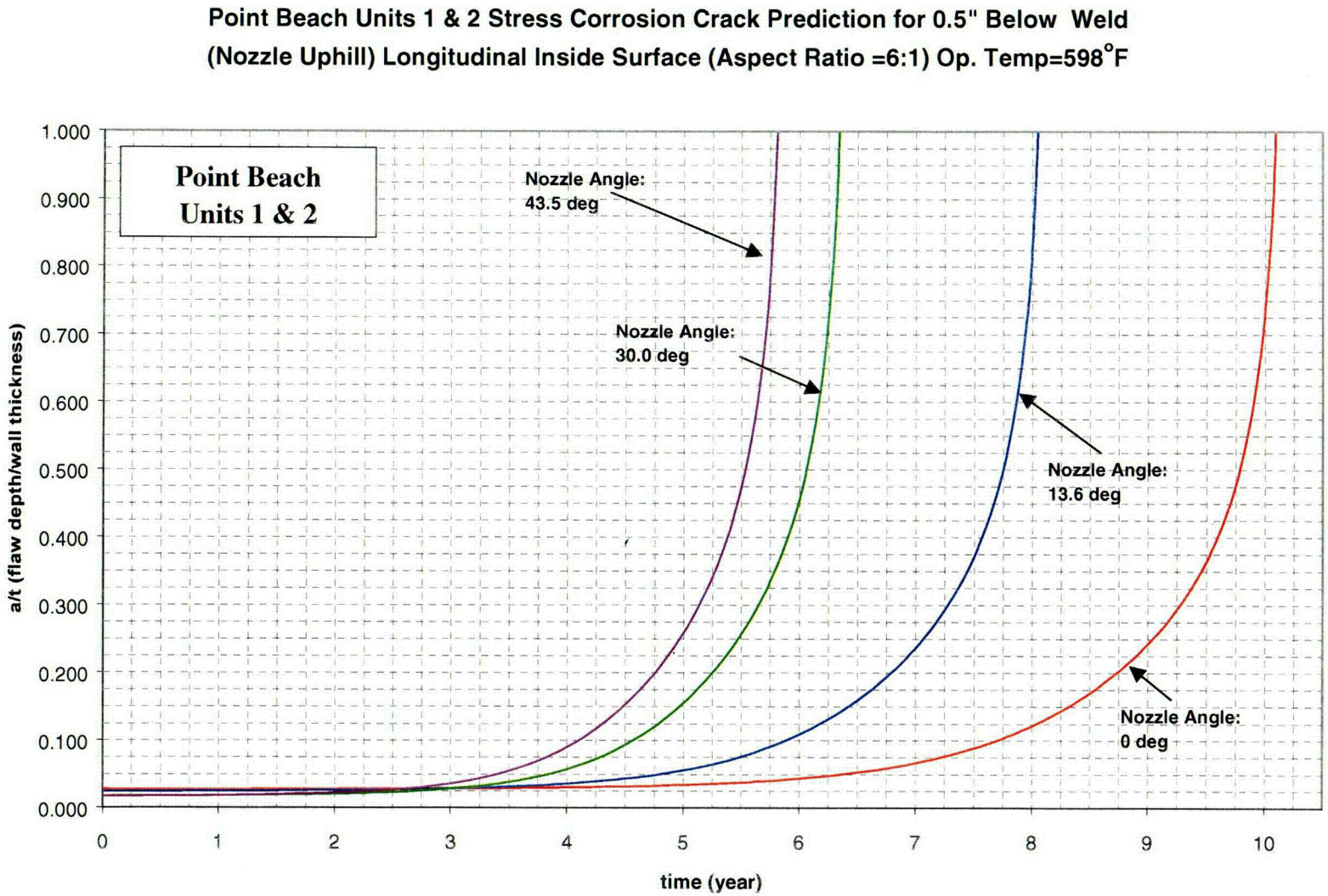

Figure 6-2 **Crack Growth Predictions for Axial Inside Surface Flaws Below the Attachment Weld by More Than 0.5 Inches – Nozzle Uphill Side. Note, all time (year) indicated in the charts are effective full power years (EFPY).**

C08

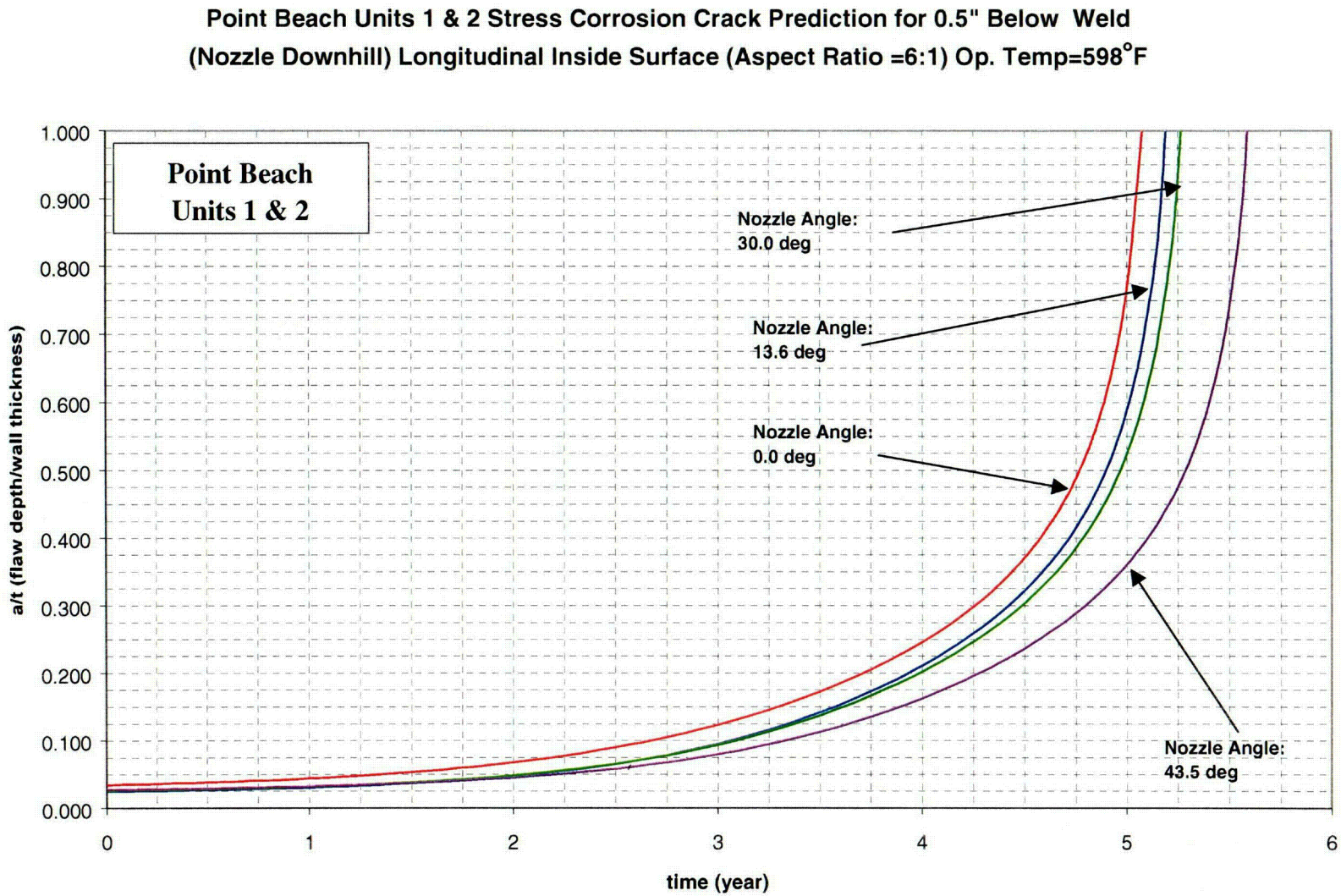

Figure 6-3 **Crack Growth Predictions for Axial Inside Surface Flaws Below the Attachment Weld by More Than 0.5 Inches – Nozzle Downhill Side. Note, all time (year) indicated in the charts are effective full power years (EFPY).**

C09

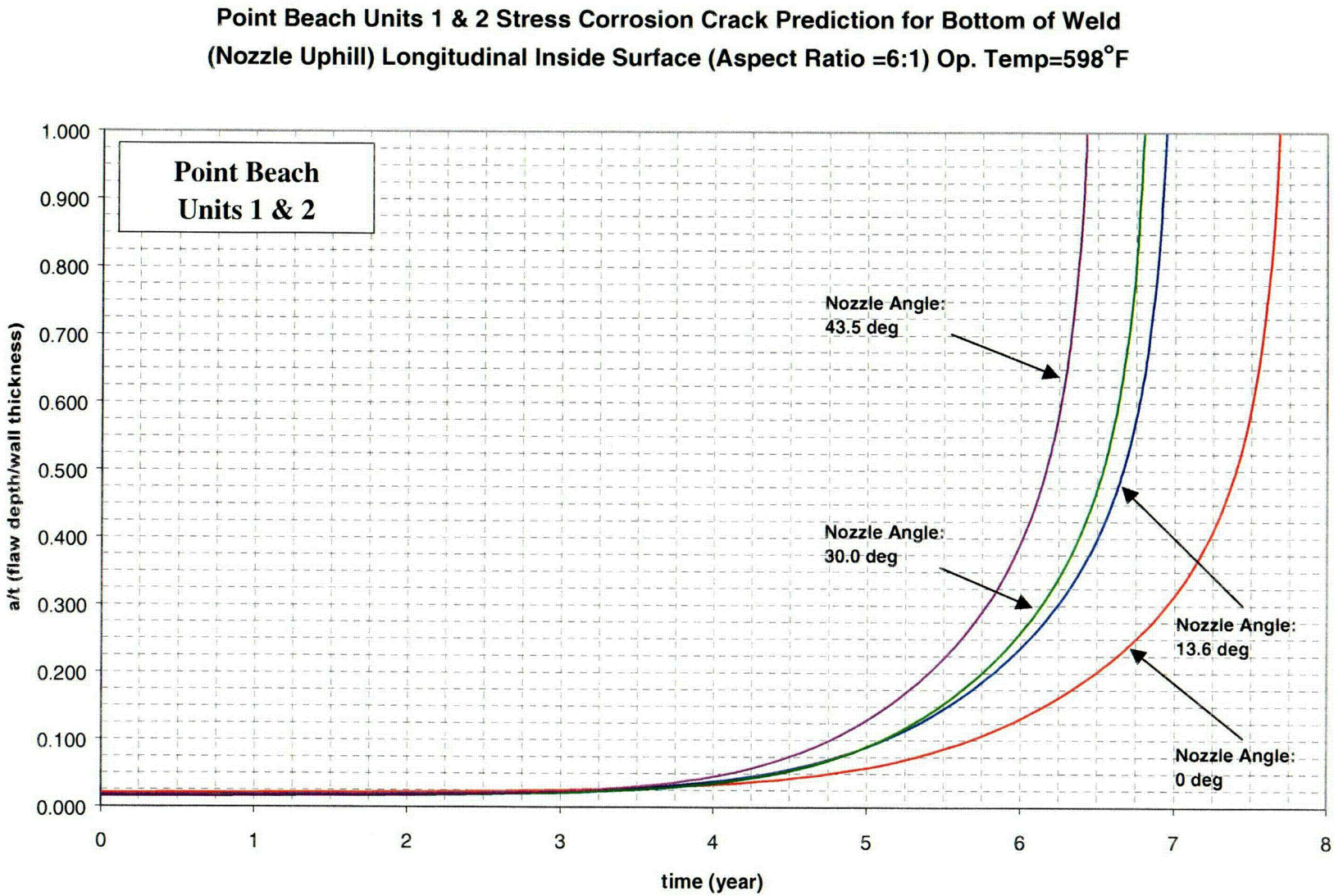

Figure 6-4 **Crack Growth Predictions for Axial Inside Surface Flaws Near the Attachment Weld – Nozzle Uphill Side. Note, all time (year) indicated in the charts are effective full power years (EFPY).**

C10

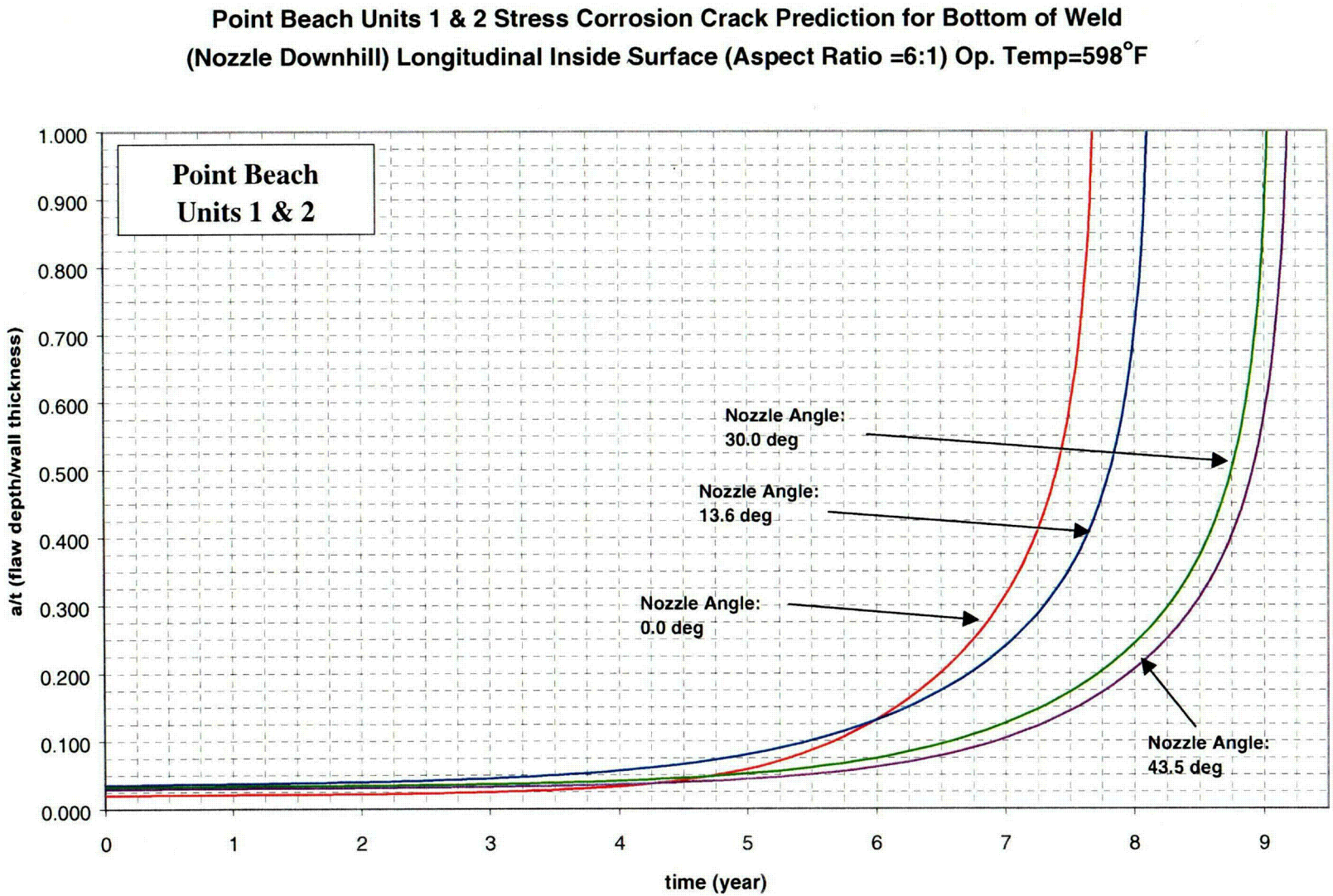

Figure 6-5 Crack Growth Predictions for Axial Inside Surface Flaws Near the Attachment Weld – Nozzle Downhill Side. Note, all time (year) indicated in the charts are effective full power years (EFPY).

C11

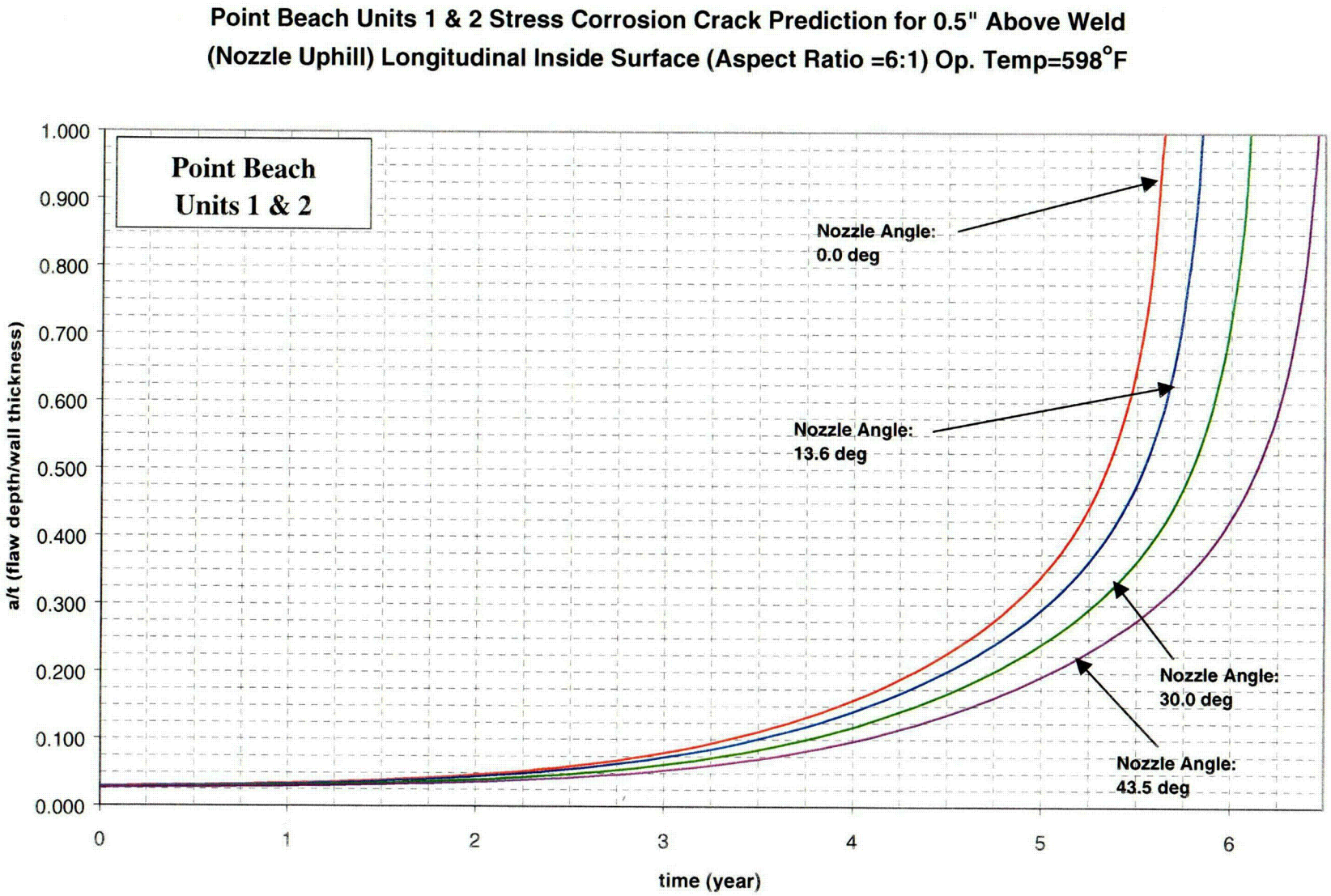

Figure 6-6 Crack Growth Predictions for Axial Inside Surface Flaws Above the Attachment Weld – Nozzle Uphill Side. Note, all time (year) indicated in the charts are effective full power years (EFPY).

C12

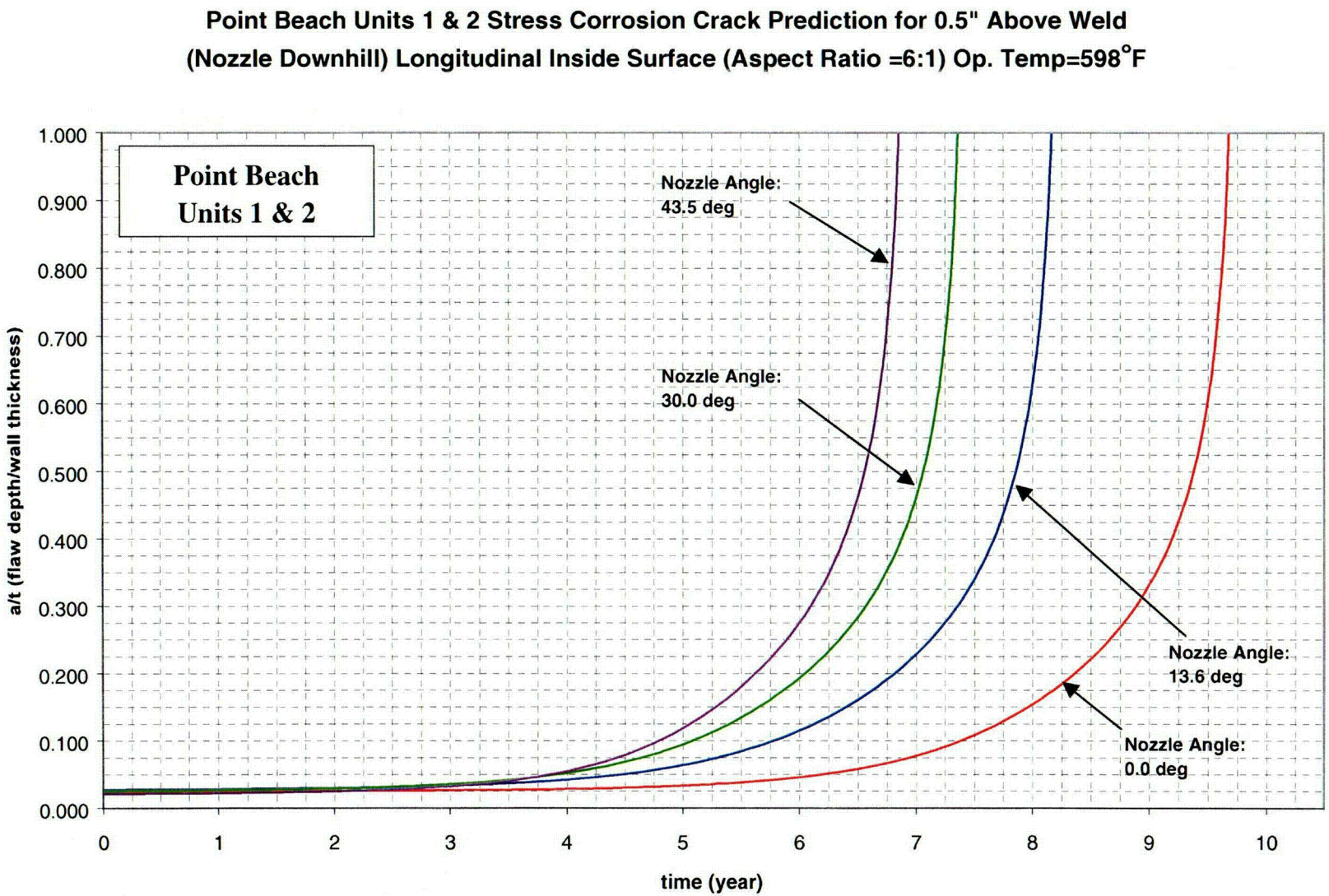

Figure 6-7 **Crack Growth Predictions for Axial Inside Surface Flaws Above the Attachment Weld – Nozzle Downhill Side. Note, all time (year) indicated in the charts are effective full power years (EFPY).**

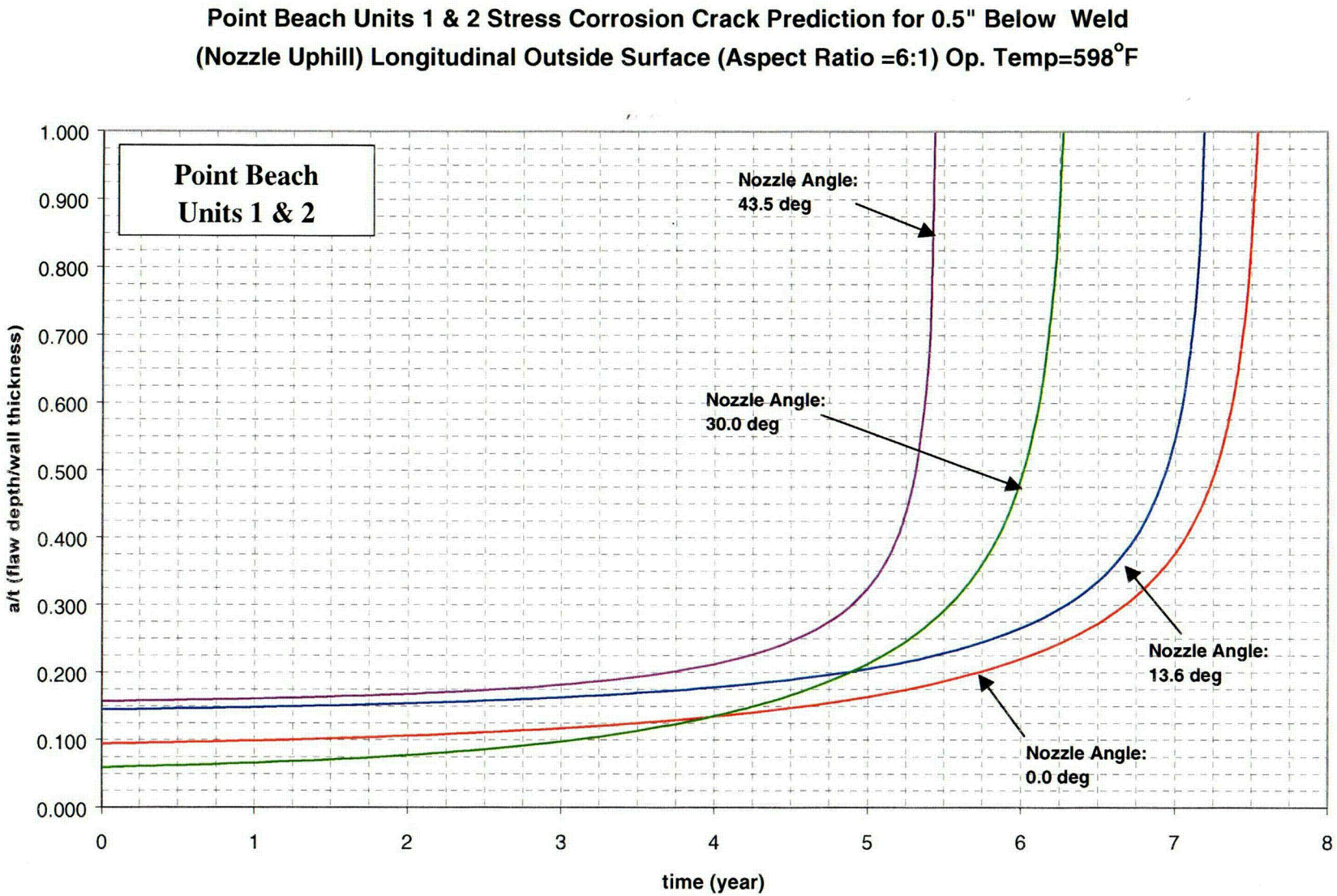

Figure 6-8 Crack Growth Predictions for Axial Outside Surface Flaws Below the Attachment Weld: Nozzle Uphill Side. Note, all time (year) indicated in the charts are effective full power years (EFPY).

C14

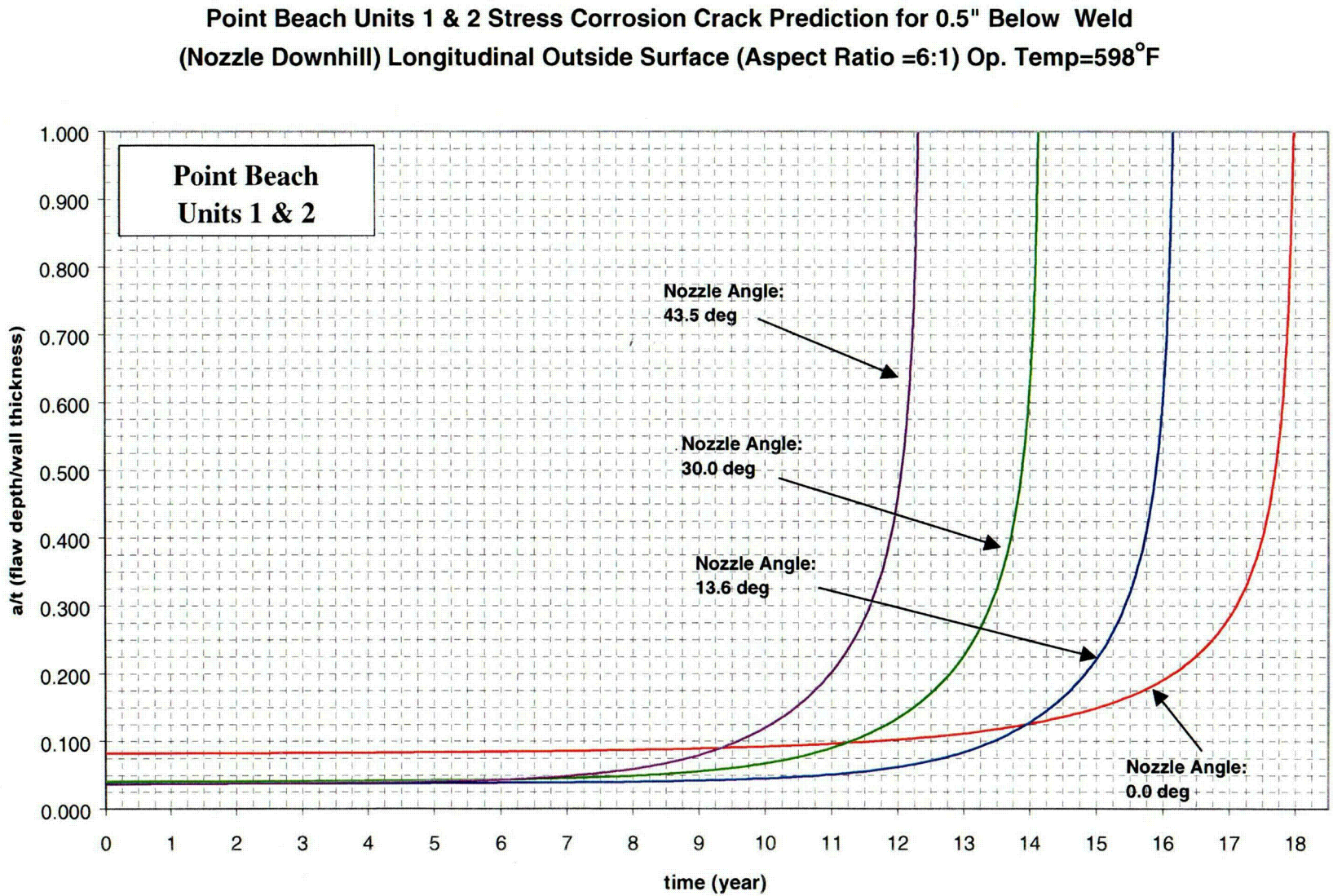

Figure 6-9 Crack Growth Predictions for Axial Outside Surface Flaws Below the Attachment Weld: Nozzle Downhill Side. Note, all time (year) indicated in the charts are effective full power years (EFPY).

C15

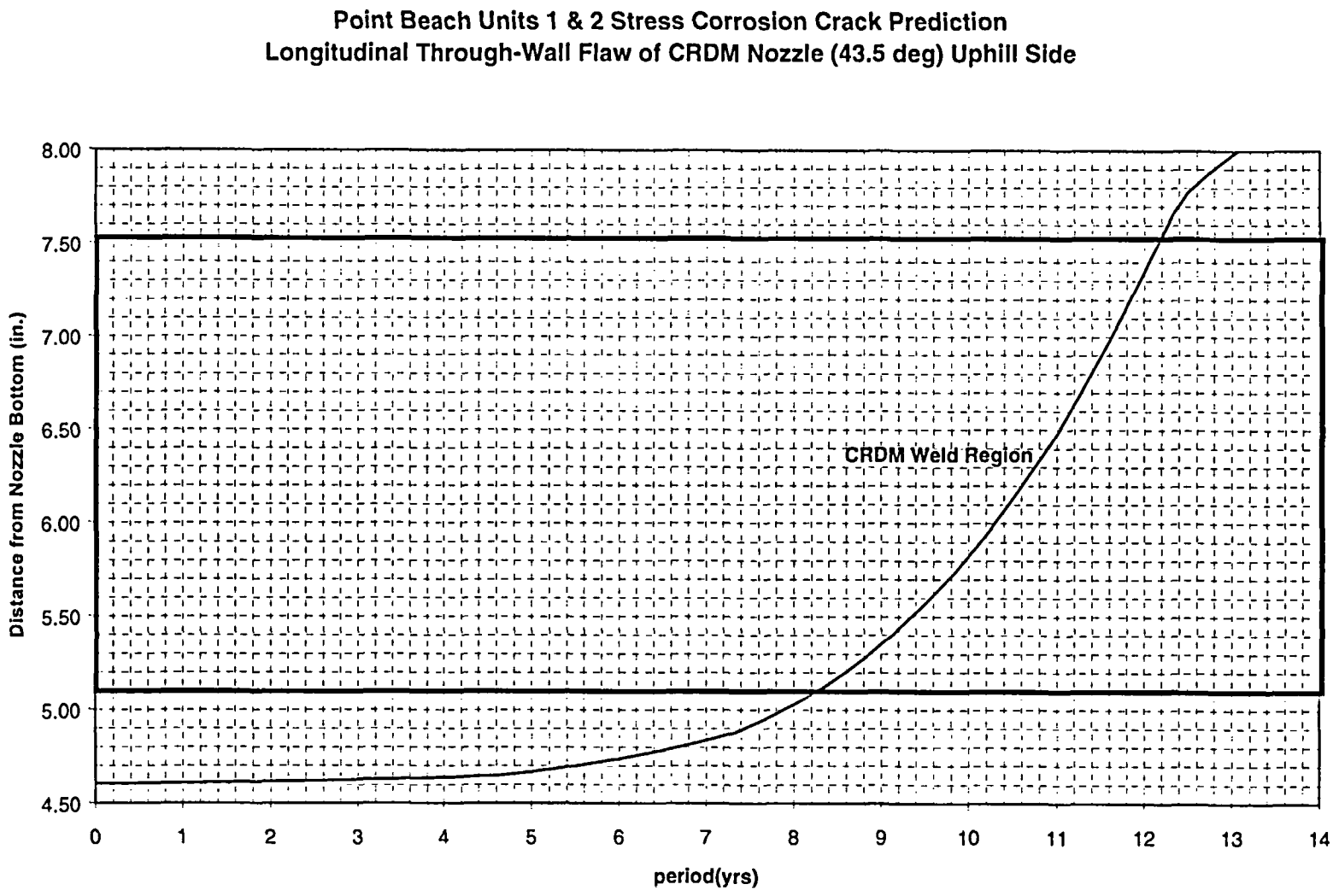

Figure 6-10 Crack Growth Predictions for Through-Wall Axial Flaws Located in the Outermost CRDM (43.5 Degree) Row of Penetrations - Uphill Side. Note, all period (yrs) indicated in the charts are effective full power years (EFPY).

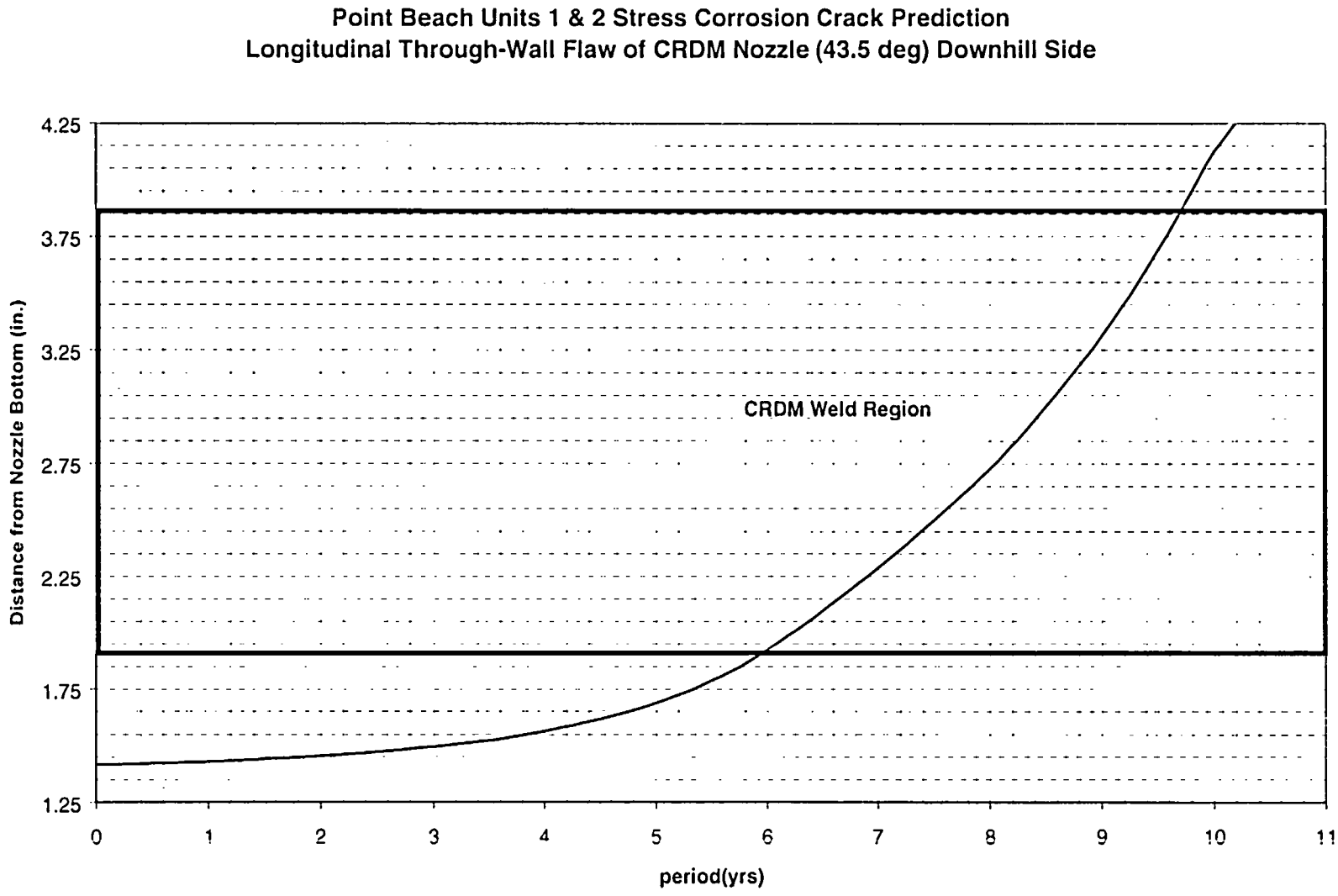

Figure 6-11 Crack Growth Predictions for Through-Wall Axial Flaws Located in the Outermost CRDM (43.5 Degree) Row of Penetrations - Downhill Side. Note, all period (year) indicated in the charts are effective full power years (EFPY).

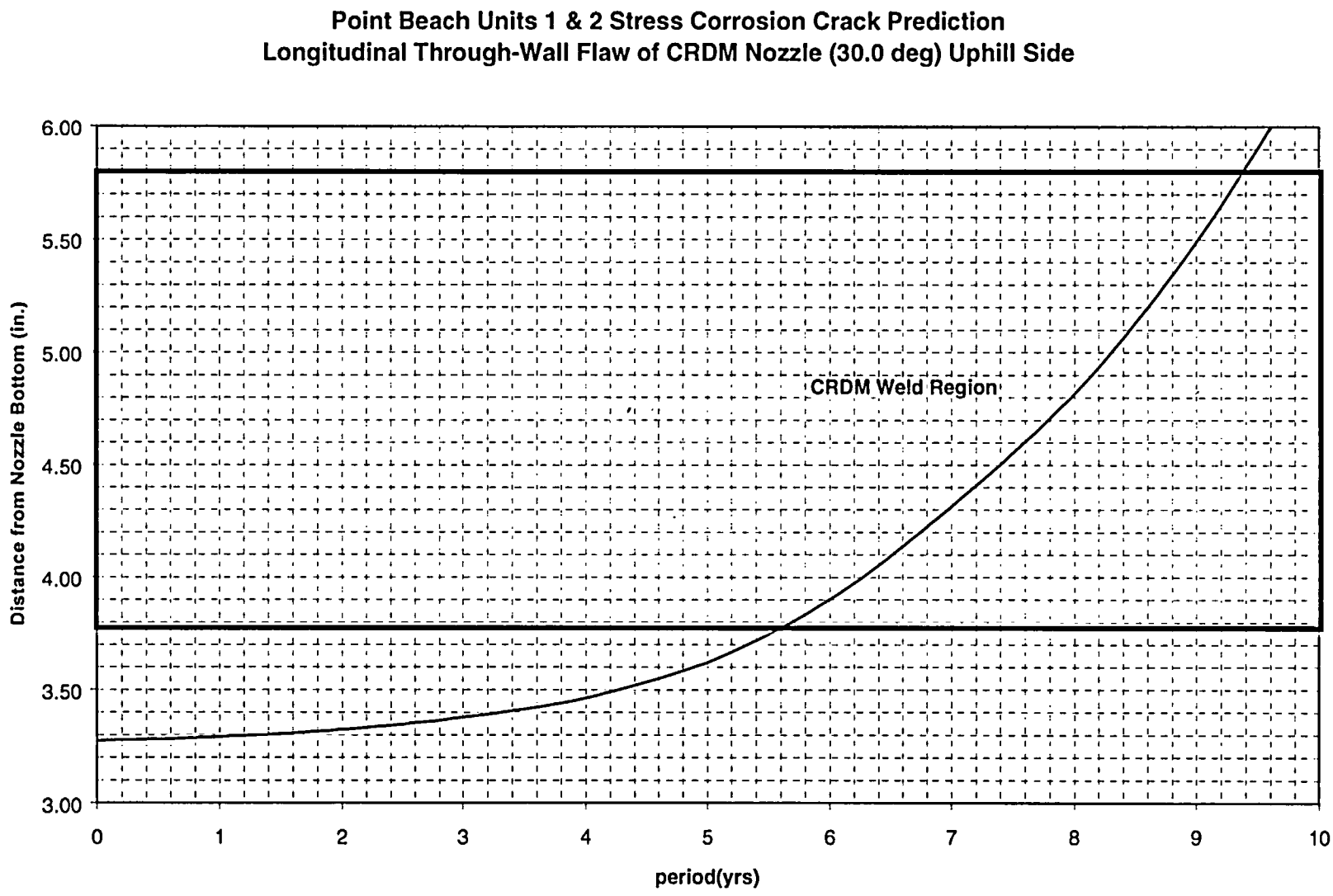

Figure 6-12 Crack Growth Predictions for Through-Wall Axial Flaws Located in the 30.0 Degree Row of Penetrations - Uphill Side. Note, all period (year) indicated in the charts are effective full power years (EFPY).

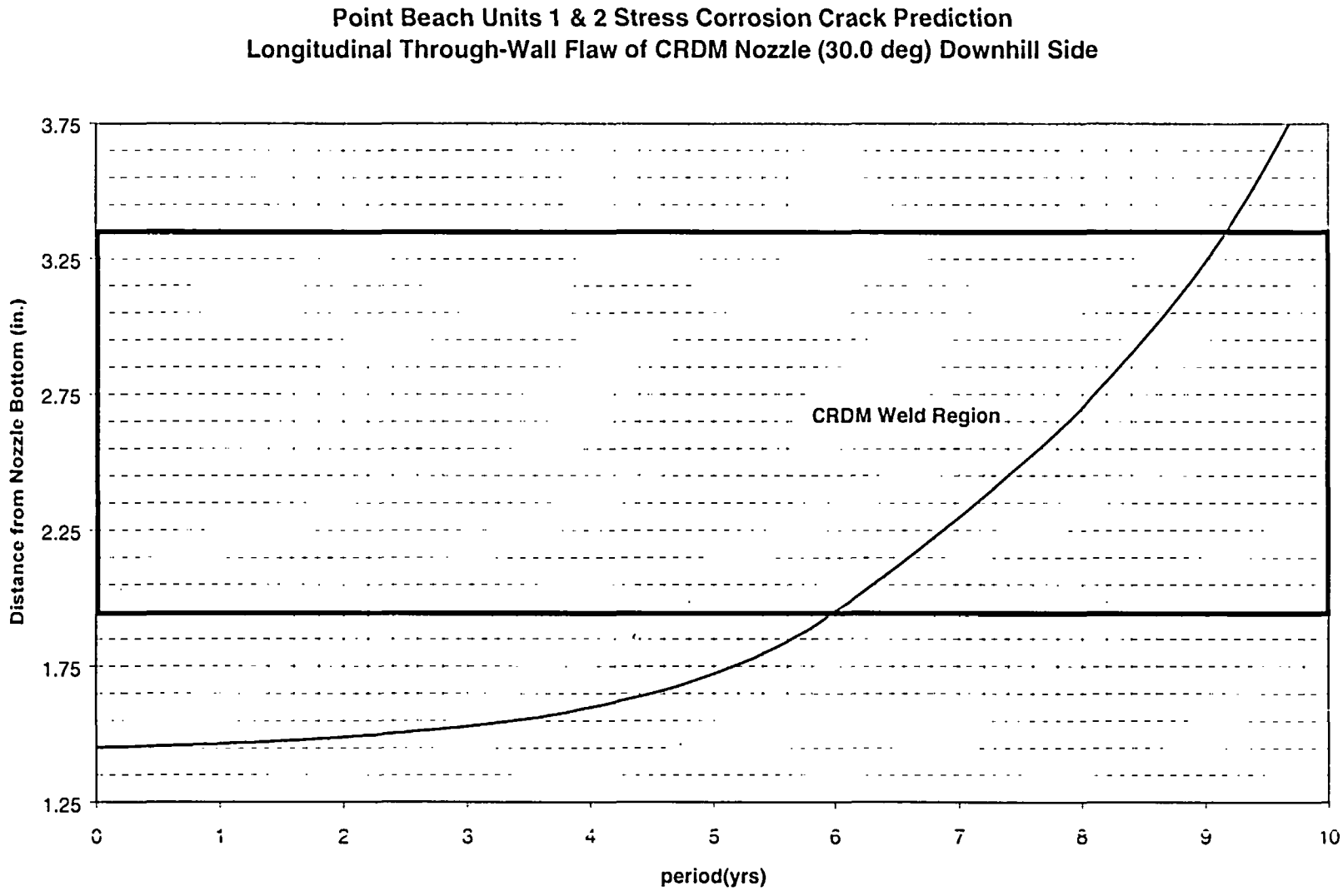

Figure 6-13 Crack Growth Predictions for Through-Wall Axial Flaws Located in the 30.0 Degree Row of Penetrations - Downhill Side. Note, all period (year) indicated in the charts are effective full power years (EFPY).

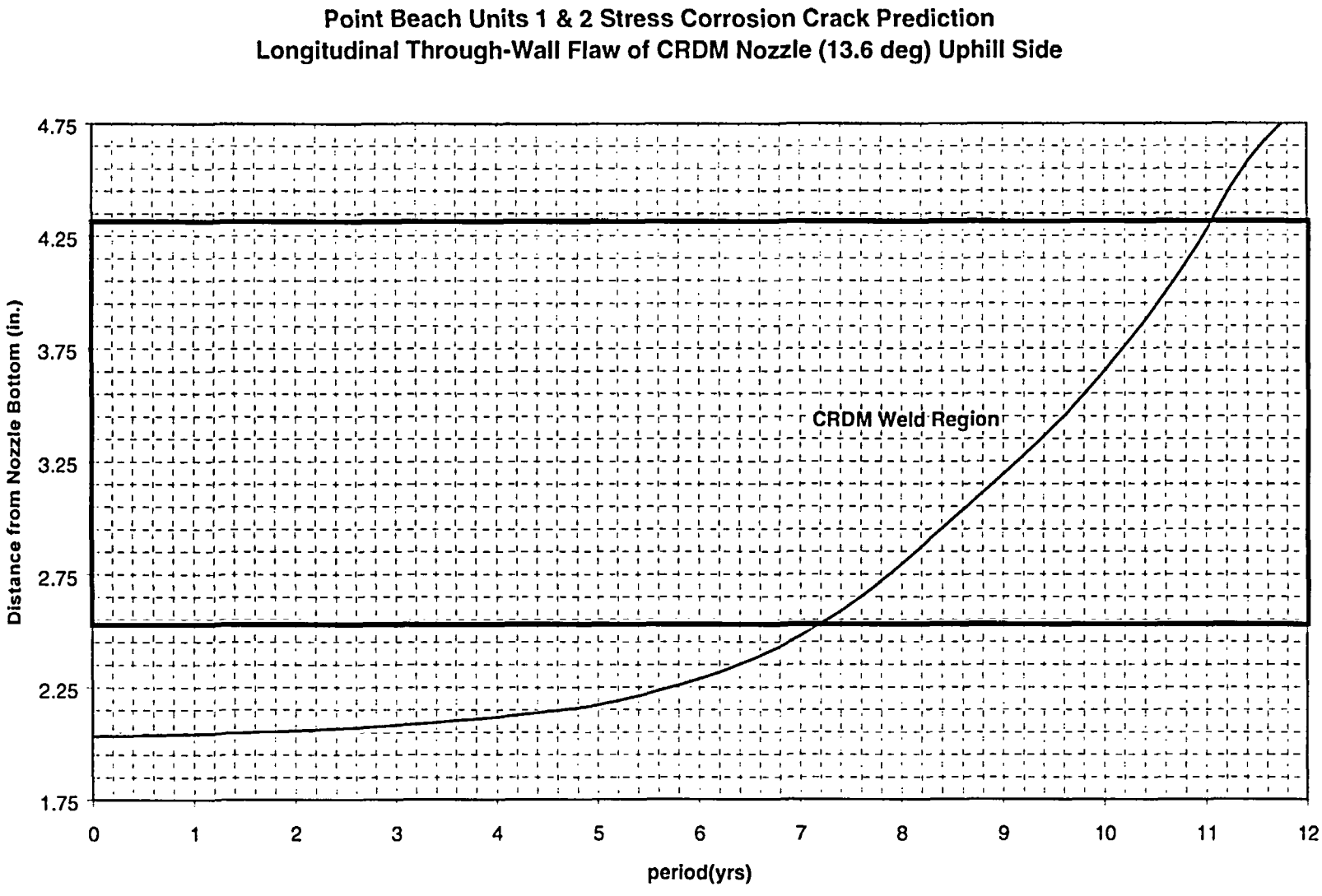

Figure 6-14 Crack Growth Predictions for Through-Wall Axial Flaws Located in the 13.6 Degree CRDM Uphill Side. Note, all period (year) indicated in the charts are effective full power years (EFPY).

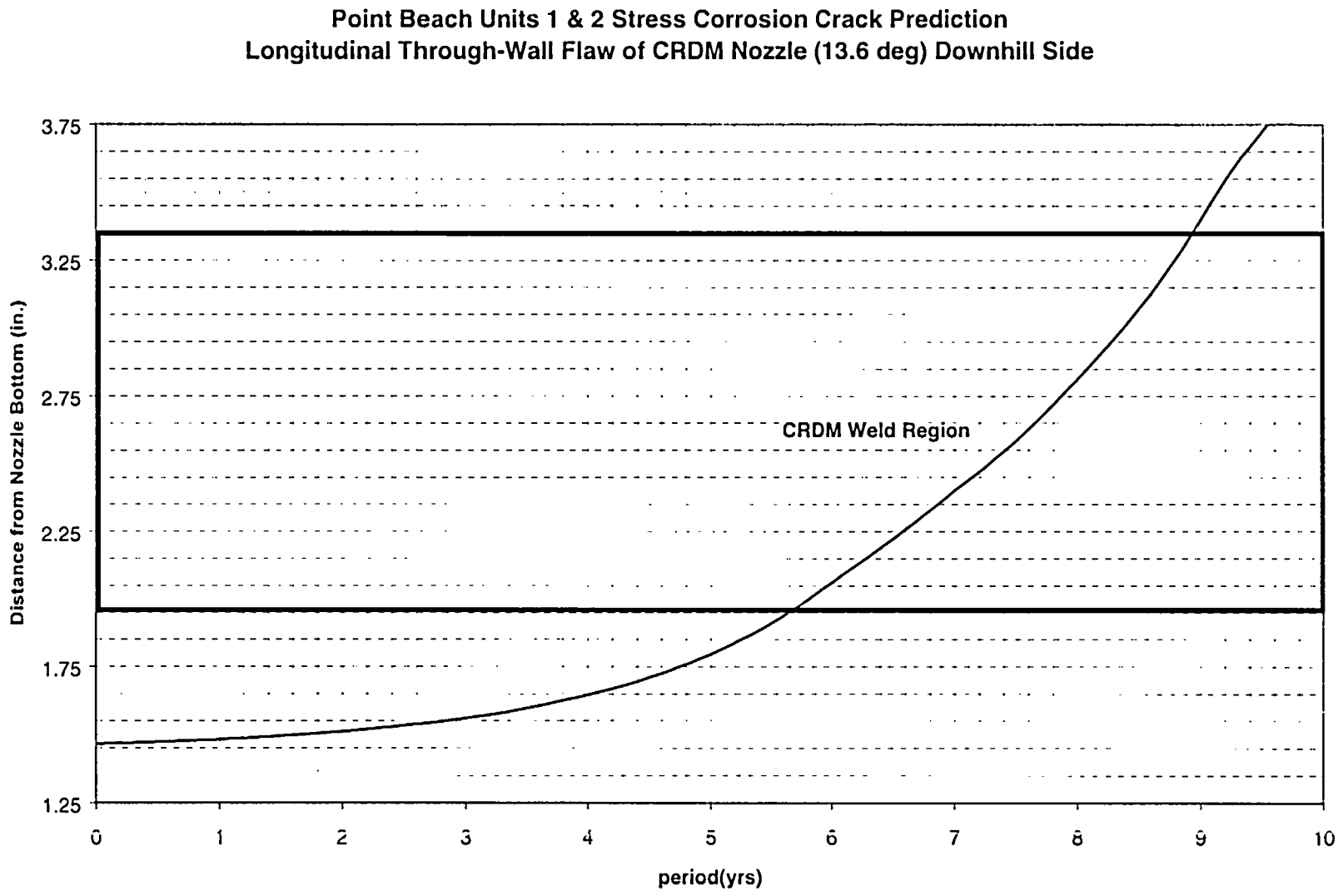

Figure 6-15 Crack Growth Predictions for Through-Wall Axial Flaws Located in the 13.6 Degree CRDM Downhill Side. Note, all period (year) indicated in the charts are effective full power years (EFPY).

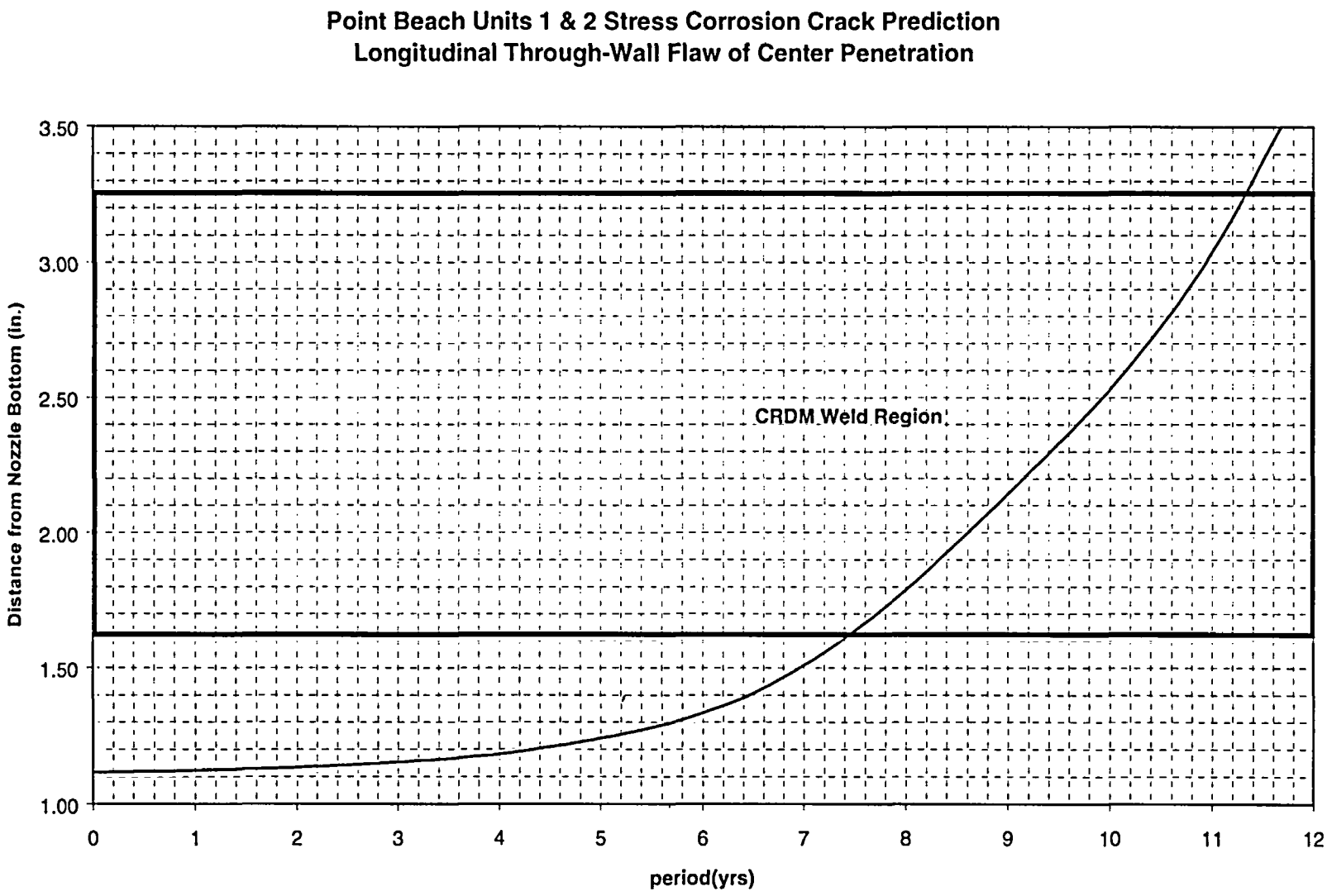

Figure 6-16 Crack Growth Predictions for Through-Wall Axial Flaws Located in the Center Penetration. Note, all period (year) indicated in the charts are effective full power years (EFPY).

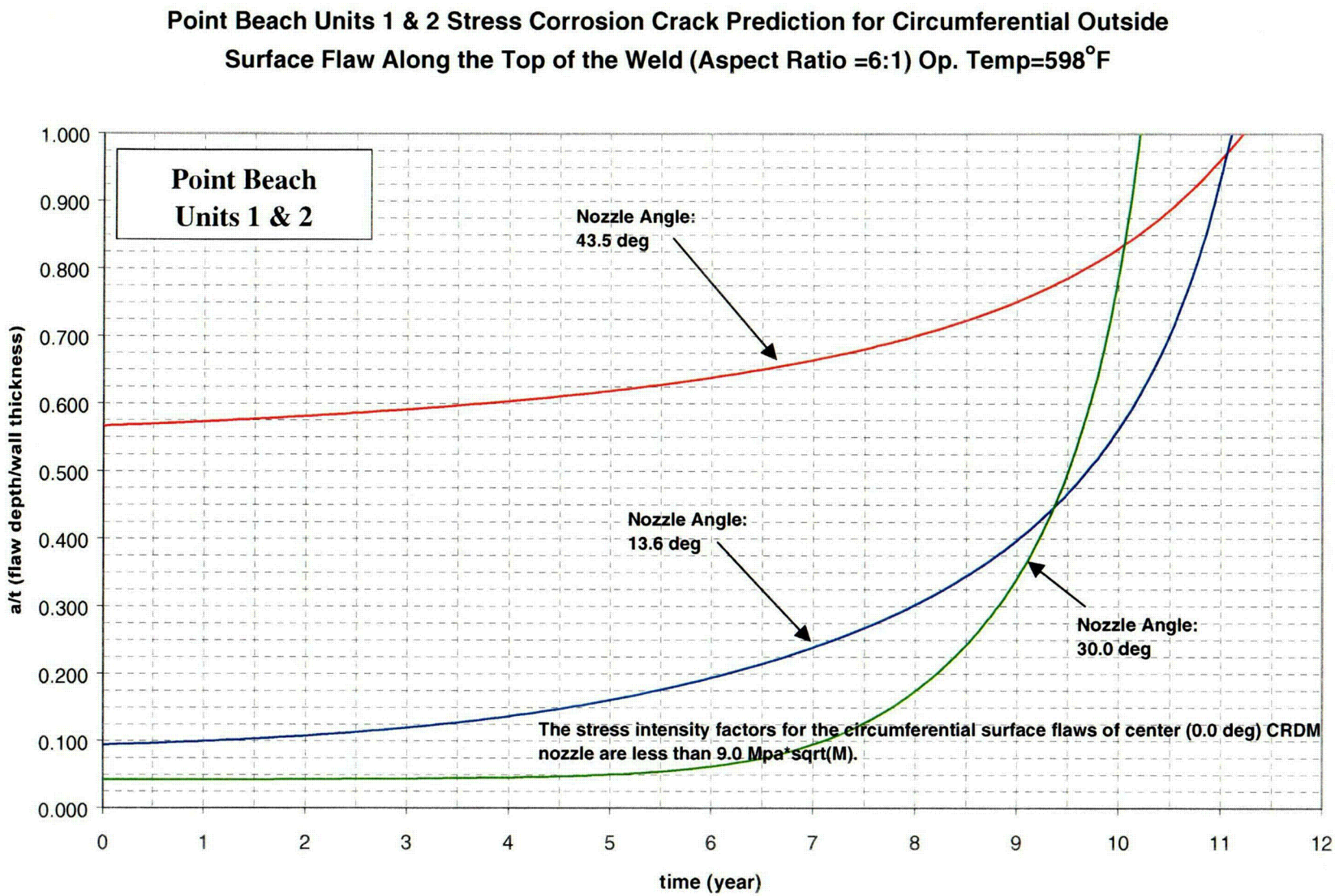

Figure 6-17 Crack Growth Predictions for Circumferential Surface Flaws Near the Top of the Attachment Weld. Note, all time (year) indicated in the charts are effective full power years (EFPY).

C16

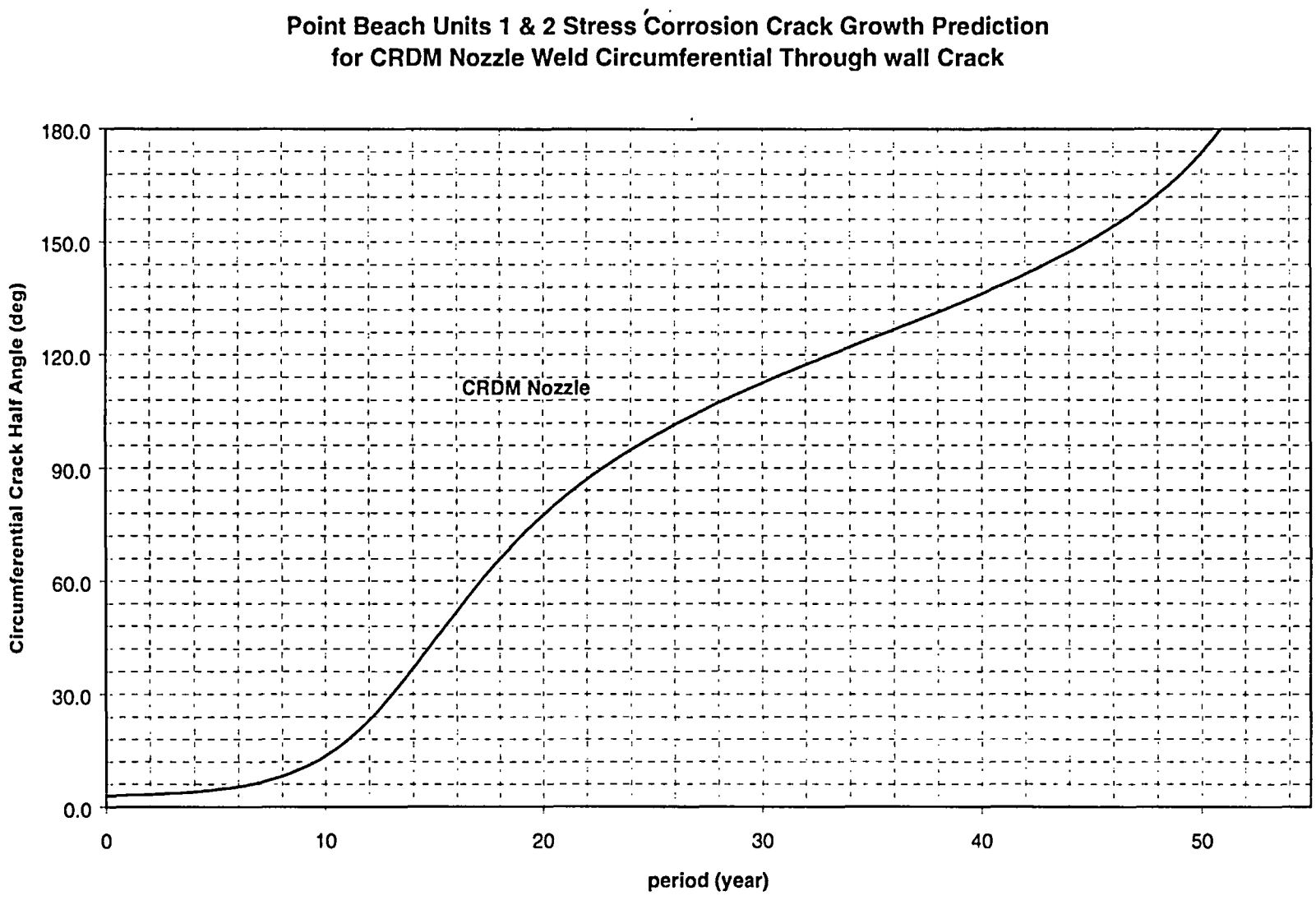

Figure 6-18 Crack Growth Predictions for Circumferential Through-Wall Cracks Near the Top of the Attachment Weld. Note, all period (year) indicated in the charts are effective full power years (EFPY).

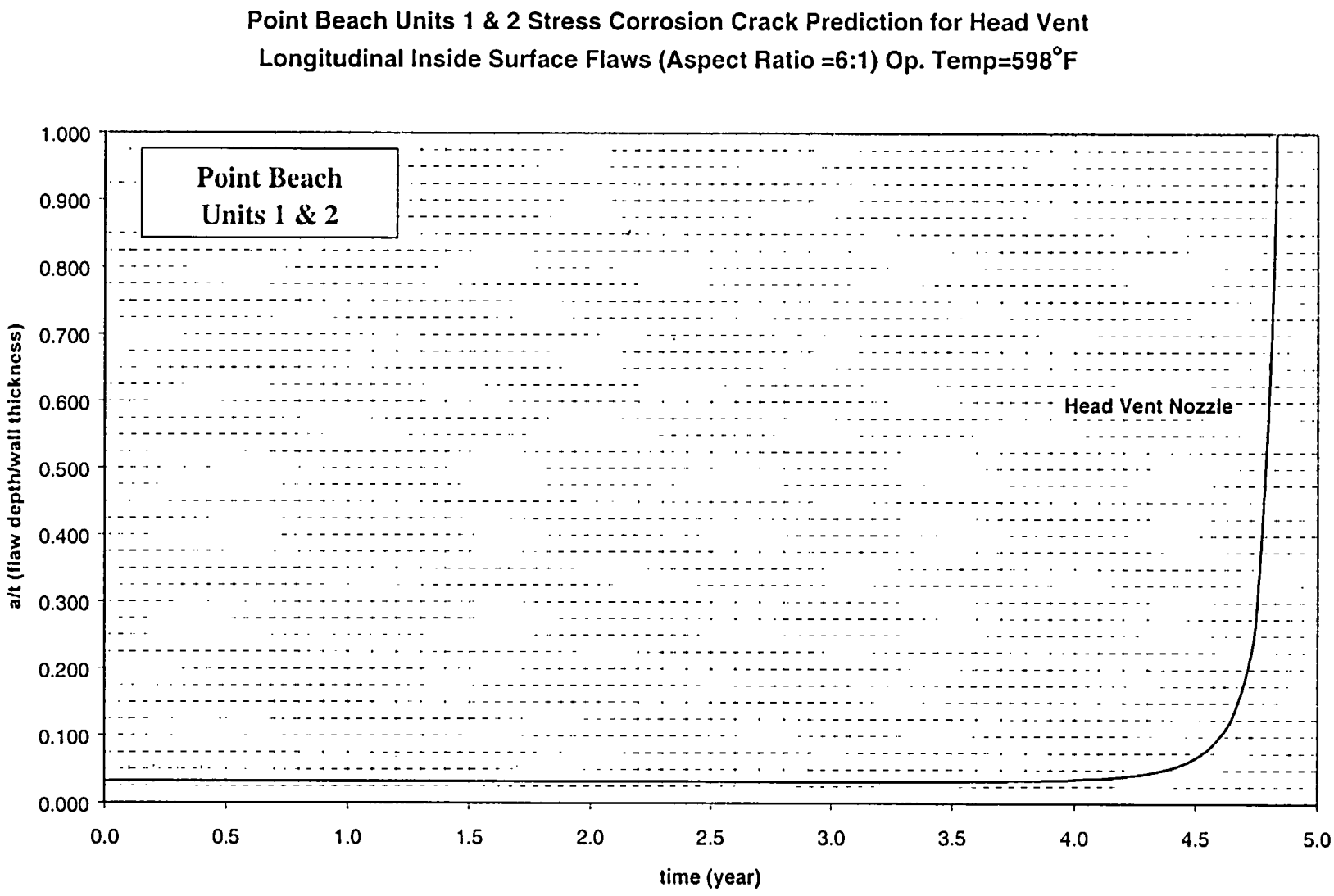

Figure 6-19 Crack Growth Predictions for Axial Inside Surface Flaws – Head Vent. Note, all time (year) indicated in the charts are effective full power years (EFPY).

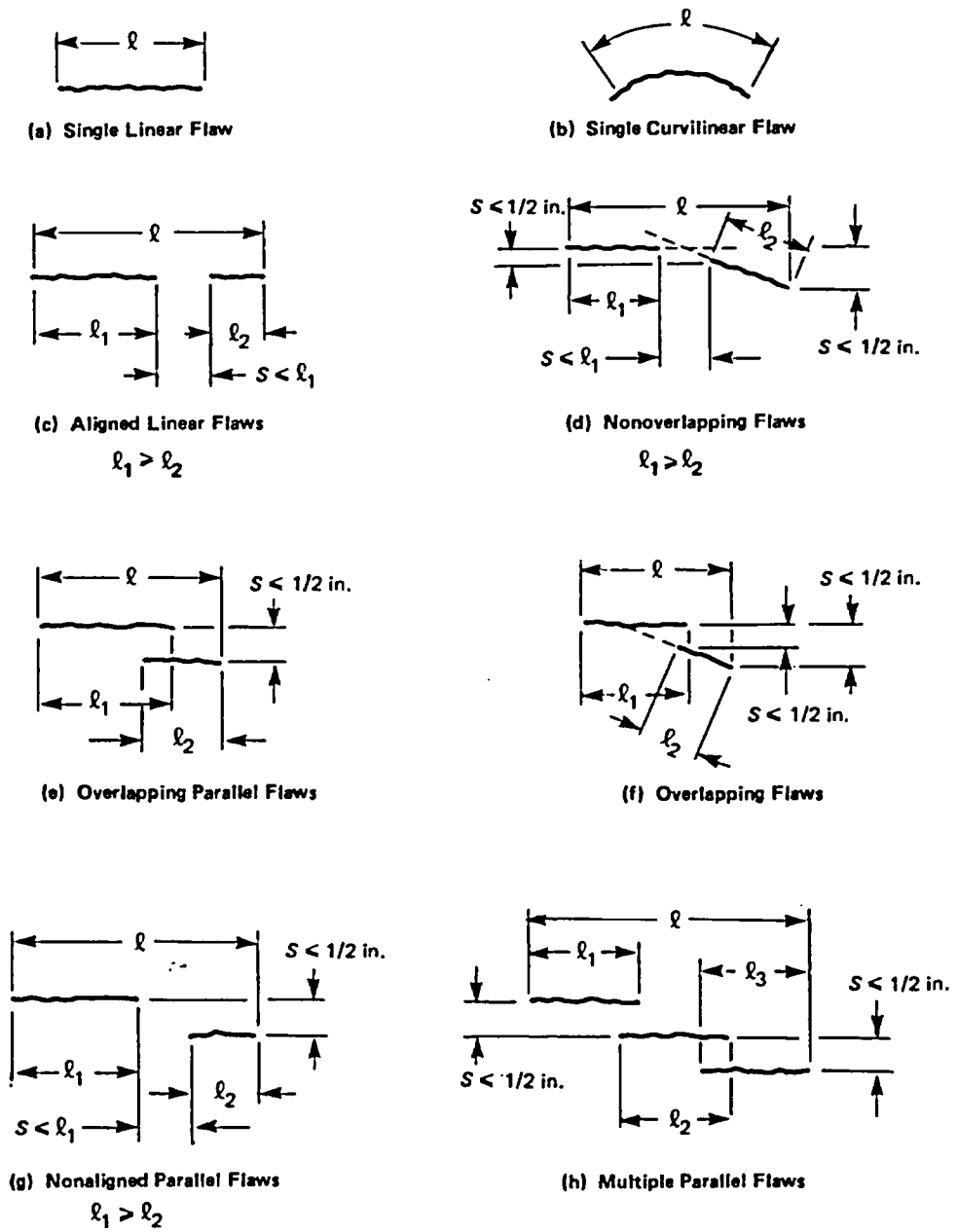

Figure 6-20 Section XI Flaw Proximity Rules for Surface Flaws (Figure IWA-3400-1)

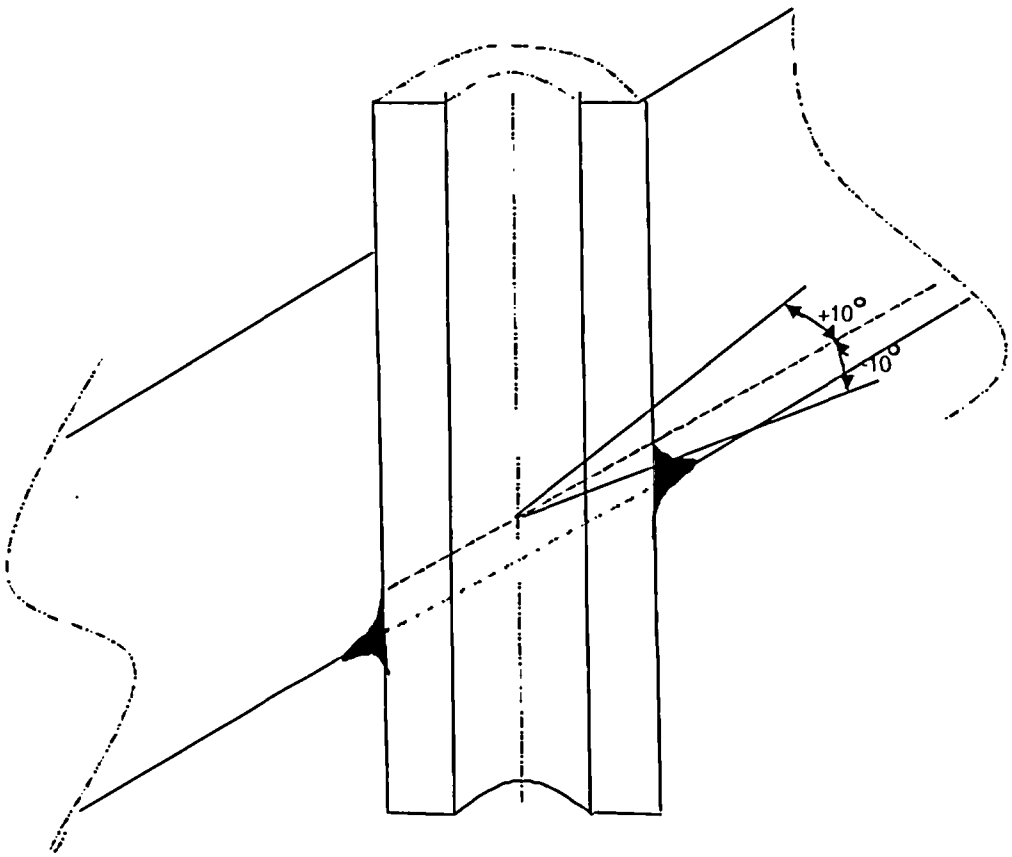

Figure 6-21 Definition of "Circumferential"

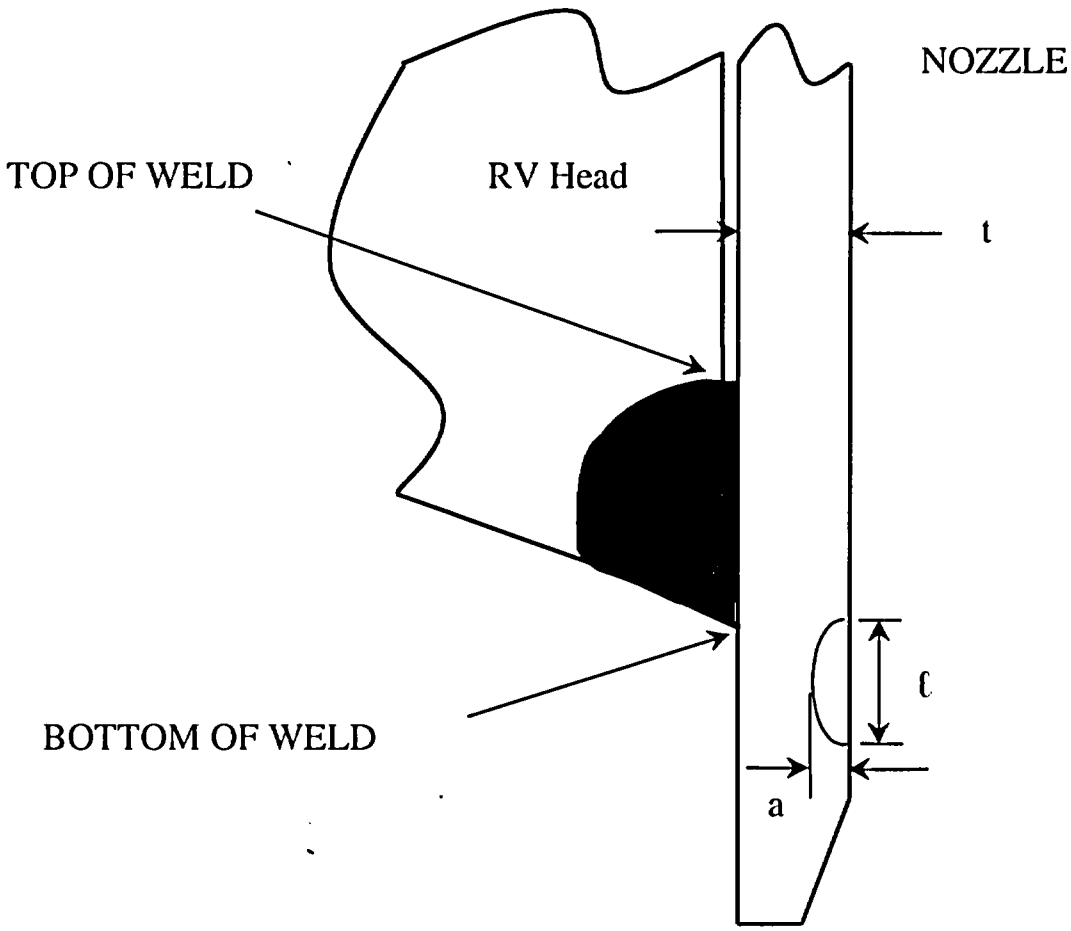

Figure 6-22 Schematic of Head Penetration Geometry

7 SUMMARY AND EXAMPLE PROBLEMS

An extensive evaluation has been carried out to characterize the loadings and stresses, which exist in the head penetrations at Point Beach Units 1 and 2. Three-dimensional finite element models were constructed, and all pertinent loadings on the penetrations were analyzed (6A, 6B). These loadings included internal pressure and thermal expansion effects typical of steady state operation. In addition, residual stresses due to the welding of the penetrations to the vessel head were considered.

Results of the analyses reported here are consistent with the axial orientation and location of flaws which have been found in service in a number of plants, in that the largest stress component is the hoop stress, and the maximum stresses were found to exist in the circumferential locations nearest and farthest away from the center of the vessel. The most important loading conditions were found to be those which exist on the penetration for the majority of the time, which are the steady state loading and the residual stresses.

These stresses are important because the cracking observed to date in operating plants has been determined to result from primary water stress corrosion cracking (PWSCC). These stresses were used in fracture calculations to predict the future growth of flaws postulated to exist in the head penetrations. A crack growth law was developed specifically for the operating temperature of the head at Point Beach Units 1 and 2, based on the EPRI recommendation, which is consistent with laboratory data as well as crack growth results for operating plants.

The crack growth predictions contained in Section 6 show that the future growth of cracks which might be found in the penetrations will be typically very slow, and that a number of effective full power years will be required for any significant extensions.

7.1 SAFETY ASSESSMENT

It is appropriate to examine the safety consequences of an indication which might be found. The indication, even if it were to propagate through the penetration wall, would have only minor consequences, since the pressure boundary would not be broken, unless it were to propagate above the weld.

Further propagation of the indication would not change its orientation, since the hoop stresses in the penetration are much larger than the axial stresses. Therefore, it is extremely unlikely that the head penetration would be severed.

If the indication were to propagate to a position above the weld, a leak could result, but the magnitude of such a leak would be very small, because the crack could not open significantly due to the tight fit between the penetration and the vessel head. Such a leak would have no immediate impact on the structural integrity of the system, but could lead to wastage in the ferritic steel of the vessel head, as the borated primary water concentrates due to evaporation. Davis Besse has demonstrated the consequence of ignoring such leaks.

Any indication is unlikely to propagate very far up the penetration above the weld, because the hoop stresses decrease in this direction, and this will cause it to slow down, and to stop before it reaches the outside surface of the head.

The high likelihood that the indication will not propagate up the tube beyond the vessel head ensures that no catastrophic failure of the head penetration will occur, since the indication will be enveloped in the head itself, which precludes the opening of the crack and limits leakage.

7.2 EXAMPLE PROBLEMS

The crack growth prediction curves in Figures 6-2 through 6-19 can be used with the acceptance criteria of Section 6.5 to determine the available service time. In this section, a few examples will be presented to illustrate the use of these figures. The example cases are listed in Table 7-1.

Example 1. For an axially oriented inside surface flaw, located below the weld, on the uphill side of penetration 20, first find the angle of the penetration in Table 1-1. The angle is 30.0 degrees. The crack growth curves of Figure 6-2 are appropriate and Figure 6-2 has been reproduced as Figure 7-1. In this case the flaw initial depth is 7.5 percent of the wall thickness, so project a line horizontally at a/t=0.075, intersecting the crack growth curve. The service life is then determined as the time for this flaw to grow to the limit of 100 percent of the wall thickness or approximately 2.1 years (labeled Service Life in Figure 7-1).

Example 2. In this case the flaw is identical in size to example 1, but located at the outside surface, in the penetration row at 30 degrees, and at the uphill side. The curve to use is in Figure 6-8. The determination of service life is illustrated in Figure 7-2, where we see the result is approximately 4.5 years.

Example 3. The axial inside surface flaw is at the weld, on the uphill side of penetration 35, whose angle can be determined from Table 1-1. The table shows that this penetration is in the row at 43.5 degrees. It is oriented on the uphill side. The curve from Figure 6-4 is used to determine the service life. The flaw depth is 7.5 percent of the wall thickness, so project horizontally at this value to intersect the crack growth curve. The allowable service life is then determined as the time for the flaw to reach a depth of 75 percent of the wall. As shown in Figure 7-3, this time is approximately 1.8 years.

Example 4. Here we have postulated an axial inside surface flaw that will require two charts for its evaluation. The flaw has a depth of 2 mm, and is located on the downhill side of CRDM 19, which has an angle with the head of 30.0 degrees. The flaw is 10 mm long and its upper extent is 1.0 inch below the weld. The first step is to estimate the time required to grow to within 0.5 inch of the weld, and this is done in Figure 6-3, reproduced here as Figure 7-4A. The flaw will grow to within 0.5 inch of the weld when its depth reaches 45 percent of the wall thickness, and the time to reach that size is estimated as 1.5 years for Figure 7-4A. Then, use Figure 6-5, for flaws within 0.5 inch of the weld, and start with the flaw depth at 45 percent. Figure 7-4B shows an additional 0.25 year of service for total of 1.75 years service.

Example 5. This case is an axial through-wall flaw whose upper-most end is 0.40 inches below the weld region on the uphill side of penetration 19, which is in the 30.0 degree row of penetrations, as seen in Table 1-1. From Figure 6-12 we obtain the appropriate curve for the crack growth prediction, and this is reproduced as Figure 7-5. This figure gives a service life estimate of approximately 2.6 years to grow to the bottom of the weld as illustrated in Figure 7-5.

It is clear from these examples that the most important figures for use in evaluating flaws in head penetrations are the surface flaw Figures 6-2 through 6-9 for axial flaws and 6-17 for circumferential flaws. The figures which project the growth of through-wall flaws are valuable, but may be of limited practical use with the acceptance criteria. There is an important safety aspect to the through-wall flaw charts, however, in that they demonstrate that flaw propagation above the weld will be very limited.

Several guidelines are important to understand when using these charts.

1. If a flaw is found in a penetration nozzle for which no specific analysis was done, interpolation between penetrations is the best approach, when there is a uniform trend.

2. If a flaw is found in a penetration nozzle not analyzed, and there is no apparent trend as a function of nozzle angle, use the result for the penetration with the closest angle.

3. If a flaw is found which has a depth smaller than any depth shown for the penetration angle of interest, assume the smallest depth which was analyzed for that particular penetration, and make the time calculation with that flaw size instead of the actual flaw size.

Table 7-1 Example Problem Inputs: Initial Flaw Sizes and Locations

Example No.	Orientation	Vertical Location	Circumferential Location	Penetration Row	Length	Depth	Penetration No.	Source Figure
1	Axial-ID	1.3" Below Weld	Uphill	30.0°	3.0 mm (0.118")	1.2 mm (0.047")	20	6-2
2	Axial-OD	1.3" Below Weld	Uphill	30.0°	3.0 mm (0.118")	1.2 mm (0.047")	20	6-8
3	Axial-ID	At Weld	Uphill	43.5°	7.2 mm (0.283")	1.2 mm (0.047")	35	6-4
4	Axial-ID	1.0" Below Weld	Downhill	30.0°	10 mm (0.394")	2 mm (0.079")	19	6-3, 6-5
5	Axial Through-Wall	0.40" Below Weld	Uphill	30.0°	--	15.9 mm (0.625")	19	6-12

Figure 7-1: Example 1

Example No.	Orientation	Vertical Location	Circumferential Location	Penetration Row	Length	Depth	Penetration No.	Source Figure
1	Axial-ID	1.3" Below Weld	Uphill	30.0°	3.0 mm (0.118")	1.2 mm (0.047")	20	6-2

Table 1-1

Nozzle No.	Type	Angle (degrees)
18	CRDM	30.0
19	CRDM	30.0
20	CRDM	30.0
21	CRDM	30.0

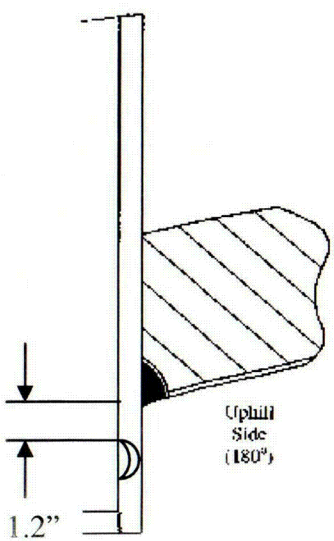

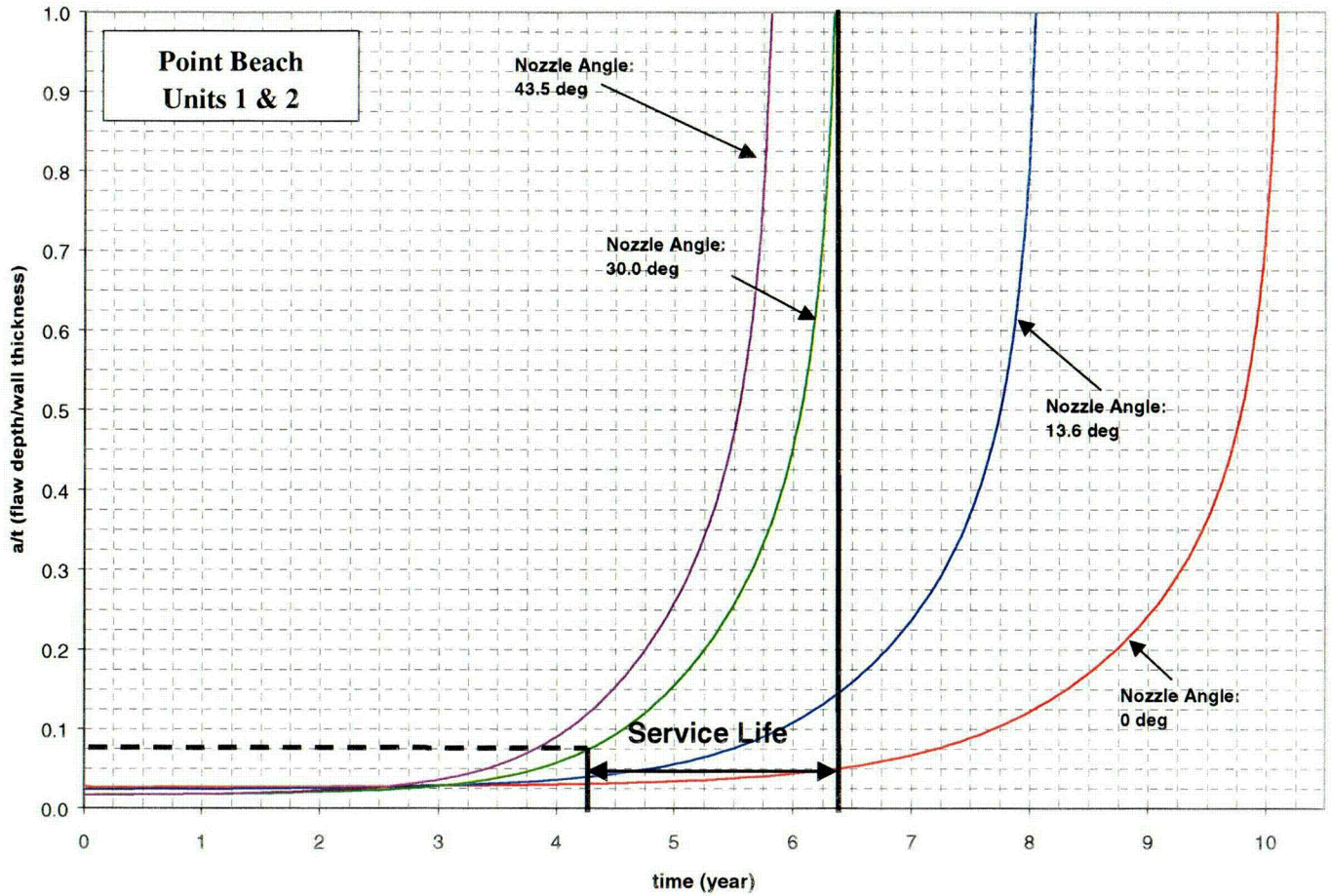

C17

Figure 7-2 Example 2

Example No.	Orientation	Vertical Location	Circumferential Location	Penetration Row	Length	Depth	Penetration No.	Source Figure
2	Axial-OD	1.3" Below Weld	Uphill	30.0°	3.0 mm (0.118")	1.2 mm (0.047")	20	6-8

Table 1-1

Nozzle No.	Type	Angle (degrees)
18	CRDM	30.0
19	CRDM	30.0
20	CRDM	30.0
21	CRDM	30.0

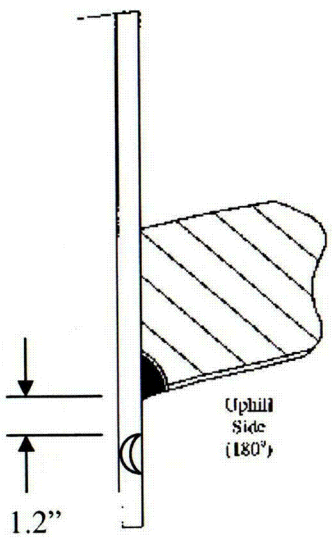

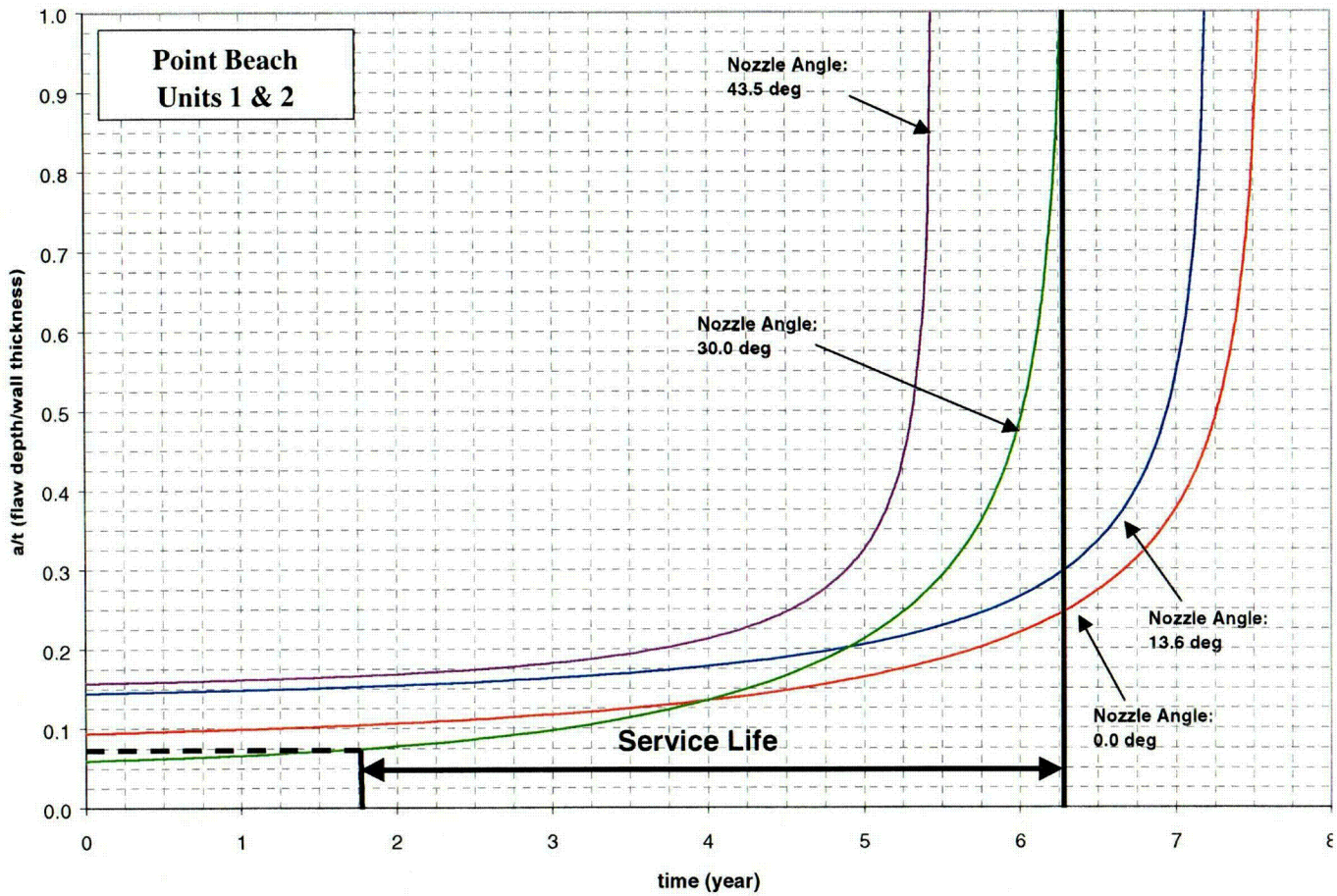

C18

Figure 7-3 Example 3

Example No.	Orientation	Vertical Location	Circumferential Location	Penetration Row	Length	Depth	Penetration No.	Source Figure
3	Axial-ID	At Weld	Uphill	43.5°	7.2 mm (0.283")	1.2 mm (0.047")	35	6-4

Table 1-1

Nozzle No.	Type	Angle (degrees)
34	CRDM	43.5
35	CRDM	43.5
36	CRDM	43.5
37	CRDM	43.5

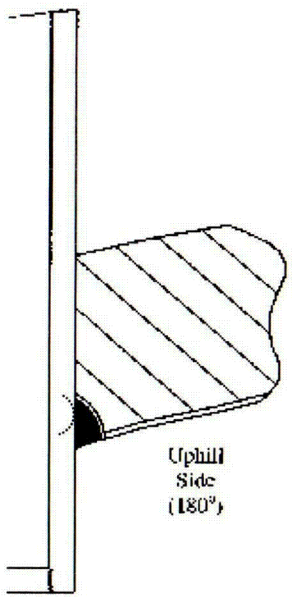

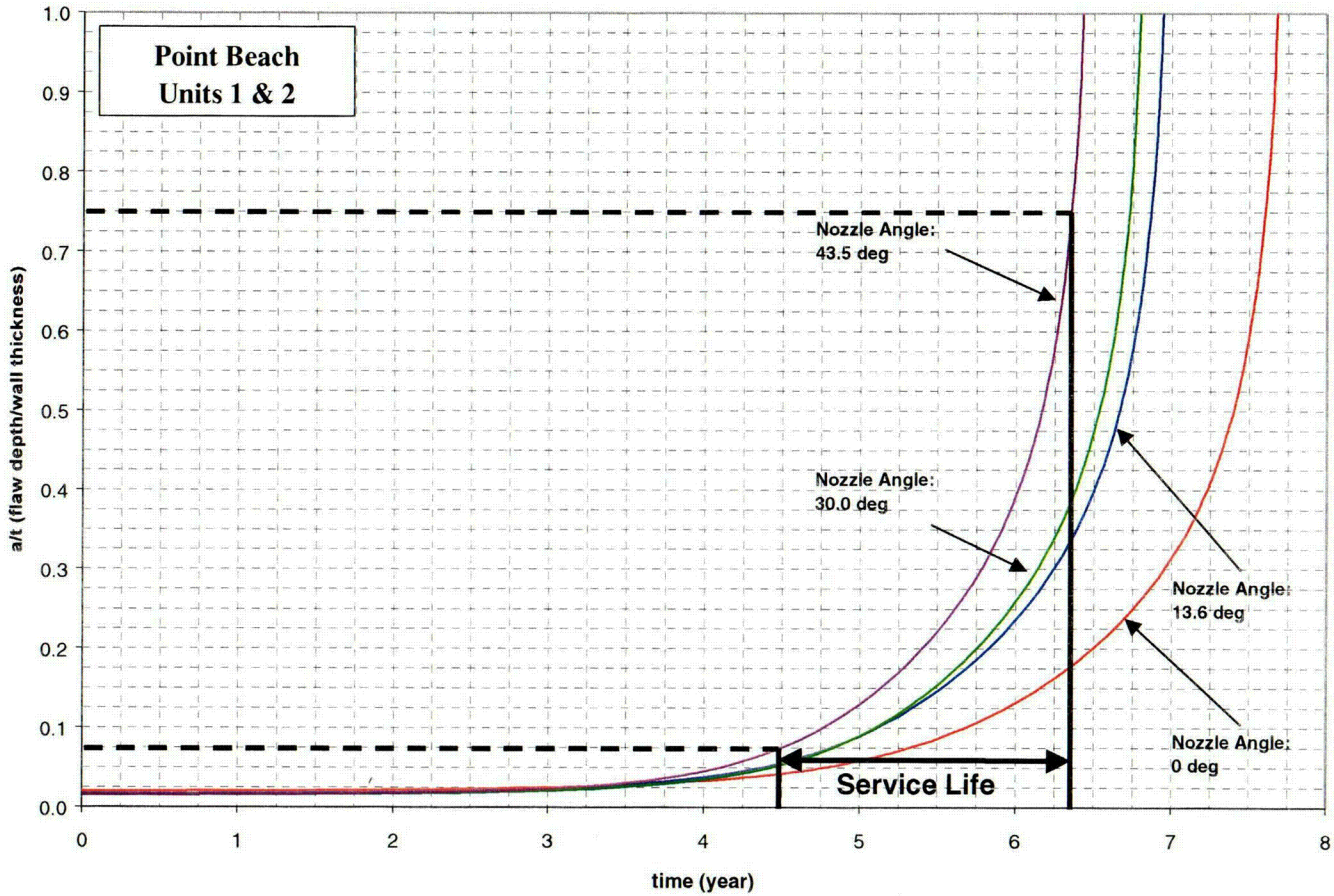

C19

Figure 7-4A Example 4 (also see 7-4B)

Example No.	Orientation	Vertical Location	Circumferential Location	Penetration Row	Length	Depth	Penetration No.	Source Figure
4	Axial-ID	1.0" Below Weld	Downhill	30.0°	10 mm (0.394")	2 mm (0.079")	19	6-3, 6-5

Table 1-1

Nozzle No.	Type	Angle (degrees)
18	CRDM	30.0
19	CRDM	30.0
20	CRDM	30.0
21	CRDM	30.0

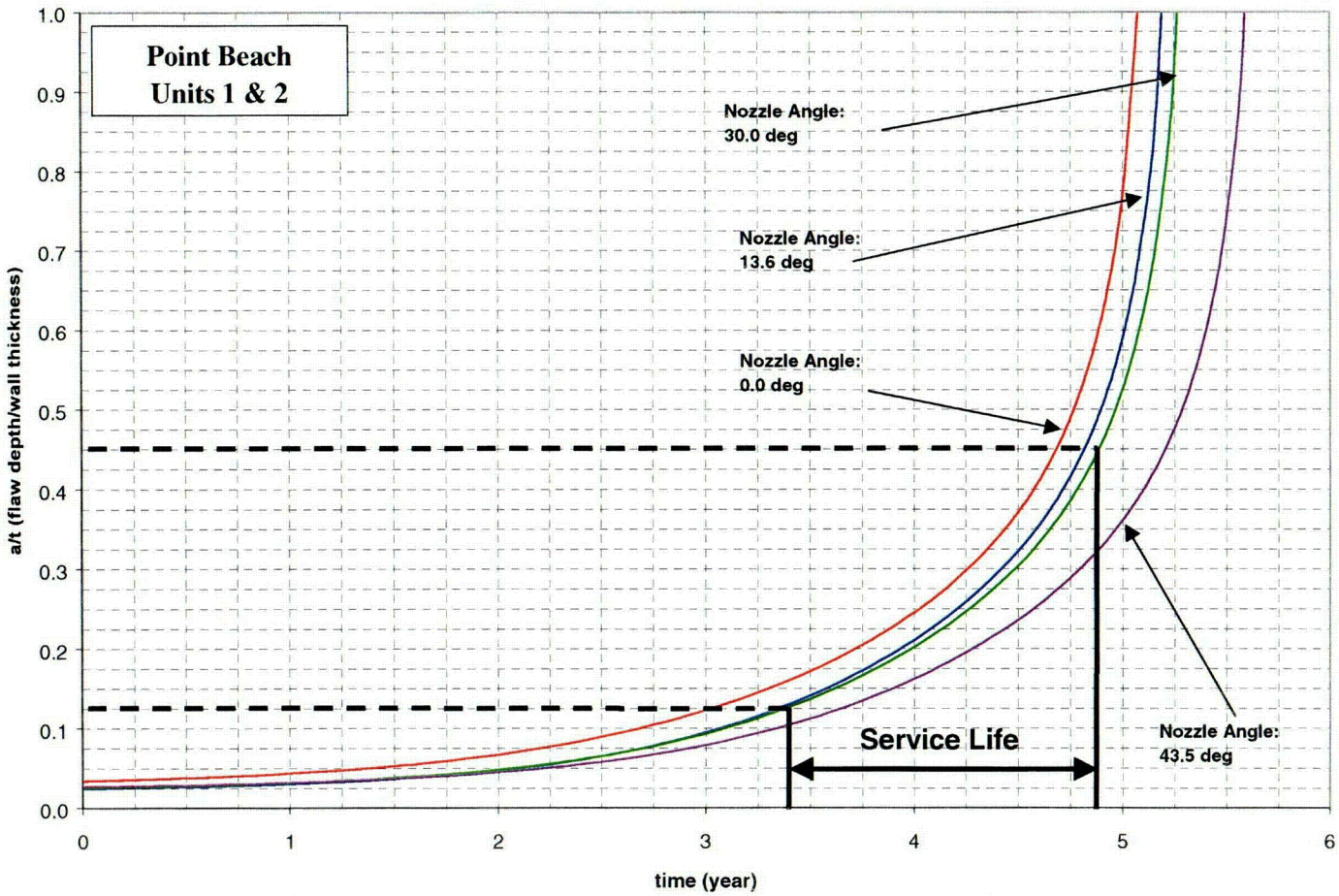

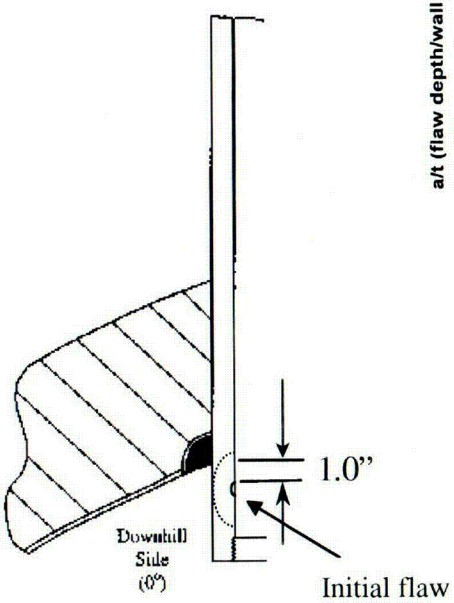

C20

Figure 7-4B Example 4 (cont.)

Example No.	Orientation	Vertical Location	Circumferential Location	Penetration Row	Length	Depth	Penetration No.	Source Figure
4	Axial-ID	1.0" Below Weld	Downhill	30.0°	10 mm (0.394")	2 mm (0.079")	19	6-3, 6-5

Table 1-1

Nozzle No.	Type	Angle (degrees)
18	CRDM	30.0
19	CRDM	30.0
20	CRDM	30.0
21	CRDM	30.0

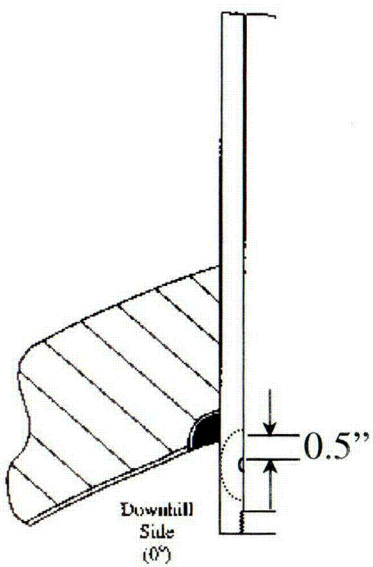

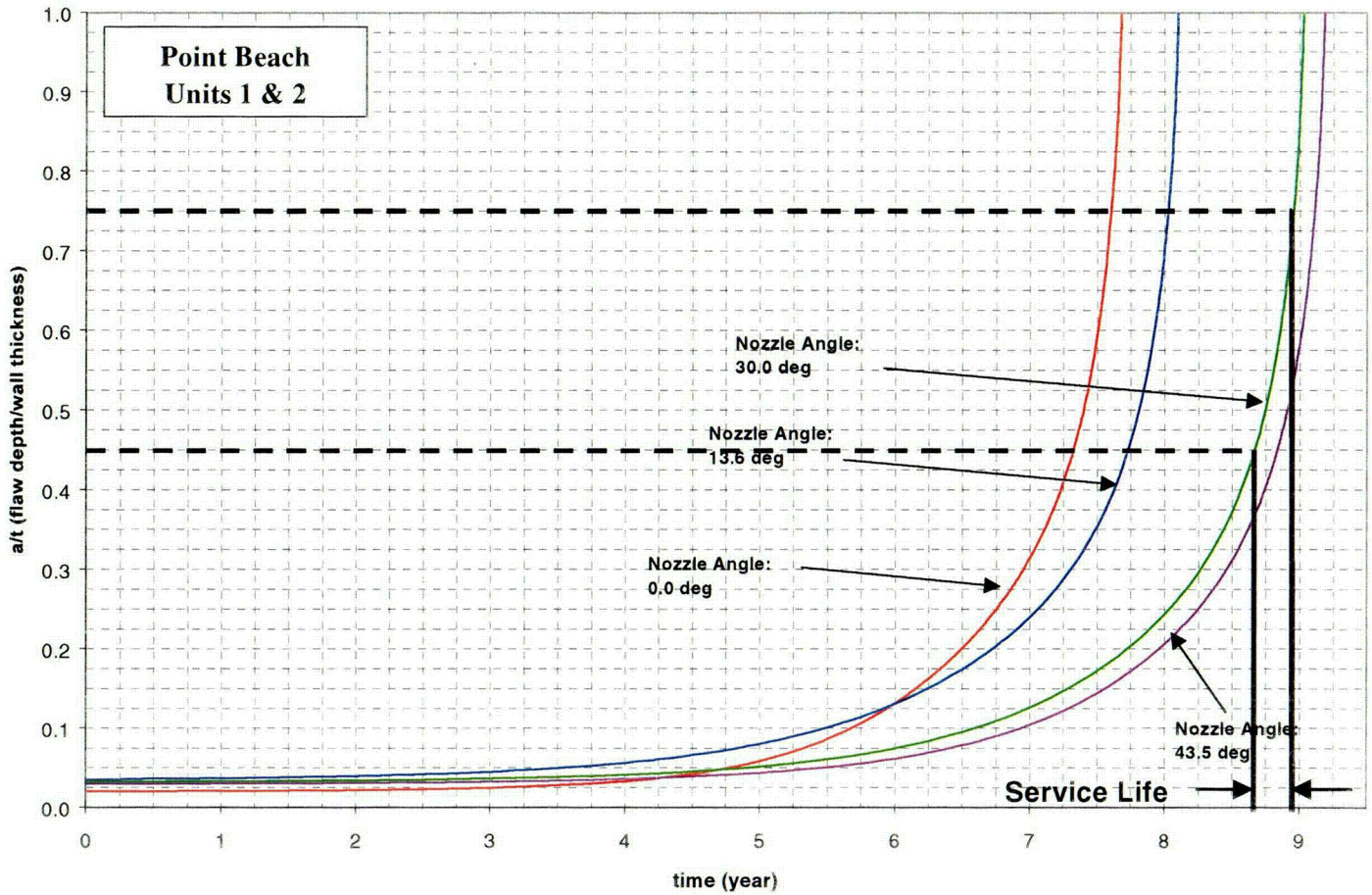

C21

Figure 7-5 Example 5

Example No.	Orientation	Vertical Location	Circumferential Location	Penetration Row	Length	Depth	Penetration No.	Source Figure
5	Axial Through-Wall	0.40" Below Weld	Uphill	30.0°	--	15.9 mm (0.625")	19	6-12

Table 1-1

Nozzle No.	Type	Angle (degrees)
18	CRDM	30.0
19	CRDM	30.0
20	CRDM	30.0
21	CRDM	30.0

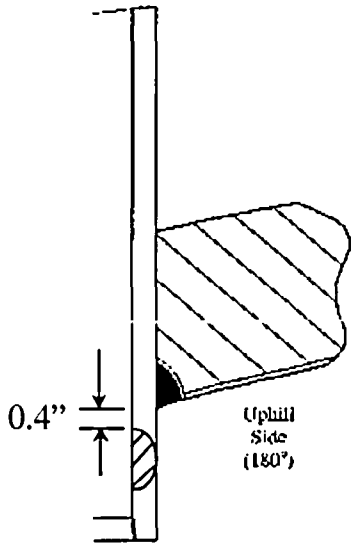

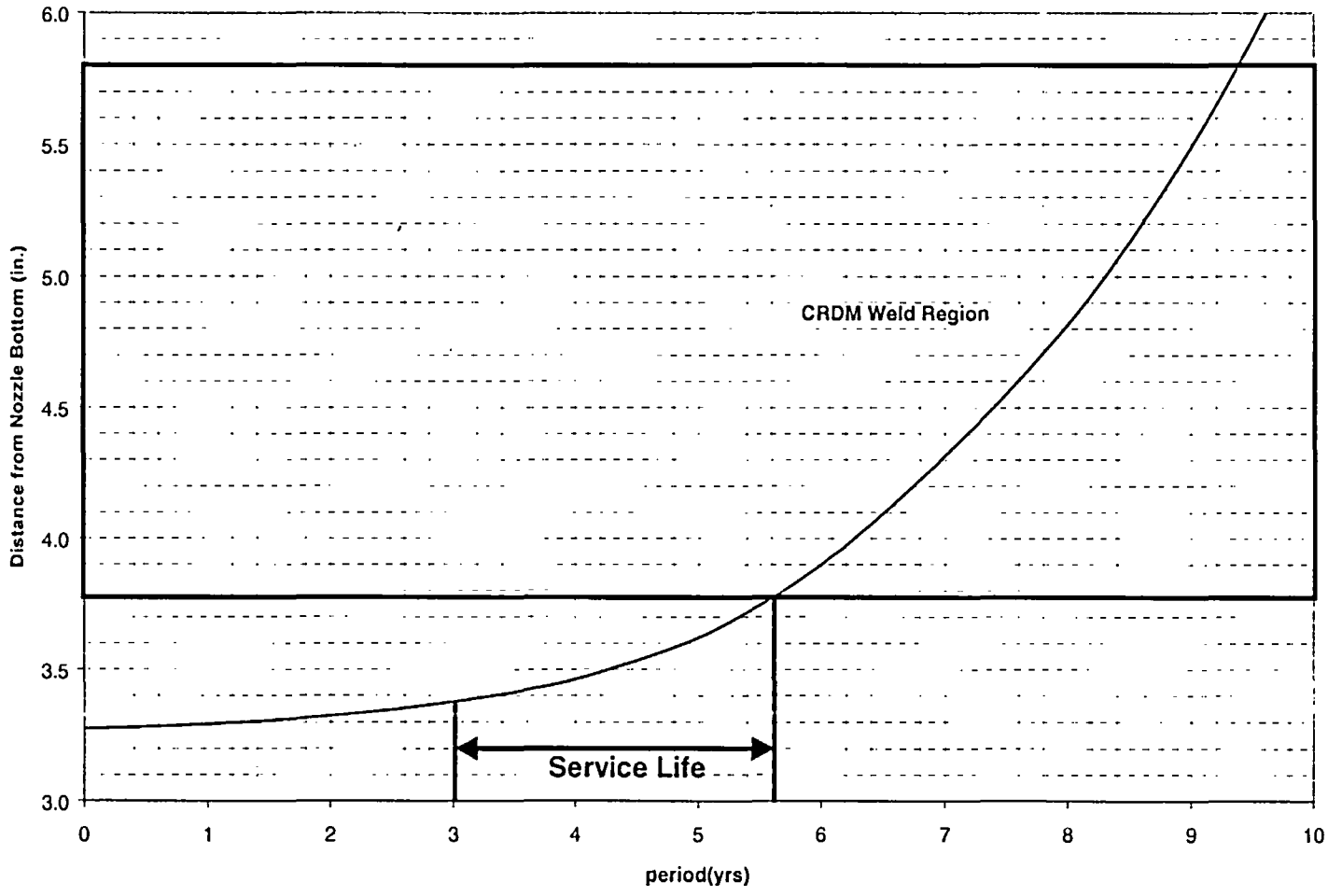

8 REFERENCES

1. Scott, P. M., "An Analysis of Primary Water Stress Corrosion Cracking in PWR Steam Generators," in Proceedings, Specialists Meeting on Operating Experience With Steam Generators, Brussels Belgium, Sept. 1991, pages 5, 6.

2. McIlree, A. R., Rebak, R. B., Smialowska, S., "Relationship of Stress Intensity to Crack Growth Rate of Alloy 600 in Primary Water," Proceedings International Symposium Fontevraud II, Vol, 1, p. 258-267, September 10-14, 1990.

3. Cassagne, T., Gelpi, A., "Measurements of Crack Propagation Rates on Alloy 600 Tubes in PWR Primary Water," in Proceedings of the 5th International Symposium on Environmental Degradation of Materials in Nuclear Power Systems-Water Reactors," August 25-29, 1991, Monterey, California.

4A. *Crack Growth and Microstructural Characterization of Alloy 600 PWR Vessel Head Penetration Materials,* EPRI, Palo Alto, CA. 1997. TR-109136.

4B. Vaillant, F. and C. Amzallag. "Crack Growth Rates of Alloy 600 in Primary Water," Presentation to the EPRI-MRP Crack Growth Rate (CGR) Review Team, Lake Tahoe, NV, August 10, 2001.

4C. Vaillant, F. and S. Le Hong. *Crack Growth Rate Measurements in Primary Water of Pressure Vessel Penetrations in Alloy 600 and Weld Metal 182,* EDF, April 1997. HT-44/96/024/A.

4D. Framatome laboratory data provided by C. Amzallag (EDF) to MRP Crack Growth Rate Review Team, October 4, 2001 (Proprietary to EDF).

4E. Cassagne, T., D. Caron, J. Daret, and Y. Lefevre. "Stress Corrosion Crack Growth Rate Measurements in Alloys 600 and 182 in Primary Water Loops Under Constant Load," *Ninth International Symposium on Environmental Degradation of Materials in Nuclear Power Systems-Water Reactors* (Newport Beach, CA, August 1-5, 1999), Edited by F. P. Ford, S. M. Bruemmer, and G. S. Was, The Minerals, Metals & Materials Society (TMS), Warrendale, PA, 1999.

4F. Studsvik laboratory data provided by Anders Jenssen (Studsvik) to MRP Crack Growth Rate Review Team, October 3, 2001 (Proprietary to Studsvik).

4G [

]a,c,e

4H. Materials Reliability Program (MRP) Recommended Crack Growth Rates for Evaluating Primary Water Stress Corrosion Cracking (PWSCC) of Thick Wall Alloy 600 Material," EPRI MRP Report 55, May 30, 2002.

5A. Newman, J. C. and Raju, I. S., "Stress Intensity Factor Influence Coefficients for Internal and External Surface Cracks in Cylindrical Vessels," in Aspects of Fracture Mechanics in Pressure Vessels and Piping, PVP Vol. 58, ASME, 1982, pp. 37-48.

5B. Hiser, Allen, "Deterministic and Probabilistic Assessments," presentation at NRC/Industry/ACRS meeting, November 8, 2001.

6A. [ ]a,c,e

6B. [ ]a,c,e

7. USNRC Letter, W. T. Russell to W. Raisin, NUMARC, "Safety Evaluation for Potential Reactor Vessel Head Adapter Tube Cracking," November 19, 1993.

8. USNRC Letter, A. G. Hansen to R. E. Link, "Acceptance Criteria for Control Rod Drive Mechanism Penetrations at Point Beach Nuclear Plant, Unit 1," March 9, 1994.

9. Westinghouse Letter, LTR-EMT-02-258, K. B. Neubert, "Point Beach Units 1 and 2 – Upper Head Mean Fluid Temperature for Flaw Handbook Calculation," September 16, 2002.

APPENDIX A

ALLOWABLE AREAS OF LACK OF FUSION: WELD FUSION ZONES

There are two fusion zones of interest for the head penetration nozzle attachment welds, the penetration itself (Alloy 600) and the reactor vessel head material (A533B ferritic steel). The operating temperature of the upper head region of the Point Beach Units 1 and 2 is 314°C (598°F), so the materials will be very ductile. The toughness of both materials is quite high, so any flaw propagation along either of the fusion zones will be totally ductile.

Two calculations were completed for the fusion zones, one for the critical flaw size, and the second for the allowable flaw size, which includes the margins required in the ASME code. The simpler case is the Alloy 600 fusion zone, where the potential failure will be a pure shearing of the penetration as the pressurized penetration tube is forced outward from the vessel head, as shown in Figure A-1.

The failure criterion will be that the average shear stress along the fusion line exceeds the limit shear stress. For the critical flaw size, the limiting shear stress is the shear flow stress, which is equal to half the tensile flow stress, according to the Tresca criterion. The tensile flow stress is the average of the yield stress and ultimate tensile stress of the material. The criterion for Alloy 600 at 314°C (598°F) is:

$$\text{Average shear stress} < \text{shear flow stress} = 26.85 \text{ ksi}$$

This value was taken from the ASME Code, Section III, Appendix I, at 600°F.

For each penetration, the axial force which produces this shear stress results from the internal pressure. Since each penetration has the same outer diameter, the axial force is the same. The average shear stress increases as the load carrying area decreases (the area of lack of fusion increases). When this increasing lack of fusion area increases the stress to the point at which it equals the flow stress, failure occurs. This point may be termed the critical flaw size. This criterion is actually somewhat conservative. Alternatively, use of the Von Mises failure criterion would have set the shear flow stress equal to 60 percent of the axial flow stress, and would therefore have resulted in larger critical flaw sizes.

The allowable flaw size, as opposed to the critical flaw size discussed above, was calculated using the allowable limit of Section III of the ASME Code, paragraph NB 3227.2. The criterion for allowable shear stress then becomes:

$$\text{Average shear stress} < 0.6\ S_m = 13.98 \text{ ksi}$$

where S_m = the ASME Code limiting design stress from Section III, Appendix I.

The above approach was used to calculate the allowable flaw size and critical flaw size for the outermost and center penetrations. The results show that a very large area of lack of fusion can be tolerated by the head penetrations, regardless of their orientation. These results can be illustrated for the outermost CRDM penetration.

The total surface contact area for the fusion zone on the outermost head penetration is 17.4 in^2. The calculations above result in a required area to avoid failure of only 1.45 in^2, and using the ASME Code criteria, the area required is 2.79 in^2. These calculations show that as much as 83.9 percent of the weld may be unfused, and the code acceptance criteria can still be met.

To envision the extent of lack of fusion which is allowable, Figure A-2 was prepared. In this figure, the weld fusion region for the outermost penetration has been shown in an unwrapped, or developed view. The figure shows the extent of lack of fusion which is allowed, in terms of limiting lengths for a range of circumferential lack of fusion. This figure shows that the allowable vertical length of lack of fusion for a full circumferential unfused region is 84 percent of the weld length. Conversely, for a region of lack of fusion which extends the full vertical length of the weld, the circumferential extent is limited to 302 degrees. The extent of lack of fusion which would cause failure is labelled "critical" on this figure, and is even larger. The dimensions shown on this figure are based on an assumed rectangular area of lack of fusion.

The full extent of this allowable lack of fusion is shown in Figure A-3, where the axes have been expanded to show the full extent of the tube-weld fusion line. This figure shows that a very large area of lack of fusion is allowable for the outer most penetration. Similar results were found for the center penetration, where the weld fusion area is somewhat smaller at 16.1 in^2.

A similar calculation was also carried out for the fusion zone between the weld and the head, and the result is shown in Figure A-4. The allowable area of unfused weld for this location is 84.8 percent of the total area. This approach to the fusion zone with the carbon steel head is only approximate, but may provide a realistic estimate of the allowable. Note that even a complete lack of fusion in this region would not result in rod ejection, because the weld to the tube would prevent the tube from moving up through the vessel head.

The allowable lack of fusion for the weld fusion zone to the head may be somewhat in doubt, because of the different geometry, where one cannot ensure that the failure would be due to pure shear. To investigate this concern, additional finite element models were constructed with various degrees of lack of fusion discretely modeled, ranging from 30 to 65 percent. The stress intensities around the circumference of the penetration were calculated, to provide for the effects of all stresses, as opposed to the shear stress only, as used above. When the average stress intensity reaches the flow stress (53.7 ksi), failure is expected to occur. The code allowable stress intensity is 1.5 Sm, or 35 ksi, using the lower of the Alloy 600 and ferritic allowables at 316°C (600°F).

The results of this series of analyses are shown in Figure A-5, where it is clear that large areas of lack of fusion are allowable. As the area of lack of fusion increases, the stresses redistribute themselves, and the stress intensity does not increase in proportion to the area lost. These results seem to confirm that the shear stress is the only important stress governing the critical flaw size for the head fusion zone as well.

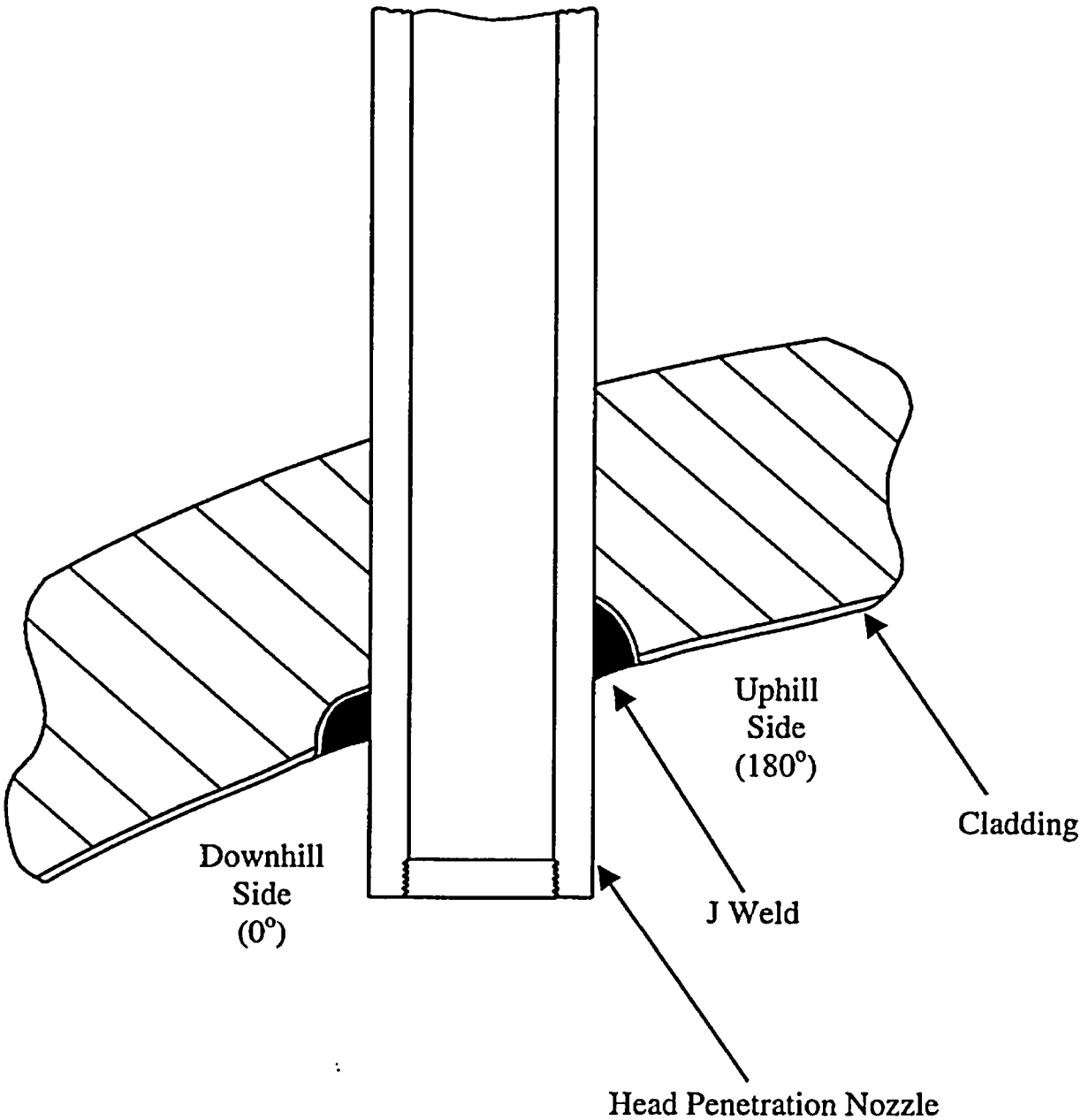

Figure A-1 Typical Head Penetration

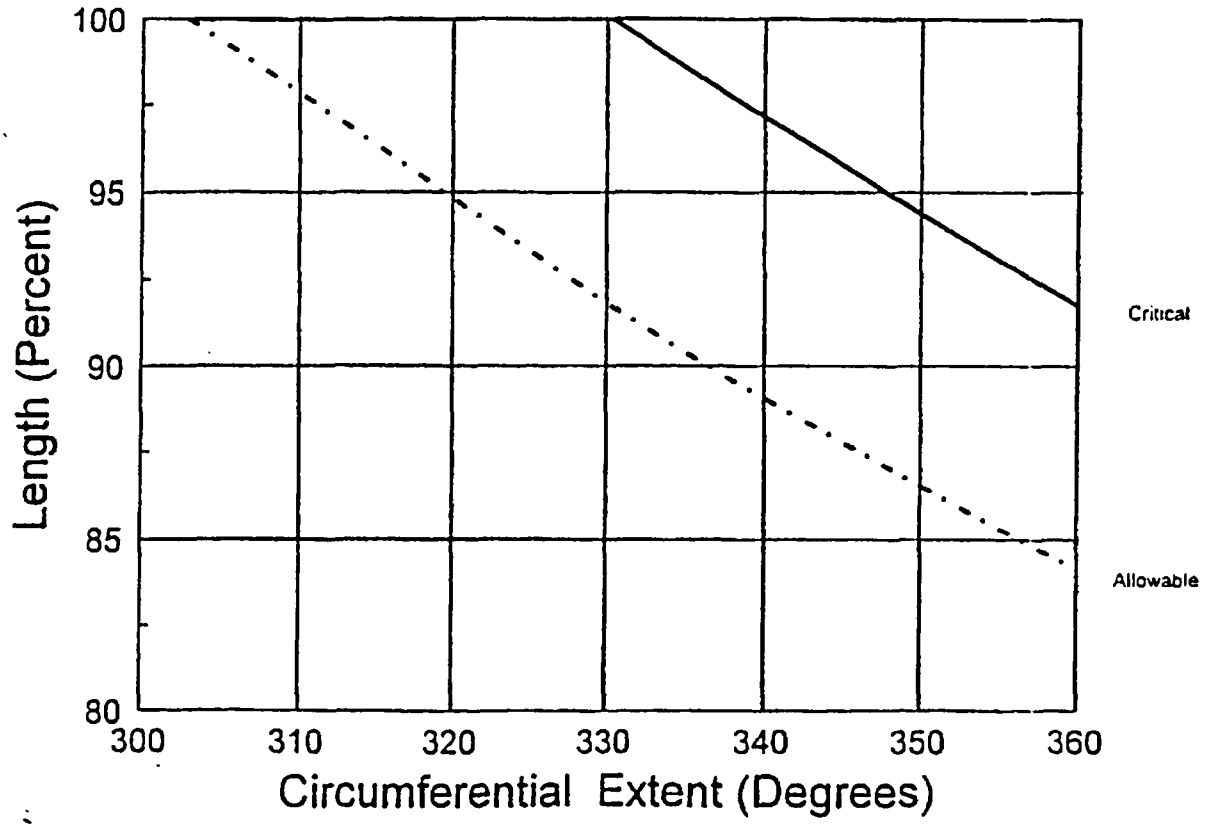

Figure A-2 Allowable Regions of Lack of Fusion for the Outermost Penetration Tube to Weld Fusion Zone: Detailed View

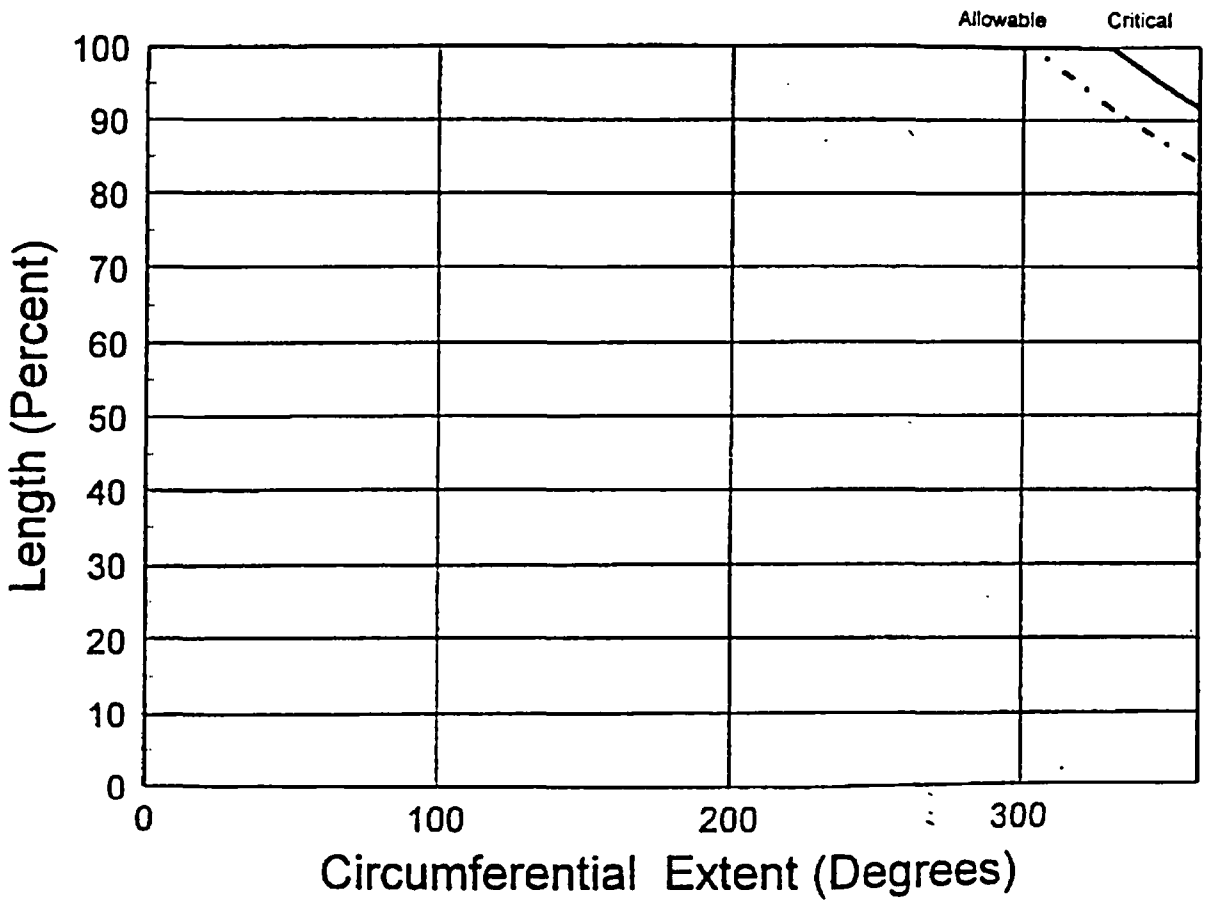

Figure A-3 Allowable Regions of Lack of Fusion for the Outermost Penetration Tube to Weld Fusion Zone

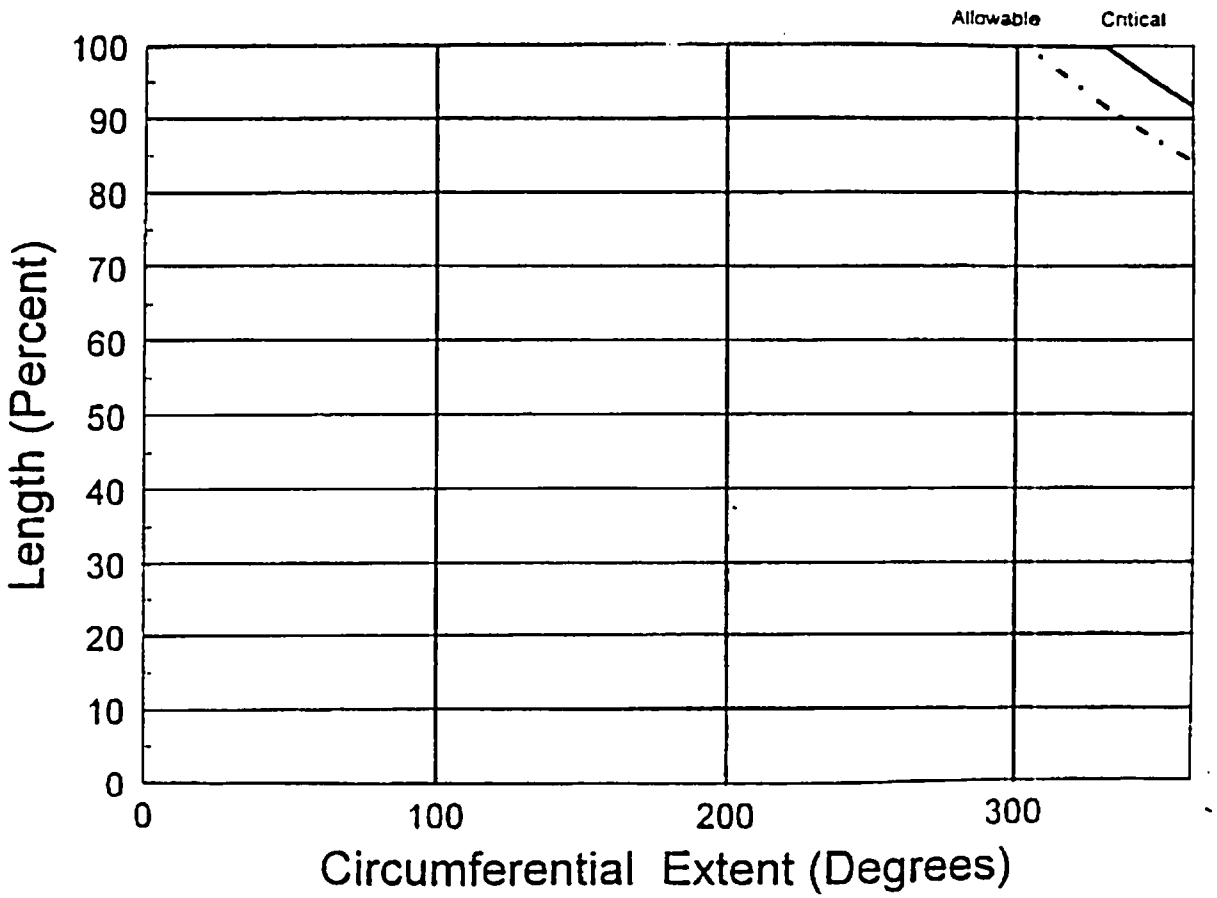

Figure A-4 Allowable Regions of Lack of Fusion for all Penetrations: Weld to Vessel Fusion Zone

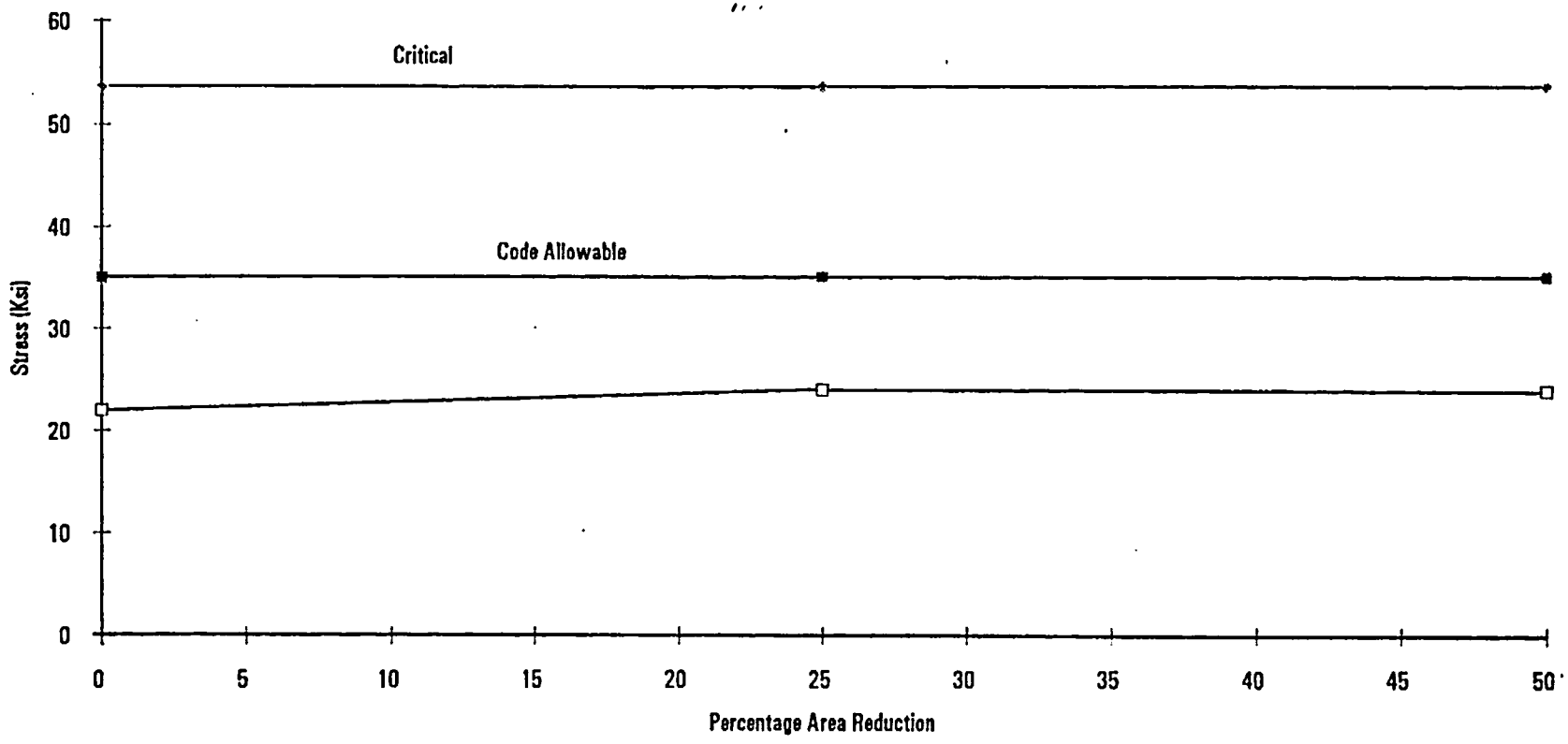

Figure A-5 Allowable Regions of Lack of Fusion for the Weld to Vessel Fusion Zone